BMR JOURNAL
OF AUSTRALIAN GEOLOGY & GEOPHYSICS

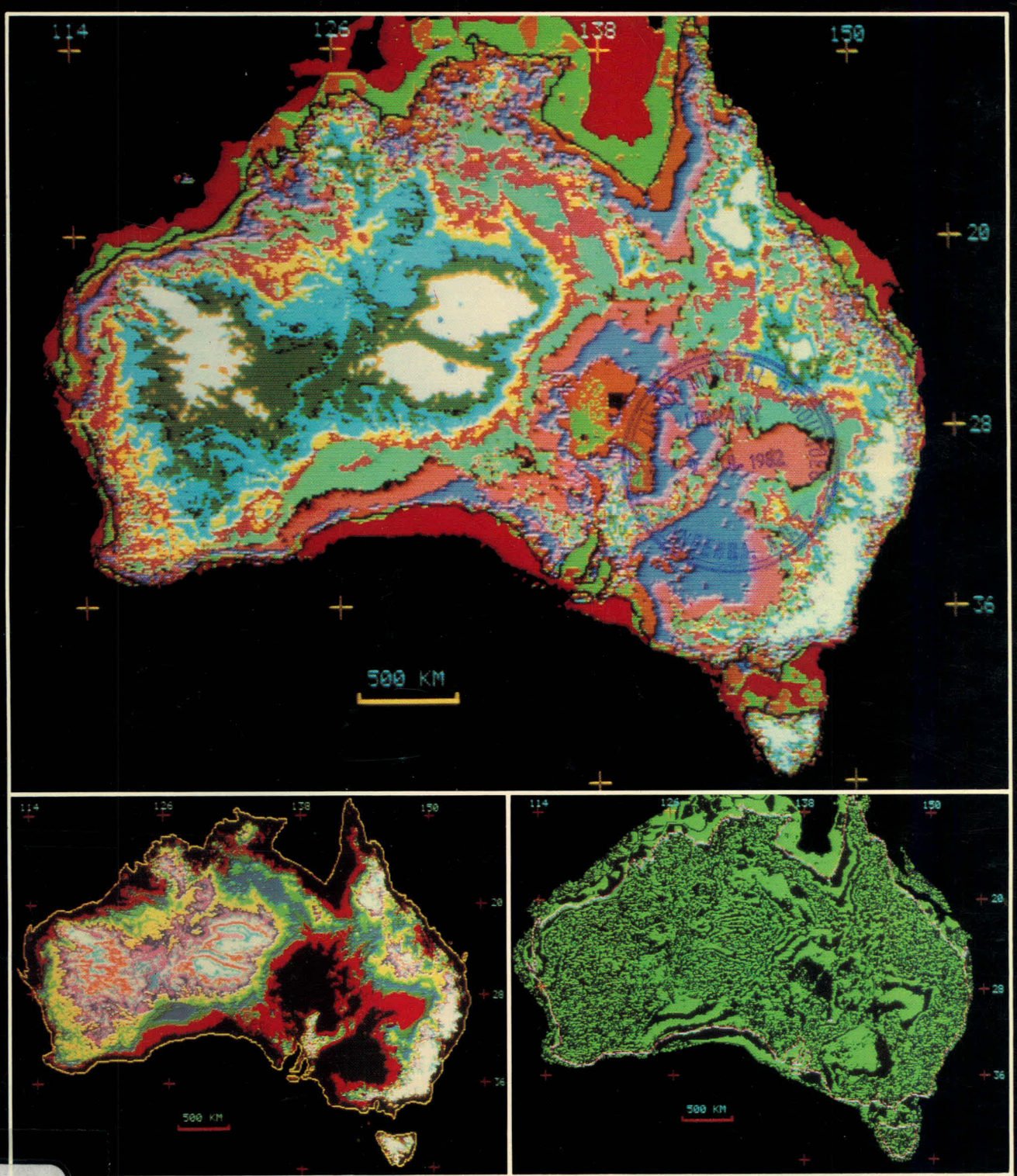

VOLUME 7 NUMBER 1 MARCH 1982

BMR JOURNAL
OF AUSTRALIAN GEOLOGY & GEOPHYSICS

We apologise to readers for the lateness of this issue of the BMR Journal, which has resulted from several causes in different stages of production. The nature of the production schedule means that some delay will inevitably flow on to subsequent issues. However, we expect that this can be progressively reduced and that by the end of the volume the Journal will appear on schedule.

Papers to appear in future issues this year include:

——————— A Proterozoic rift zone at Mount Isa, and implications for mineralisation (G.M. Derrick);

——————————— Eastern Creek Volcanics as the source of copper at Mammoth Mines, NW Queensland (K.M. Scott & G.F. Taylor);

——— Distribution and geochemistry of volcanic rocks in the Duchess-Urandangi region, Queensland (R.J. Bultitude & L.A.I. Wyborn);

——— A review of the Corella Formation, Mount Isa Inlier (D.H. Blake);

——————————— The role of pre-existing sulphides in copper-ore formation at Mount Isa (C.W. Robertson);

——————————————— Geological evolution, tectonic style, and economic potential of the Lawn Hill Platform Cover, NW Queensland (L.J. Hutton & I.P. Sweet);

——————————————— Proterozoic intrusive breccia bodies near Duchess, NW Queensland (D.H. Blake, R.J. Bultitude & P.J. Donchak);

——————— A latest Devonian palynoflora from the Buttons Beds, Bonaparte Gulf Basin, WA (G. Playford);

——————————————— The multielement composition of Icriodus expansus Branson & Mehl from the Upper Devonian of the Canning Basin, WA (R.S. Nicoll);

——————————————— The extent of Archaean and Late Proterozoic rocks under the ice cap of Princess Elizabeth Land, Antarctica, inferred from geophysics (P. Wellman & J.W. Williams).

BMR JOURNAL
OF AUSTRALIA GEOLOGY & GEOPHYSICS

VOLUME 7 NUMBER 1 MARCH 1982

CONTENTS

K. S. Jackson
Geochemical evaluation of the petroleum potential of the Toko Syncline, Georgina Basin, Queensland 1

J. P. Cull
An appraisal of Australian heat-flow data 11

C. M. Brown, K. S. Jackson, K. L. Lockwood, & V. L. Passmore
Source rock potential and hydrocarbon prospectivity of the Darling Basin, New South Wales 23

R. V. Burne
Relative fall of Holocene sea level and coastal progradation, northeastern Spencer Gulf, South Australia 35

V. Anfiloff
Elevation and gravity profiles across Australia: some implications for tectonism 47

G. D. Karner
Spectral representation of isostatic models 55

NOTES

R. F. Moore & C. J. Simpson
Computer manipulation of a digital terrain model (DTM) of Australia .. 63

H. J. Harrington, C. J. Simpson, & R. F. Moore
Analysis of continental structures using a digital terrain model (DTM) of Australia 68

D. L. Strusz
On *Australina* Clarke and its junior synonyms, *Lissatrypa, Lissatrypoidea,* and *Tyrothyris* (Silurian-Devonian Brachiopoda) 73

D. L. Strusz & C. J. Jenkins
The stratigraphic implications of *Monograptus exiguus* from Camp Hill, Canberra, ACT 78

AUSTRALIAN GOVERNMENT PUBLISHING SERVICE CANBERRA 1982

Department of National Development and Energy, Australia

Minister: Senator the Hon. Sir John L. Carrick

Secretary: A. J. Woods

Bureau of Mineral Resources, Geology and Geophysics

Director: R. W. R. Rutland

Editor, BMR Journal: I. M. Hodgson

The BMR Journal of Australian Geology and Geophysics is a quarterly journal of research and related activities. Contributions are from officers of the BMR, from BMR officers working in collaboration with others, or requested work sponsored by the BMR. In addition to articles the Journal may include shorter notes and discussion of papers published in it. Discussion of papers is invited from anyone.

Annual subscriptions to the Journal is at the rate of $14 (Australian). Individual numbers, if available, cost $4. Subscriptions, etc., made payable to the Receiver of Public Moneys in Australian dollars should be sent to the Director, Bureau of Mineral Resources, Geology and Geophysics, P.O. Box 378, Canberra, A.C.T. 2601, Australia.

Other matters concerning the Journal should be sent to the Director, marked for the attention of the Editor, BMR Journal.

Front cover: The first published coloured images of the topography of Australia (DTM) created from a digital data file at the Bureau of Mineral Resources. Their generation and use for the analysis of continental structures are described in two notes in this issue.

Cover design: Stuart Fereday.

The text figures in this issue were drafted by a cartographic team of P. Jorritsma, P. Griffiths, C. Williams, & B. Pashley.

ISSN 0312-9608

Printed by Graphic Services Pty Ltd, 516-518 Grand Junction Road, Northfield, S.A. 5085

BMR Journal of Australian Geology & Geophysics, 7, 1-10.

GEOCHEMICAL EVALUATION OF THE PETROLEUM POTENTIAL OF THE TOKO SYNCLINE, GEORGINA BASIN, QUEENSLAND, AUSTRALIA

K. S. Jackson

In the Georgina Basin, the Toko Syncline is considered the most prospective region for petroleum exploration. The syncline contains up to 5000 m of Middle Cambrian to Middle Ordovician sediments and has been the site of six petroleum exploration wells, three of which showed traces of gas, oil, and solid bitumen. Geochemical data for cores from two stratigraphic holes, GSQ Mount Whelan Nos. 1 and 2, and data from four exploration wells, held on open file at BMR, are used to evaluate the organic maturation and rock potential of the sediments in the Toko Syncline. Source rocks are not recognised in the Ordovician; however, source rocks of generally good quality are present in the Middle and Upper Cambrian. While doubts do exist over the stratigraphic correlations for the wells involved in this study, the Middle Cambrian Marqua beds are considered to be the best source interval. Maturity for oil generation is achieved in the Upper Cambrian to Lower Ordovician Ninmaroo Formation at the Mount Whelan location. However, in the deeper western area, where the better exploration prospects are likely to exist, maturity in Mirrica No. 1 is reached in the Lower to Middle Ordovician Carlo Sandstone. Over-maturity for oil generation, but still in the gas generation phase, is generally observed in the Middle Cambrian. An oil stain in the Lower Ordovician Coolibah Formation in GSQ Mount Whelan No. 2 (also described as bitumen plugging porosity) is interpreted as having originated in and having migrated from the Cambrian source rock intervals.

Introduction

Solid bitumen and traces of oil and gas considered indicative of hydrocarbon generation have been noted in three petroleum exploration wells drilled in the Toko Syncline (Figs. 1 & 2), in which the preservation of up to 5000 m of Middle Cambrian to Middle Ordovician sediments suggests this as the most petroleum prospective sequence in the Georgina Basin (Harrison, 1979). BMR seismic data have been previously published in discussions of the petroleum prospects and structural aspects of the Toko Syncline (Harrison, 1979, 1980); this study presents geochemical data in an evaluation of the potential for hydrocarbon generation.

Between July and November 1977, the Queensland Department of Mines drilled two deep stratigraphic holes, GSQ Mount Whelan Nos. 1 and 2 on the eastern flank of the Toko Syncline (Fig. 2) Attention was focussed on these wells with the observation of bitumen plugging porosity in the Ordovician Coolibah Formation of Mount Whelan No. 2, and the detection of a petroliferous odour when micritic beds in the Middle Cambrian Georgina Limestone and Thorntonia Limestone of Mount Whelan No. 1 are freshly broken (Green & Balfe, 1980). These wells provided an almost complete section through the Cambrian and Ordovician of the Georgina Basin (the upper part of the Georgina Limestone and lower part of the Ninmaroo Formation were not intersected in either well), and organic geochemical analyses of selected core from them form the major part of this study.

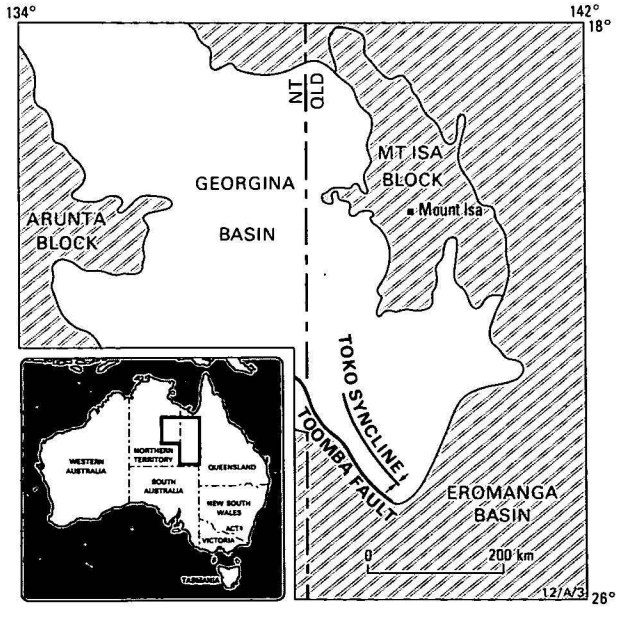

Figure 1. Regional setting of the Toko Syncline, Georgina Basin.

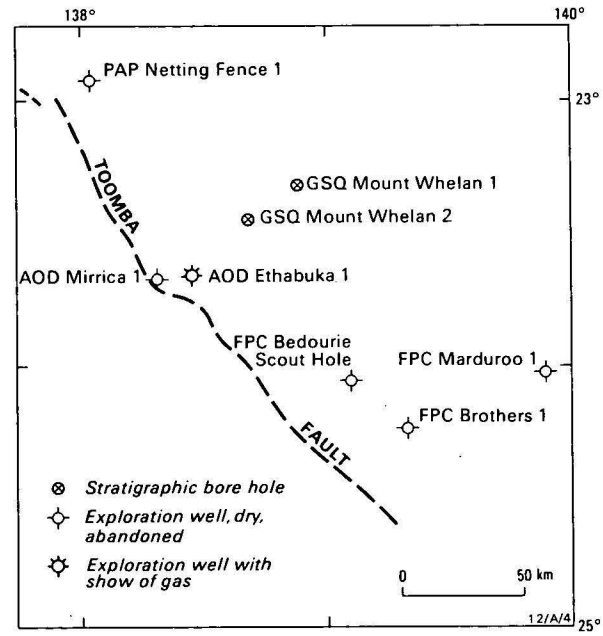

Figure 2. Well locations in the Toko Syncline.

Data have also been used from four exploration wells: Netting Fence No. 1, Ethabuka No. 1, Mirrica No. 1, and The Brothers No. 1. Netting Fence No. 1 drilled a complete Cambrian sequence with several shows of

bitumen, tar, oil stains, and small gas traces being reported (PAP, 1965). The Mirrica-Ethabuka structure, discussed by Harrison (1979), has now been tested by two exploration wells. Ethabuka No. 1 drilled from September 1973 to October 1974, had technical problems and reached total depth in the Lower Ordovician Kelly Creek Formation without reaching zones of interest in the Cambrian. It did, however, encounter a modest gas flow estimated at 7080 m^3/day open hole, from the Lower Ordovician Coolibah Formation (Mulready, 1975). Mirrica No. 1, drilled as a follow-up in 1980, penetrated the primary target in the Cambrian, reaching a total depth of 3314 m. However, the results were disappointing with only a minor gas show in DST 4 at 2745.4–2754.9 m in the Cambrian (Tracer's Exogram and Oil and Gas Review, 1980a & b).

Stratigraphy

The stratigraphy of the Georgina Basin has been described by several workers, including Smith (1972) and Shergold & Druce (1980). Harrison (1979) summarised the stratigraphy of the Toko Syncline; this has been modified to provide a stratigraphic framework for Ordovician and Cambrian units of interest to this study (Table 1).

For the GSQ Mount Whelan Nos. 1 & 2 core samples, the stratigraphy of Green & Balfe (1980) has been adopted (Table 3). However, alternative interpretations and correlations between GSQ Mount Whelan No. 1, Netting Fence No. 1, and Mirrica No. 1 complicate this issue. The most important of these is that the unit designated Georgina Limestone in GSQ Mount Whelan No. 1 (Green & Balfe, 1980) is better correlated with the Middle Cambrian Marqua beds recognised in Mirrica No. 1 (Gausden, Alliance Oil Development N.L., personal communication, June 1981). Gausden also correlates the 'Netting Fence Formation' in Netting Fence No. 1 (PAP, 1965) with the Marqua beds in Mirrica No. 1, a correlation supported by Kennard (1981) after examination of core from Netting Fence No. 1. Table 2 summarises these alternative interpretations.

Petroleum geochemistry

Source rock richness

The following source rock analyses were carried out in the Petroleum Technology Laboratory, BMR, on 33 core samples from GSQ Mount Whelan Nos. 1 & 2 (Table 3):

- TOC—total organic carbon, calculated for whole rock;
- EOM—total extractable organic matter, using 60 benzene 40 methanol as solvent.

The EOM was fractionated by liquid chromatography into:

- SATS—saturated hydrocarbons, which were further, characterised by capillary gas chromatographic analysis:
- AROM—aromatic hydrocarbons;
- POLAR—polar organic compounds, usually containing some or all of N,S, and O.

Table1. Stratigraphy of the Toko Syncline, Georgina Basin. Modified from Harrison, 1979.

Age	*Stratigraphic unit*	*Maximum thickness (m)*	*Lithology*	*Environment*
MIDDLE ORDOVICIAN	Ethabuka beds	1170?	sandstone conglomerate	open coastal?
	Mithaka Fm.	126	sandstone, shale, siltstone	lagoonal or tidal flat
LOWER-MIDDLE ORDOVICIAN	Carlo Sst.	174	sandstone	shoals, barrier island
LOWER ORDOVICIAN	Nora Fm.	231	siltstone, sandstone, limestone	shallow intertidal & subtidal
	Coolibah Fm.	79	limestone, marl	intertidal to subtidal
	Kelly Ck. Fm.	182?	siltstone, sandstone, dolomite, evaporites	intertidal to supratidal
LOWER ORDOVICIAN UPPER CAMBRIAN	Ninmaroo Fm.	488+	sandstone, limestone, dolomite	regressive intertidal and subtidal
			UNCONFORMITY	
UPPER CAMBRIAN	Georgina Lst.	601	limestone, dolomite, sandstone	intertidal to subtidal
MIDDLE CAMBRIAN	Steamboat Sst.	221	sandstone, limestone	shallow marine
	Marqua beds	410	limestone, dolomite, sandstone, shale	marine
	Inca Fm correlative	8	shale	marine
	Thorntonia Lst.	49	limestone, dolomite, calc. shale	shallow marine
			UNCONFORMITY	
ADELAIDEAN—LOWER CAMBRIAN	Field River Beds		tillite, arkose	marine, glacigene

Table 2. Stratigraphic interpretations from GSQ Mount Whelan No. 1, Mirrica No. 1, and Netting Fence No. 1 wells.

GSQ Mount Whelan No. 1 (Green & Balfe, 1980)	*Mirrica No. 1 (Gausden, pers. comm.)*	*Netting Fence No 1*	
		(Kennard, 1981)	*(PAP, 1965)*
Georgina Lst.	Marqua beds	Arrinthrunga Fm. Marqua beds	Georgina Lst. Netting Fence Fm.

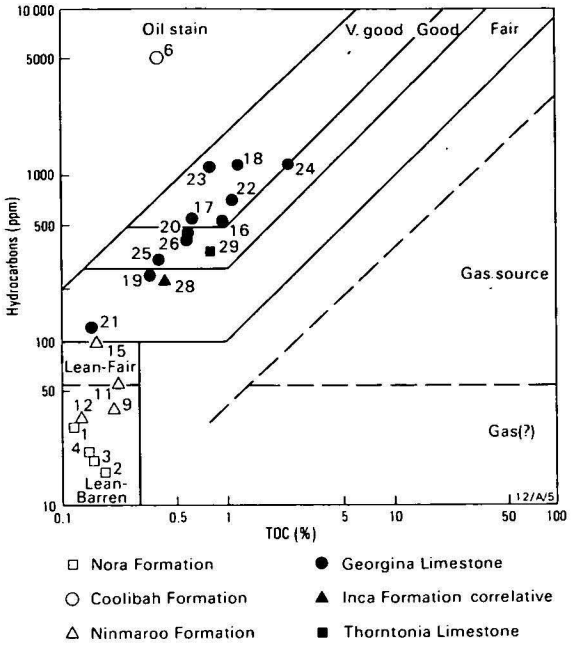

Figure 3. Total hydrocarbons and organic carbon in cores from GSQ Mount Whelan Nos. 1 (solid symbols) and 2 (open symbols).

Also calculated were (Table 3):

- EPOC—EOM as a percentage of TOC,
- HPE—total hydrocarbons (SATS + AROM) as a percentage of EOM.

Total hydrocarbons (SATS + AROM) have been plotted against total organic carbon (TOC) to obtain source rock richness ratings (Fig. 3), with the ratings shown being appropriate for clastic rocks (Hunt, 1979). For carbonate rocks, they may be on the conservative side: for example, Pontigo & others (1979) suggested that carbonates with 0.26–0.50 per cent TOC have fair source potential, while those with greater than one per cent are rated excellent.

In the GSQ Mount Whelan No. 1 sequence, the unnamed tillite overlying Proterozoic basement shows no source potential, with TOC values of 0.08 per cent. The Middle Cambrian Thorntonia Limestone samples show good source potential, and the Inca Formation correlative rates as fair (Fig. 3). Of the 12 samples from the Upper Cambrian Georgina Limestone (of Green & Balfe, 1980) or Marqua beds (of Gausden, pers. comm), 6 rate as very good, 3 as good, 2 as fair, and only one as barren or non-source. A sample from 227.7 m in GSQ Mount Whelan No. 1 has the surprisingly high value of 2.3 per cent, which may reflect its minor shale content, as such values are not expected for carbonates.

The Lower to Middle Ordovician rocks from GSQ Mount Whelan No. 2, show no petroleum source potential. The highest TOC value from 8 Ninmaroo Formation samples is 0.21 per cent at 809.5 m in Mount Whelan No. 2. The one Kelly Creek Formation sample proved barren, and 5 samples from the Nora Formation rate lean to barren with 0.18 per cent as the highest TOC recorded.

A core from the Lower Ordovician Coolibah Formation in Mount Whelan No. 2 at 397.6 m contains bitumen plugging porosity (Green & Balfe, 1980). The analytical data (TOC-0.39%, EOM-6650 ppm, HPE-77.8%), support the interpretation that this is no more than an oil-stained core.

To complement the data obtained by analysis of the GSQ Mount Whelan core material, geochemical data held on open file at BMR are also included in the paper (Table 4); the stratigraphy shown has been taken from the data sources referred to in the table. The wells quoted are Netting Fence No. 1, The Brothers No. 1, and Ethabuka No. 1.

The interpretation of source rating, when based on a TOC value only, is considered less reliable than that based on a plot of TOC against total hydrocarbons. From the data (Table 4), the Ordovician again rates as poor to non-source. Source potential is seen within the Cambrian with some variation from the Mount Whelan data. The Georgina Limestone (of PAP, 1965) or Arrinthrunga Formation (of Kennard, 1981) does not rate as a source. But the 'Netting Fence Formation' (of PAP, 1965) or the Marqua beds (of Gausden, pers. comm.) and the Thorntonia Limestone (of PAP, 1965) rate as good to very good source rock. The data for the cores from The Brothers No. 1 indicate likely good source rock potential for the Cambrian.

Thus, if the alternative stratigraphic correlations of Gausden and Kennard are accepted, the geochemical results for GSQ Mount Whelan No. 1 and Netting Fence No. 1 are compatible and indicate the Marqua beds as a good hydrocarbon source.

Organic maturation

It has proved difficult to assess organic maturation levels in Cambrian and Ordovician rocks. Conodont colour alteration has been examined within the Ordovician sediments of Ethabuka No. 1 by Nicoll (BMR, personal communication, 1979), who related the differences to temperature effects. This paper attempts to evaluate maturation levels in the GSQ Mount Whelan wells using the chemical data.

As organic maturation progresses, the EPOC value increases to a maximum, and begins to decrease as overmaturity for oil generation is reached. The HPE value will increase with maturation; McKirdy & Kantsler (1980), suggested from the work of Powell (1978), that values less than 20 per cent relate to immature sediments; 20-30 per cent, marginally mature; 30-50 per cent, mature; and 50-80 per cent overmature for oil generation.

As well as the maturation effect, migration of hydrocarbons into or out of sediments can produce marked variations in the HPE value over narrow depth ranges: the high HPE value of 77.8 per cent for the oil-stained Coolibah Formation core is likely an indication of hydrocarbons migrating into this unit. The EPOC values have been plotted stratigraphically (Fig. 4), with the oil-stained Coolibah Formation sample being obviously inconsistent with the maturation trend. The lack of organic carbon, or non-source nature of the Ordovician section, makes the analyses of these rocks particularly sensitive to minor levels of migrating hydrocarbons, which may explain the high HPE values obtained for the Nora Formation samples (Table 3).

Table 3. Source rock analytical data for core from GSQ Mount Whelan Nos. 1 and 2

Index No.	*Sample depth (m)*	*Stratigraphic unit*	*Lithology*	*TOC %*	*EOM ppm*	*SATS ppm*	*AROM ppm*	*POLAR ppm*	*EPOC %*	*HPE %*	*Source rating*
				GSQ MOUNT WHELAN No. 2							
1	201.04	Nora Fm	slt Mdst	0.12	51	10	21	18	4.25	60.8	Lean-barren
2	277.03	Nora Fm	slt Mdst	0.18	28	8	7	12	1.55	53.6	Lean-barren
3	293.71	Nora Fm	slt Mdst	0.15	31	5	14	10	2.07	61.3	Lean-barren
4	328.09	Nora Fm	slt Mdst	0.14	32	12	10	8	2.28	68.7	Lean-barren
5	398.39	Nora Fm	slt Mdst, Sst & Lst	0.09	—	—	—	—	—	—	Barren
6	397.60	Coolibah Fm	Lst Lam in slt Mdst	0.39	6650	4396	778	1450	170.5	77.8	Oil stain
7	435.38	Kelly Creek Fm	slt Mdst & Sst	0.03	—	—	—	—	—	—	Barren
8	716.37	Ninmaroo Fm	sd Mdst	0.10	—	—	—	—	—	—	Barren
9	738.66	Ninmaroo Fm	Mdst & sd Lst	0.20	65	16	22	24	3.25	58.5	Lean-barren
10	769.14	Ninmaroo Fm	slt Mdst	0.09	—	—	—	—	—	—	Barren
11	809.54	Ninmaroo Fm	sd Lst	0.21	98	16	38	41	4.67	55.1	Lean-fair
12	825.28	Ninmaroo Fm	md Lst	0.13	125	17	16	89	9.61	26.4	Lean-barren
13	851.41	Ninmaroo Fm	Lst	0.05	—	—	—	—	—	—	Barren
14	867.04	Ninmaroo Fm	md Lst	0.05	—	—	—	—	—	—	Barren
15	902.01	Ninmaroo Fm	Mct	0.16	121	43	54	23	7.56	80.2	Lean-fair
				GSQ MOUNT WHELAN No. 1							
16	47.22	Georgina Lst	Lst	0.90	888	364	141	378	9.87	56.9	Very good
17	60.66	Georgina Lst	md Lst	0.61	962	476	94	380	15.78	59.2	Very good
18	97.76	Georgina Lst	md Lst	1.02	1987	979	119	886	19.48	55.3	Very good
19	108.37	Georgina Lst	md Lst	0.33	698	234	28	432	21.15	37.5	Fair
20	117.40	Georgina Lst	md Lst, mnr Sh	0.58	1017	422	30	560	17.53	44.4	Good
21	128.18	Georgina Lst	md Lst	0.14	407	87	32	285	29.07	29.2	Fair
22	144.30	Georgina Lst	md Lst	0.96	1388	609	93	682	14.46	50.6	Very good
23	189.25	Georgina Lst	md Lst	0.75	1821	995	88	735	24.28	59.5	Very good
24	227.72	Georgina Lst	md Lst, mnr Sh	2.30	1751	1009	77	661	7.61	62.0	Good-very good
25	246.48	Georgina Lst	md Lst, mnr Sh	0.37	691	275	31	380	18.67	44.3	Good
26	254.68	Georgina Lst	md Lst	0.54	537	270	130	131	9.94	74.5	Good
27	386.66	Georgina Lst	md Lst, some Mct	0.01	—	—	—	—	—	—	Barren
28	432.66	Inca Fm correlative	calc Sh	0.41	320	150	77	90	7.80	70.9	Fair
29	448.57	Thorntonia Lst	md Lst, mnr Sh	0.77	405	275	81	45	5.26	87.9	Good
30	522.07	Unnamed Tillite	slt Mdst	0.08	—	—	—	—	—	—	Barren
31	535.76	Unnamed Tillite	pbl Sltst	0.08	—	—	—	—	—	—	Barren
32	574.83	Unnamed Tillite	slt Mdst	0.06	—	—	—	—	—	—	Barren
33	591.18	Unnamed Tillite	slt Mdst	0.08	—	—	—	—	—	—	Barren

Table 4. Source rock analytical data for samples from Netting Fence No. 1, The Brothers No. 1, and Ethabuka No. 1.

Stratigraphic unit	*Sample type*	*Depth m*	*TOC %*	*VTREF %*	*EOM ppm*	*SATD ppm*	*AROM ppm*	*POLAR ppm*	*ASPH ppm*	*Source rating*	*Reference**
					NETTING FENCE No. 1						
Carlo Sst	Cuttings	198.1	0.30							Lean	1
Carlo Sst	Cuttings	201.1	0.30							Lean	1
Carlo Sst	Cuttings	216.4	0.20							Lean-barren	1
Carlo Sst	Cuttings	228.6	0.20							Lean-barren	1
Coolibah Fm	Cuttings	441.9	0.20							Lean-barren	1
Coolibah Fm	Core	443.8	0.17		43	8	6		7	Lean-barren	2
Coolibah Fm	Cuttings	454.1	0.20							Lean-barren	1
Georgina Lst	Core	996.6	0.20							Lean-barren	1
Georgina Lst	Core	997.3	0.11		18	9	4		1	Lean-barren	2
Georgina Lst	Core	997.3	0.12							Lean-barren	3
Georgina Lst	Core	998.5	0.10		89	37	6		39	Lean-barren	2
Georgina Lst	Cuttings	1011.9	0.20							Lean-barren	1
Steamboat Sst	Core	1496.5	0.18		192				103	Lean-barren	3
Steamboat Sst	Core	1496.6	0.40							Lean-fair	1
Steamboat Sst	Core	1600.2	0.11		133				96	Lean-barren	3
Netting Fence Fm	Cuttings	1859.0	0.40							Lean-fair	1
Netting Fence Fm	Core	1882.4	0.34		902	476	162	138	126	V. good-oil stain?	3
Netting Fence Fm	Core	1882.4	0.50							Fair-good	1
Netting Fence Fm	Core	1883.7	0.40	0.50	625	256	110	152		Good	4
Netting Fence Fm	Core	1884.9	0.50	1.00	1000					Good	5
Netting Fence Fm	Cuttings	1885.4	0.60							Good	1
Netting Fence Fm	Core	1885.5	0.60							Good	1
Thorntonia Lst	Cuttings	1920.2	1.10							Good	1
Thorntonia Lst	Cuttings	1950.7	1.10							Good	1
Thorntonia Lst	Core	1954.9	1.60	1.00	1000					Good	5
Thorntonia Lst	Core	1955.0	1.80							Good	1
Thorntonia Lst	Core	1955.0	1.30		131	102	10		7	Fair	2
Thorntonia Lst	Core	1955.5	1.30							Good	1
Thorntonia Lst	Core	1955.6	1.68		582	202	105	104	170	Fair	3
Thorntonia Lst	Core	1955.9	1.05	0.52	712	361	169	117		V. good	4
Thorntonia Lst	Cuttings	1956.8	0.30							Lean-fair	1
					THE BROTHERS No. 1						
Undiff. Cambrian	Core	880.8	0.48		186				132	Fair	3
Undiff. Cambrian	Core	1049.9	0.25							Lean-barren	3
Undiff. Cambrian	Core	1051.8	2.60	0.88	200					Good	5
Undiff. Cambrian	Core	1192.1	1.00	0.76	200					Good	5
Undiff. Cambrian	Core	1194.1	0.91							Good	3
Undiff. Cambrian	Core	1194.4	0.64							Fair	3
					ETHABUKA No. 1						
Nora Fm	Cuttings	1549.9	0.09							Barren	6
Nora Fm	Cuttings	1732.8	0.16							Lean-barren	6
Coolibah Fm	Cuttings	1781.6	0.11							Lean-barren	6

*1. Buiskool Toxopeus & van Lieshout, 1979.
2. McKirdy, 1977.
3. Metter, 1977.
4. Raphael & Saxby, 1979.
5. van der Veen & Lijmbach, 1979.
6. Robertson Research (Singapore), 1978.

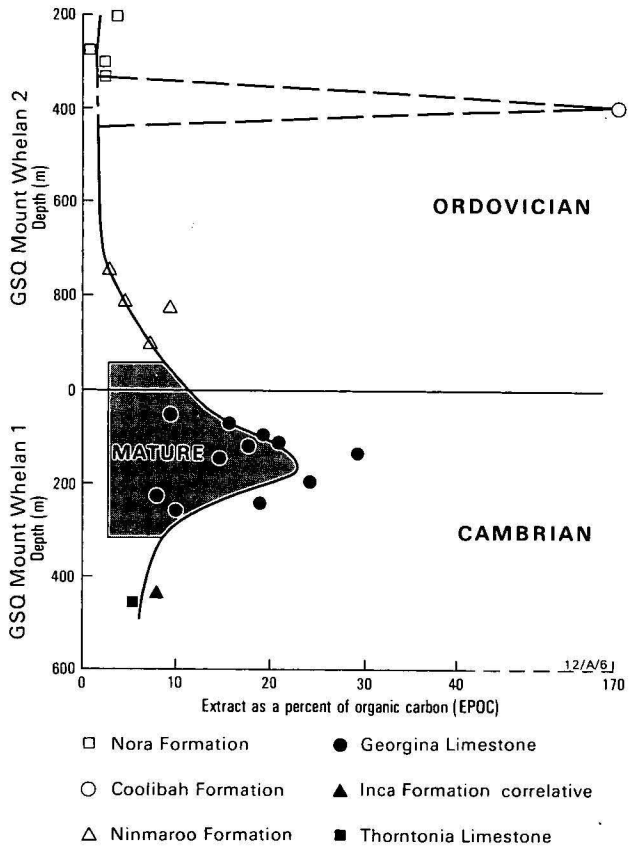

Figure 4. EPOC variation with depth in GSQ Mount Whelan Nos. 1 (solid symbols) and 2 (open symbols).

The EPOC data (Fig. 4) suggest that maturity for oil generation has certainly been achieved in the Upper Cambrian Georgina Limestone (or the Marqua beds of Gausden), with overmaturity for oil, but suitability for gas generation, likely in the Middle Cambrian Inca Formation correlative and Thorntonia Limestone. The Ordovician Ninmaroo Formation would appear to be transitional between immature and mature, with EPOC values still increasing with depth (maturation). The HPE values shown in Table 3, differ from the EPOC values in that they imply a higher level of maturity for the Ninmaroo Formation.

The pristane/n.C_{17} and phytane/n.C_{18} ratios, obtained from the capillary gas chromatograms for the SATS fraction, have been plotted in Figure 5, according to the technique of Connan & Cassou (1980). They suggest a mature Cambrian section with possible overmaturity in the Middle Cambrian. The Ordovician also appears mature, with a possible lower maturity in the Nora Formation.

In summary, maturity for oil generation has likely been reached in the Lower Ordovician Ninmaroo Formation with overmaturity likely in the Middle Cambrian sediments.

Head space gas analyses, Mirrica No. 1

Canned cuttings from Mirrica No. 1 were made available to the BMR Petroleum Technology Laboratory by Alliance Oil Development N.L. for head space gas analysis (Table 5). These have enabled an interpretation of source rock richness and maturation for the deeper, western margins of the Toko Syncline, where the main structural and stratigraphic plays are likely to be located (Harrison, 1979, 1980). Head space gas analyses from canned cuttings have been used successfully in areas such as the Western Canada Basin (Bailey & others, 1974).

The important parameters of total gas and percentage wet gas (C_2-C_4) are plotted against depth in Figure 6. The total gas contents suggest that source potential is poor for the Ordovician with only the Kelly Creek Formation rating as poor to fair. Source potential generally improves in the Cambrian, with the Marqua beds rating as fair to good source. The Georgina Limestone in Mirrica No. 1 has a lowered source potential compared to the results from the GSQ Mount Whelan No. 1 core for those samples designated Georgina Limestone by Green & Balfe (1980). However, the geochemical results appear to be consistent with Gausden's stratigraphic interpretation (Table 2).

With increasing levels of organic maturation, wet gas content increases; the onset of organic maturity for oil generation is taken at 50 per cent wet gas. As maturation approaches overmaturity, wet gas content

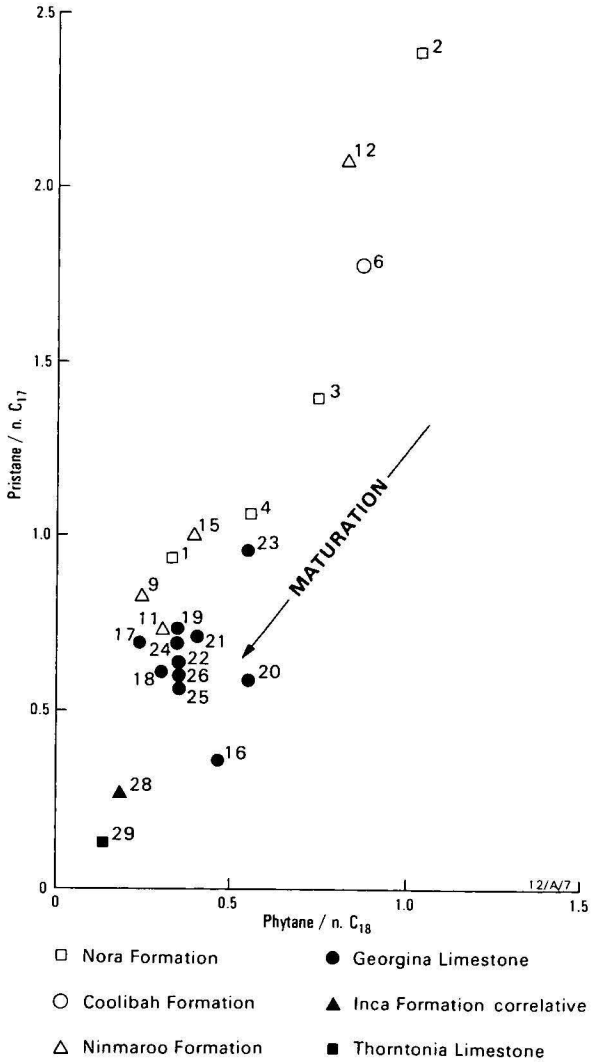

Figure 5. Pristane/n.C_{17} and phytane/n.C_{18} for core samples from GSQ Mount Whelan Nos. 1 (solid symbols) and 2 (open symbols).

Table 5. Head space gas analytical data for canned cuttings from Mirrica No. 1.

Depth m	Gas concentration (volume gas per million volumes cuttings)							Gas composition (%)					
	Methane (M) C1	Ethane (E) C2	Propane (P) C3	iButane (iB) iC4	nButane (nB) nC4	Total C1-C4	Wet/Total %	M	E	Total gas P	iB	nB	iB/nB
45.0	0.987	2.458	0.881	0.000	0.000	4.325	77.191	22.8	56.8	20.4	0.0	0.0	—
90.0	0.143	1.373	0.203	0.000	0.000	1.720	91.663	8.3	79.9	11.8	0.0	0.0	—
135.0	0.549	2.335	0.700	0.000	0.000	3.583	84.693	15.3	65.2	19.5	0.0	0.0	—
180.0	1.195	4.452	0.308	0.000	0.000	5.955	79.939	20.1	74.8	5.2	0.0	0.0	—
225.0	12.463	0.226	0.332	0.926	0.000	13.947	10.638	89.4	1.6	2.4	6.6	0.0	—
310.0	1.106	0.000	0.000	0.000	0.000	1.106	0.000	100.0	0.0	0.0	0.0	0.0	—
355.0	14.038	2.083	0.863	0.000	0.000	16.984	17.345	82.7	12.3	5.1	0.0	0.0	—
390.0	16.218	5.577	1.869	0.195	0.461	24.321	33.315	66.7	22.9	7.7	0.8	1.9	0.42
435.0	16.230	15.372	7.679	1.264	0.000	40.546	59.971	40.0	37.9	18.9	3.1	0.0	—
480.0	22.401	2.103	0.763	0.141	0.000	25.409	11.837	88.2	8.3	3.0	0.6	0.0	—
525.0	3.163	1.207	0.238	0.000	0.000	4.609	31.365	68.6	26.2	5.2	0.0	0.0	—
570.0	12.027	3.644	1.590	0.110	0.000	17.370	30.761	69.2	21.0	9.2	0.6	0.0	—
615.0	42.429	19.373	6.683	0.474	0.864	69.824	39.235	60.8	27.7	9.6	0.7	1.2	0.55
660.0	3.402	3.986	3.065	0.000	0.000	10.453	67.458	32.5	38.1	29.3	0.0	0.0	—
705.0	12.525	9.049	3.470	0.000	0.000	25.044	49.988	50.0	36.1	13.9	0.0	0.0	—
750.0	0.325	3.278	1.037	0.163	0.000	4.804	93.234	6.8	68.2	21.6	3.4	0.0	—
795.0	23.556	11.929	3.673	0.251	1.266	40.675	42.088	57.9	29.3	9.0	0.6	3.1	0.20
840.0	1.342	1.170	2.395	0.572	3.521	9.001	85.087	14.9	13.0	26.6	6.4	39.1	0.16
885.0	2.485	1.649	0.279	0.000	0.000	4.413	43.692	56.3	37.4	6.3	0.0	0.0	—
930.0	49.509	25.625	25.191	1.947	13.151	115.421	57.106	42.9	22.2	21.8	1.7	11.4	0.15
975.0	20.778	10.197	5.219	0.429	2.660	39.283	47.107	52.9	26.0	13.3	1.1	6.8	0.16
1020.0	0.103	1.934	1.451	0.065	0.000	3.554	97.096	2.9	54.4	40.8	1.8	0.0	—
1065.0	0.869	4.869	2.679	0.153	0.286	8.856	90.189	9.8	55.0	30.2	1.7	3.2	0.53
1110.0	0.211	1.695	0.645	0.000	0.000	2.552	91.733	8.3	66.4	25.3	0.0	0.0	—
1155.0	3.093	0.806	0.284	0.000	0.131	4.315	28.306	71.7	18.7	6.6	0.0	3.0	—
1200.0	0.051	0.653	0.010	0.000	0.000	0.715	92.824	7.2	91.4	1.5	0.0	0.0	—
1245.0	0.552	1.625	0.904	0.024	0.000	3.105	82.237	17.9	52.3	29.1	0.8	0.0	—
1290.0	0.145	0.178	0.420	0.000	0.000	0.743	80.539	19.5	24.0	56.5	0.0	0.0	—
1335.0	85.798	11.377	30.716	6.057	18.044	151.992	43.551	56.4	7.5	20.2	4.0	11.9	0.34
1380.0	28.673	146.422	52.827	35.004	71.384	334.309	91.423	8.6	43.8	15.8	10.5	21.4	0.49
1425.0	16.204	9.485	25.242	13.598	25.470	90.000	81.995	18.0	10.5	28.0	15.1	28.3	0.53
1470.0	15.418	8.236	22.760	12.815	27.969	87.198	82.319	17.7	9.4	26.1	14.7	32.1	0.46
1515.0	35.903	14.461	29.515	11.521	26.476	117.876	69.542	30.5	12.3	25.0	9.8	22.5	0.44
1560.0	120.493	46.772	97.867	37.098	95.267	397.498	69.687	30.3	11.8	24.6	9.3	24.0	0.39
1605.0	33.993	11.049	34.249	16.565	56.985	152.841	77.760	22.2	7.2	22.4	10.8	37.3	0.29
1650.0	19.821	4.687	16.255	3.637	13.591	57.991	65.820	34.2	8.1	28.0	6.3	23.4	0.27
1695.0	26.600	6.590	25.186	12.203	37.184	107.762	75.316	24.7	6.1	23.4	11.3	34.5	0.33
1740.0	8.569	1.764	5.597	2.289	6.282	24.500	65.026	35.0	7.2	22.8	9.3	25.6	0.36

Depth m	as concentration (volume gas per million volumes cuttings)							Gas composition (%)					
	Methane (m) C1	Ethane (E) C2	Propane (P) C3	iButane (iB) iC4	nButane (nB) nC4	Total C1-C4	Wet/Total %	M	E	Total gas P	iB	nB	iB/nB
1785.0	10.104	2.763	10.678	3.458	8.333	35.336	71.405	28.6	7.8	30.2	9.8	23.6	0.42
1830.0	71.535	24.174	37.711	6.471	18.350	158.241	54.794	45.2	15.3	23.8	4.1	11.6	0.35
1875.0	50.371	15.853	42.431	4.169	23.546	136.370	63.063	36.9	11.6	31.1	3.1	17.3	0.18
1920.0	61.109	6.035	26.716	6.867	15.701	116.429	47.514	52.5	5.2	22.9	5.9	13.5	0.44
1965.0	14.909	1.365	3.179	2.245	5.295	26.994	44.771	55.2	5.1	11.8	8.3	19.6	0.42
2010.0	63.244	21.133	53.045	8.428	14.948	160.797	60.668	39.3	13.1	33.0	5.2	9.3	0.56
2055.0	0.362	1.106	5.879	2.370	9.627	19.343	98.130	1.9	5.7	30.4	12.3	49.8	0.25
2100.0	16.612	5.264	101.580	2.378	6.993	132.827	87.494	12.5	4.0	76.5	1.8	5.3	0.34
2145.0	15.049	5.140	14.872	3.025	3.407	41.494	63.731	36.3	12.4	35.8	7.3	8.2	0.89
2190.0	3.493	1.776	4.780	1.383	1.485	12.917	72.959	27.0	13.7	37.0	10.7	11.5	0.93
2235.0	3.292	0.534	2.339	0.609	1.466	8.240	60.052	39.9	6.5	28.4	7.4	17.8	0.42
2280.0	319.316	19.641	19.055	2.860	3.777	364.050	12.432	87.6	5.4	5.2	0.8	1.0	0.78
2325.0	22.150	2.564	11.648	15.269	27.847	79.479	72.131	27.9	3.2	14.7	19.2	35.0	0.55
2370.0	34.963	2.122	5.056	4.014	10.244	56.401	38.011	62.0	3.8	9.0	7.1	18.2	0.39
2415.0	8.086	1.537	1.731	0.424	1.180	12.958	37.599	62.4	11.9	13.4	3.3	9.1	0.36
2460.0	17.881	2.484	8.856	2.885	4.968	37.074	51.770	48.2	6.7	23.9	7.8	13.4	0.58
2505.0	105.255	79.952	11.827	0.937	0.990	198.960	47.097	52.9	40.2	5.9	0.5	0.5	0.95
2550.0	73.555	60.215	10.884	0.581	0.809	146.044	49.635	50.4	41.2	7.5	0.4	0.6	0.72
2595.0	288.622	156.565	26.556	0.959	1.958	474.660	39.194	60.8	33.0	5.6	0.2	0.4	0.49
2640.0	558.627	248.768	40.985	1.587	3.061	853.227	34.504	65.5	29.2	4.8	0.2	0.4	0.52
2685.0	521.703	382.998	46.624	1.136	2.737	955.197	45.383	54.6	40.1	4.9	0.1	0.3	0.33
2730.0	568.090	224.022	24.444	1.053	1.527	819.136	30.648	69.4	27.3	3.0	0.1	0.2	0.69
2775.0	329.453	70.860	16.233	0.908	1.057	418.512	21.280	78.7	16.9	3.9	0.2	0.3	0.86
2820.0	417.588	161.905	21.420	0.840	1.141	602.894	30.736	69.3	26.9	3.6	0.1	0.2	0.74
2865.0	366.702	154.996	21.693	1.253	0.987	545.632	32.793	67.2	28.4	4.0	0.2	0.2	1.27
2910.0	440.015	69.658	14.051	1.492	1.016	526.231	16.384	83.6	13.2	2.7	0.3	0.2	1.46
2955.0	439.484	58.098	14.133	2.544	1.107	515.366	14.724	85.3	11.3	2.7	0.5	0.2	2.30
2990.0	274.742	120.516	19.793	0.886	0.668	416.605	34.052	65.9	28.9	4.8	0.2	0.2	1.33
3035.0	325.319	224.050	32.328	1.022	1.434	584.153	44.309	55.7	38.4	5.5	0.2	0.2	0.71
3080.0	305.767	276.557	31.819	1.101	1.682	616.925	50.437	49.6	44.8	5.2	0.2	0.3	0.65
3125.0	408.032	377.516	34.377	1.154	1.614	822.694	50.403	49.6	45.9	4.2	0.1	0.2	0.71
3170.0	228.584	261.405	19.042	0.402	0.717	510.150	55.193	44.8	51.2	3.7	0.1	0.1	0.56
3215.0	970.032	622.148	31.706	0.898	1.150	1625.934	40.340	59.7	38.3	2.0	0.1	0.1	0.78
3260.0	1738.385	217.200	3.818	0.000	0.000	1959.402	11.280	88.7	11.1	0.2	0.0	0.0	—
3305.0	492.326	117.020	14.605	0.000	0.000	623.951	21.095	78.9	18.8	2.3	0.0	0.0	—
3318.0	35.433	9.995	3.403	0.000	0.000	48.831	27.438	72.6	20.5	7.0	0.0	0.0	—

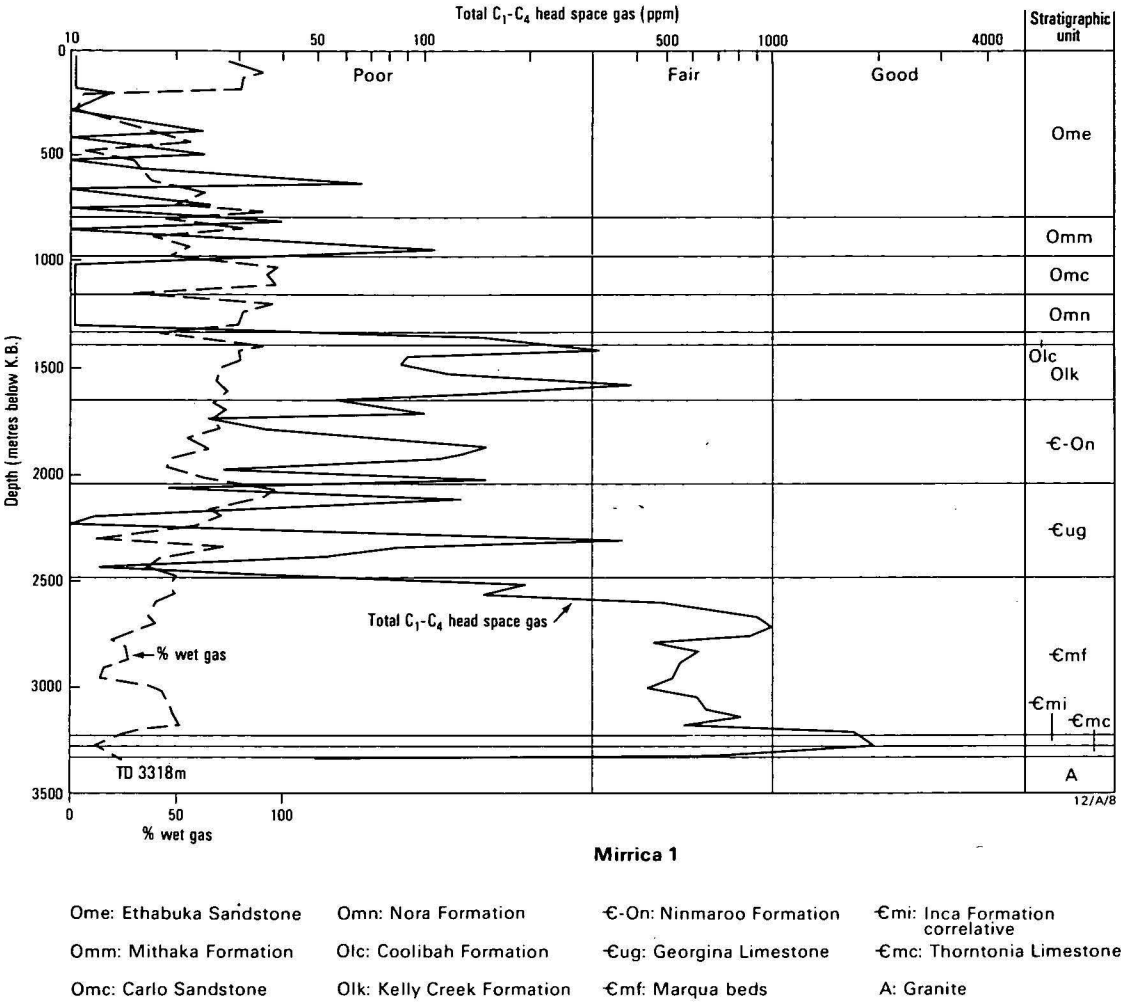

Figure 6. Plot of head space gas analytical data for canned cuttings from Mirrica No. 1.
Stratigraphic information provided by Alliance Oil Development N.L.

decreases. Based on this, maturity is generally reached at around 1000 m in the Ordovician Carlo Sandstone, with, possibly, an element of overmaturity for oil generation being observed at around 2700 m in the Middle Cambrian Marqua beds. Even at the higher maturity levels, the total gas contents imply fair to good gas source potential.

The ratio of iso- to normal-butane ($i.C_4$ to $n.C_4$) has been considered a function of organic maturation, the ratio increasing with maturity (Durand & Espitalie, 1971; Cassou & others, 1977). However, as shown by Leythaeuser & others (1979), this ratio is also very dependent on kerogen type, with the more hydrogen rich kerogens producing light hydrocarbons with a lowered $i.C_4$ to $n.C_4$ ratio. The $i.C_4$ to $n.C_4$ ratio has been calculated and is included in Table 5. It is difficult to interpret the observed variation in the ratio, but a general increase at depths of around 1600 m to 3215 m may well reflect the maturation process. However, a better guide to maturation levels is the increased abundance of iso- and normal-butane in the total gas. This occurs between 1335 m and about 2505 m, and is considered indicative of oil-mature sediments; the butane content diminishes below 2505 m, indicating overmaturity for oil generation.

Conclusions and discussion

This study has shown that:

- Source rocks exist in the Middle and Upper Cambrian, particularly the Marqua beds, at levels of organic maturation suitable for hydrocarbon generation through the geologic past up to the present time. However, at what time in the past, peak hydrocarbon generation, particularly from the Middle Cambrian, occurred is difficult to determine. It is possible that this peak may pre-date the major structural phase related to faulting, which culminated during the Alice Springs Orogeny of late Devonian to early Carboniferous time. (Harrison, 1979, 1980).

- In the wells studied, the Ordovician appears to have poor source potential.

- The oil stain seen in the Coolibah Formation of the GSQ Mount Whelan No. 2 well represents migration from underlying Cambrian source rocks.

- These conclusions support those of Kantsler (1980), who in an organic microscopy study of kerogen extracts from cuttings of the Ordovician section in Ethabuka No. 1, failed to identify a source rock, but recognised

'live' hydrocarbons and a widespread occurence of a variety of asphaltic bitumens, leading him to conclude that hydrocarbon generation and migration have taken place, probably from the Cambrian.

• The source rock richness for the Cambrian of the Toko Syncline compares well with that reported for the Cambrian of the Officer Basin in South Australia (McKirdy & Kantsler, 1980), both sequences giving high TOC and EOM values. Oil shows were encountered in the Cambrian Observatory Hill beds in SADME Byilkaoora No. 1 in the Officer Basin. McKirdy & Kantsler (1980) described these as immature oils with varying degrees of biodegradation, and thought they were probably generated from source beds in the playa lake evaporitic sequence which forms their reservoir. Organic maturity levels in the Toko Syncline are more advanced than in the Officer Basin, as seen by McKirdy & Kantsler, but the apparent generation of oil from carbonates of similar chemical characteristics in the Officer Basin is encouraging for the prospects of hydrocarbon generation in the Toko Syncline.

Acknowledgements

The analytical work on the core material from the Mount Whelan wells and the head space gas analyses were performed by Z. Horvath, BMR Petroleum Technology Laboratory. The support and cooperation of geologists at BMR involved in the Georgina Basin study are gratefully acknowledged. The Geological Survey of Queensland gave permission and much assistance for sampling of core from the Mount Whelan wells. Alliance Oil Development N.L. assisted this study by providing canned cuttings from the Mirrica No. 1 well, and by supplying stratigraphic information for this well. Editorial assistance was provided by Mrs E. Nicholas, Dr D. Forman and Dr J. Shergold.

References

BAILEY, N. J. L., EVANS, C. R., & MILNER, C. W. D., 1974—Applying petroleum geochemistry to search for oil: Examples from Western Canada Basin. *American Association of Petroleum Geologists, Bulletin*, 58, 2284-94.

BUISKOOL TOXOPEUS, J. M. A., & VAN LIESHOUT, J. B., 1979—Source rock evaluation and maceral description of some samples in well Netting Fence -1, Australia. Technical service report, RKTR 0092.79, to Shell Australia. *Bureau of Mineral Resources, Australia, Source Rock Report* R343 (unpublished).

CASSOU, A. M., CONNAN, J., & PORTHAULT, B., 1977—Relations between maturation of organic matter and geothermal effect, as exemplified in Canadian east coast offshore wells. *Bulletin of Canadian Petroleum Geology*, 25, 174-94.

CONNAN, J., & CASSOU, A. M., 1980—Properties of gases and petroleum liquids derived from terrestrial kerogen at various maturation levels. *Geochimica et Cosmochimica Acta*, 44, 1-23.

DURAND, B., & ESPITALIE, J., 1971—Formation et évolution des hydrocarbures de C_1 à C_{15} et des gaz permanents dans les argiles du Toarcien du bassin de Paris. *Advances in Organic Geochemistry*, 455-65.

GREEN, P. M., & BALFE, P. E., 1980—Stratigraphic report—GSQ Mt Whelan 1 and 2. *Queensland Government Mining Journal*, 81, 162-78.

HARRISON, P. L., 1979—Recent seismic studies upgrade the petroleum prospects of the Toko Syncline, Georgina Basin. *The APEA Journal*, 19(1), 30-42.

HARRISON, P. L., 1980—The Toomba Fault and the western margin of the Toko Syncline, Georgina Basin, Queensland and Northern Territory. *BMR Journal of Australian Geology & Geophysics*, 5, 201-14.

HUNT, J. M., 1979—Petroleum geochemistry and geology. *W. H. Freeman, San Francisco.*

KANTSLER, A. J., 1980—AOD Ethabuka No. 1, notes and comments on the organic petrology of kerogen extracts and cuttings samples. *Open file report to the Bureau of Mineral Resources, Geology and Geophysics* (unpublished).

KENNARD, J. M., 1981—The Arrinthrunga Formation: Upper Cambrian epeiric carbonates in the Georgina Basin, central Australia. *Bureau of Mineral Resources, Australia, Bulletin* 221.

LEYTHAEUSER, D., SCHAEFER, R. G., CORNFORD, C., & WEINER, B., 1979—Generation and migration of light hydrocarbons (C_2-C_7) in sedimentary basins. *Organic Geochemistry*, 1, 191-204.

MCKIRDY, D. M., 1977—The diagenesis of microbial organic matter: a geochemical classification and its use in evaluating the hydrocarbon generating potential of Proterozoic and Lower Palaeozoic sediments, Amadeus Basin, central Australia. *Ph.D Thesis, Australian National University, Canberra,* (unpublished).

MCKIRDY, D. M., & KANTSLER, A. J., 1980—Oil geochemistry and potential source rocks of the Officer Basin, South Australia. *The APEA Journal*, 20, 68-86.

METTER, R. E., 1977—Source rock analyses: Galilee Basin and Toko Syncline, Australia. Report to Esso Australia Ltd. *Bureau of Mineral Resources, Australia, Source Rock Report* R242 (unpublished).

MULREADY, J., 1975—AOD Ethabuka No. 1 well completion report. *Bureau of Mineral Resources, Australia, Petroleum Search Subsidy Acts File* 73/224 (unpublished).

PAP (Papuan Apinaipi Petroleum Co. Ltd.), 1965—Netting Fence No. 1 well completion report. *Bureau of Mineral Resources, Australia, Petroleum Search Subsidy Acts File* 64/4068 (unpublished).

PONTIGO, F. A., Jnr, APPLEGATE, A. V., ROOKE, J. H., & BROWN, S. N., 1979—South Florida's Sunniland oil potential. *Oil and Gas Journal*, 77(31), 226-32.

POWELL, T. G., 1978—An assessment of the hydrocarbon source rock potential of the Canadian Arctic Islands. *Geological Survey of Canada, Paper* 78-12.

RAPHAEL, N. M., & SAXBY, J. D., 1979—Source rock analyses on samples from the Otway, Sydney, Bowen, Surat, Bass, Gippsland, Georgina and Ngalia Basins—report to the Bureau of Mineral Resources. *CSIRO Restricted Investigation* 1030R (unpublished).

ROBERTSON RESEARCH (SINGAPORE), 1978—Organic carbon analysis of cuttings samples from Ethabuka -1—memorandum to Alliance Oil Development Australia N.L. *Bureau of Mineral Resources, Australia, Source Rock Report* R289 (unpublished).

SHERGOLD, J. H., & DRUCE, E. C., 1980—Upper Proterozoic and Lower Palaeozoic rocks of the Georgina Basin. *In* HENDERSON, R. A. & STEPHENSON, P. J. (editors), The geology and geophysics of northeastern Australia. *Geological Society of Australia Inc., Queensland Division*, 149-74.

SMITH, K. G., 1972—Stratigraphy of the Georgina Basin. *Bureau of Mineral Resources, Australia, Bulletin* 111.

TRACER'S EXOGRAM AND OIL AND GAS REVIEW, 1980a, volume 26, number 13, p. 11.

TRACER'S EXOGRAM AND OIL AND GAS REVIEW, 1980b, volume 26, number 15, p. 11.

VAN DER VEEN, F. M., & LIJMBACH, G. W. M., 1979—Geochemical analysis of rock extracts from Netting Fence No. 1 and The Brothers No. 1, Georgina Basin, Queensland. Technical service report, RKER 79.004 to Shell Australia. *Bureau of Mineral Resources, Australia, Source Rock Report* R355 (unpublished).

BMR Journal of Australian Geology & Geophysics, 7, 11-21.

AN APPRAISAL OF AUSTRALIAN HEAT-FLOW DATA

J. P. Cull

Estimates of heat flow in Australia have been compiled in standard format rating the principal facts of each determination. Quality is assessed using a code that contains a summary of the sources of error. Estimates of precision vary according to the techniques used both in recording and processing of relevant geothermal data, but less obvious systematic errors are generated by changes in equipment design, core sampling rates, and local site conditions. Each factor must be considered when heat-flow values from different sources are being compared. The rating system has been tested for consistency, and a calibration provided that will allow the subjective quality factors to be used for numerical estimates of error. Heat-flow estimates were considered in two groups according to quality. Errors of 10 per cent (one standard deviation) were calculated for the group with better quality, but other estimates may contain errors of 20 per cent. New determinations of heat flow are presented according to the adopted format, and other data related to geothermal studies have been included to complement the existing data bank.

Introduction

Compilations of surface heat-flow values have been used to establish major constraints in models of crustal evolution and global tectonism. Steady state models of mantle convection are consistent with oceanic heat-flow patterns (Turcotte & Oxburgh, 1969), but more complicated models involving episodic evolution are required for continental patterns.

Most heat is generated within the Earth by the decay of radioactive trace elements contained in crustal rocks (Roy & others, 1968). Consequently, it is expected that correlations will exist between surface heat flow and factors such as the age, thickness, and type of crustal material present. In addition, thermal transients may be associated with the formation of major structural features, including fold mountains, rift valleys, and zones of active volcanism (Lachenbruch & Sass, 1977).

Other anomalies in heat flow indicate geothermal energy prospects, fault systems, dome structures, coalfield boundaries, and mineral deposits undergoing exothermic reactions (Poley & Van Steveninck, 1970; Krcmar & Masin, 1969). Values of greater precision may be used to investigate the thermal history of sedimentary basins for studies of the maturation of hydrocarbons, for stratigraphic correlations and bulk assays (Burne & Kantsler, 1977; Facer & others, 1980; Beck, 1976). Estimates of error are required for heat-flow values before valid models can be formulated to resolve fine detail in each application.

Geothermal data in Australia have been obtained over many years, using a variety of instruments subject to different types of error (Beck, 1965). Furthermore, the original reduction techniques have been modified progressively, and numerous corrections have been suggested according to local environments (e.g. Hyndman & Sass, 1966). Consequently, the accuracy of each heat-flow determination cannot be readily specified from the quoted statistics of data reduction. Individual factors that contribute to the total error (quality factors) must be assessed before it is possible to compare values from areas of different geological and physical environments without bias from poor determinations.

The primary aim of this work, therefore, is to present the available Australian heat-flow values together with some new determinations (Appendix 1) in a standard format detailing the principal facts relevant to estimates of error. Subjective weights are assigned, and data can be extracted according to individual applications requiring different levels of precision.

Sources of data

In Australia the first estimates of heat flow were published by Newstead & Beck (1953). Since then, several workers at the Australian National University (ANU) have published data, and, by 1977, heat-flow values had been determined for 90 well-distributed sites. Compilations were published by Sass & others (1976) and Lilley & others (1978), and regional trends were considered by Cull & Denham (1979).

Marine data have not been accumulated on a routine basis, and values used in previous publications were extracted from Sclater & others (1972), Erikson & others (1975), MacDonald & others (1973), Jongsma (1976), and Anderson & others (1977). Most of these marine data are listed by Jessop & others (1976) in their world review; they have been included here to allow the extrapolation of contours offshore (Figs. 1, 2), but different criteria are required to assess their quality.

Each of the above compilations contains references to the many original reports detailing the individual determinations of heat flow. The style of presentation varies considerably and the principal facts are not always obvious. Hence, it is difficult to assess the quality and reliability of the determination. However, the concepts of Jessop & others (1976) can be adopted with some modifications.

For the purposes of this paper, all data relating to estimates of heat flow have been extracted from the original publications. Individual references are documented in Table 1 in chronological order, and are numbered sequentially. This reference number then constitutes part of an identifying code for individual values of heat flow.

Calculations of heat flow

Heat flow, Q(mW m^{-2}) is computed from the expression: $Q = \lambda\beta$; where β (mK m^{-1}) is the geothermal gradient, and λ(W m^{-1} K^{-1}) is the thermal conductivity of the rock in which the gradient is measured. On land, temperatures are usually measured in boreholes at depths greater than 100 m (and preferably 300 m) to avoid seasonal climatic perturbations.

Figure 1. Heat flow in Australia.
Contours are derived from a 1° grid of values rated better than 333.

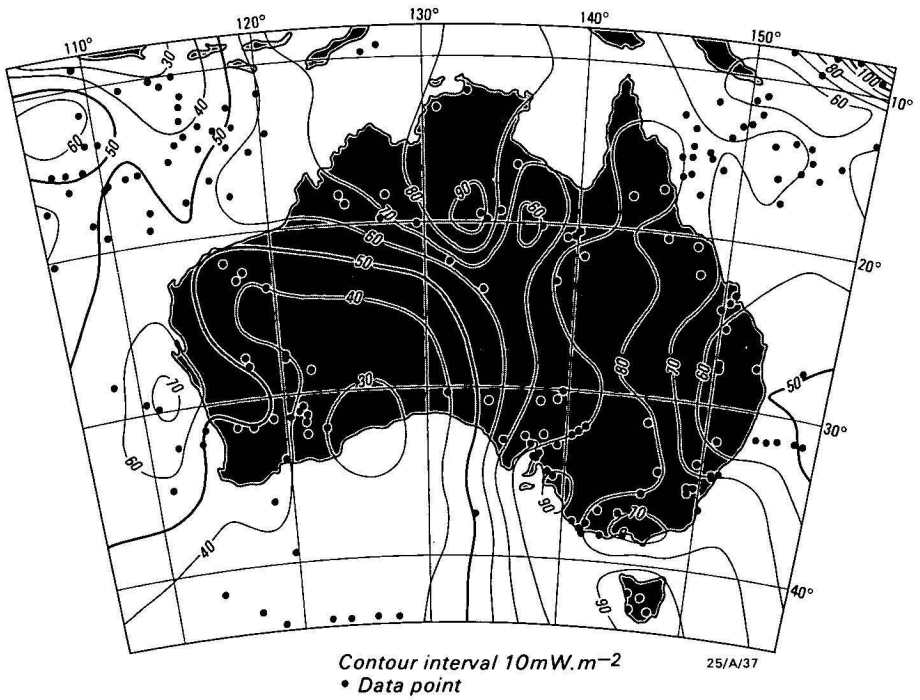

Figure 2. Heat flow in Australia.
Contours derived from a 3° grid.

Anomalous temperature gradients can be expected to persist to greater depth in regions of Quaternary glaciation (Cull, 1979). However, values of heat flow reported for Tasmania and the Snowy Mountains are consistently above the world average (60 mW m^{-2}). No routine corrections have been applied for climatic changes in Australia and, consequently, present data represent minimum values. Independent isolated attempts to include climatic corrections would result in significant positive anomalies unrelated to surface geology—particularly in the southeast of Australia, where surface temperatures may have increased by 10°C following glacier retreat about 15 000 years B.P. (Bowler & others, 1976). To resolve uncertainties in the data for this region, observations are required in boreholes at depths greater than 1000 m (Cull, 1979).

Although failure to correct for climatic perturbation may result in major systematic errors, many geological problems can be solved using relative values of heat flow (Cull, 1981). However, more serious deficiencies appear in some estimates of heat flow contained in early

reports. Complex corrections are required where temperatures have been measured in tunnels, mines, flowing bores, or cased and uncased holes of different depths. Many of these corrections remain contentious, and new procedures must be adopted to ensure a consistent data set.

In Australia, thermal conductivities have been measured almost exclusively with variants of the divided bar apparatus (Beck, 1965). Comparable values have been obtained for identical samples processed at ANU, BMR, and Oxford University (Cull, Lilley, & Sloane, personal communications). In general, core samples were extracted from each borehole in which temperatures were measured. However, errors are introduced where lithology is highly variable, through poor sampling, anisotropy, and refraction. Where no continuous core has been available, representative spot core samples have been selected or cuttings have been used with cell techniques, giving less accurate determinations.

In most instances, heat flow was calculated by combining average conductivities with a linear least-squares thermal gradient over the full length of the hole. Occasionally, several linear segments of gradient were identified and heat flow was calculated for each. More recently in BMR, individual determinations of thermal conductivity have been combined with geothermal gradients calculated for appropriate 10-m intervals to give heat flow as a function of depth. Bullard-type reductions (Bullard, 1939) have been used only rarely.

Local perturbations

In addition to errors inherent in the reduction technique, other non-representative values of heat flow may be related to local features of near-surface geology. Low values are observed on the recharge margins of the Great Artesian Basin, and regional values may need correction for this effect to obtain the mean heat flow below the basin margin. A corresponding discharge zone of high heat flow is apparent north of Spencer Gulf. Hot springs in the area (e.g. Paralana) are probably associated with outflow from the Great Artesian Basin, but small-scale recent tectonism may also cause thermal anomalies.

High values of heat flow are also observed in regions of recent volcanism in Queensland and western Victoria; these values are higher than those predicted from heat flow/age relations derived elsewhere. Other anomalies may be caused by mining-grade concentrations of radioactive materials in the crust—e.g. near Tennant Creek (20°S, 134°E), or by exothermic reactions associated with mineral hydration/oxidation or related to hydrocarbon maturation.

In some instances, corrections may be required where local topographic features exceed a few tens of metres, or where there are extensive bodies of surface water close by. In addition, there may be some need to consider correction for sedimentary deposition or for uplift and erosion.

Compilation format

Because of the large disparity in the quality of borehole observations, and the many techniques used for data reduction, it is essential to establish criteria for any comparison. Major points to be considered have been discussed above. No attempt has been made to derive individual estimates of error, but ratings have been assigned to each of the major factors contributing to reliability. The system chosen here adheres closely to the recommendations of Jessop & others (1976), but there are some modifications. A data-file format appears in Table 2.

Identification

Each value is assigned a unique number containing year of determination, literature reference number (Table 1), and sequential file number, which is combined with a location name for easy reference. However, site coordinates are also quoted for greater precision. At locations such as Mount Isa, Tennant Creek, and Kalgoorlie, where multiple determinations have been made, a best value (usually a simple average) has been adopted for a mean location. Data are available for 109 locations on land, and at sea there are 241 determinations in the region 90-170°E, 0-45°S. However, there are still large gaps in the data bank, notably on land, in the desert region of Western Australia, on Cape York Peninsula, and in southern Queensland.

Elevation is seldom important, but it completes the specification of position and may indicate some need for topographic corrections. The elevation of the solid surface at the measuring point provides a datum for isothermal maps that can be related to geological structure. Depth of measurement is also included as a prime indication of data quality.

A best value for heat flow constitutes the next item in each entry to the file; a number of determinations are grouped where appropriate. Usually, the value adopted is the same as that suggested in the original reference. However, in some cases a number of alternatives are given and a subjective factor is introduced to select a 'best' value. Data are quoted to the nearest 1.0 mW m^{-2}, representing an uncertainty of about one per cent, but total error is highly variable, and the following descriptive codes are included to indicate the quality of each determination.

Major factors

The descriptive codes detailed in Table 3 are an attempt to condense the words written by the authors about their measurements. There are often several pages of information condensed into single item indicators and many details may not be fully considered. The primary factors relate to thermal gradient, thermal conductivity, and borehole condition.

(a) thermal gradients. In general, temperatures are well determined, usually with thermistor probes. Errors in the geothermal gradient are, therefore, related to the depth of determination and the interval of interpolation. Perturbations caused by changes in climate or refraction effects associated with surface features usually decrease with depth. Consequently, measurements at great depth (>500 m) are assigned maximum weight (5), and intervals closer to the surface have lower weights. Where an average gradient is quoted

Table 1. Principal Sources of data.

01 Newstead & Beck, 1953—*Australian Journal of Physics*, 6, 480-9.
02 Beck, 1956—Ph.D. Thesis, *Australian National University, Canberra* (unpublished).
03 Jaeger, 1961—*Journal of Geophysical Research*, 66, 563-9.
04 Le Marne & Sass, 1962—*Journal of Geophysical Research*, 67, 3981-3.
05 Jaeger & Sass, 1963—*Geofisica Pura e Applicata*, 54, 55-63.
06 Sass & Le Marne, 1963—*Geophysical Journal of the Royal Astronomical Society*, 7, 477-89.
07 Howard, 1963—Ph.D. Thesis, *Australian National University, Canberra* (unpublished).
08 Howard & Sass, 1964—*Journal of Geophysical Research*, 69, 1617-26.
09 Sass, 1964—*Journal of Geophysical Research*, 69, 229-308.
10 Sass, 1964—*Journal of Geophysical Research*, 69, 2889-93.
11 Sass, 1965—Ph.D. Thesis, *Australian National University, Canberra* (unpublished).
12 Hyndman & Sass, 1966—*Journal of Geophysical Research*, 71, 587-601.
13 Hyndman, 1967—*Journal of Geophysical Research*, 72, 527-539.
14 Sass, Clark, & Jaeger, 1967—*Journal of Geophysical Research*, 72, 2635-47.
15 Hyndman, 1967—Ph.D. Thesis, *Australian National University, Canberra* (unpublished).
16 Hyndman & Everett, 1968—*Geophysical Journal of the Royal Astronomical Society*, 14, 479-86.
17 Hyndman, Lambert, Heier, Jaeger, & Ringwood, 1968—*Physics of the Earth and Planetary Interiors*, 1, 129-35.
18 Hyndman, Jaeger, & Sass, 1968—*Earth and Planetary Science Letters*, 7, 12-16.
19 Jaeger, 1970—*Earth and Planetary Science Letters*, 8, 285-92.
20 Bunker, Bush, Munroe & Sass, 1975—*United States Geological Survey, Open File Report*, 75-393.
21 Munroe, Sass, Milburn, Jaeger, & Tammemagi, 1975—*United States Geological Survey Open File Report*, 75-567.
22 Wirubov, 1975—B.Sc. Thesis, *University of Melbourne* (unpublished).
23 Taplin, 1976—B.A. (Honours) Thesis, *Macquarie University, Sydney* (unpublished).
24 Sass, Jaeger, & Munroe, 1976—*United States Geological Survey Open File Report*, 76-250.
25 Wronski, 1977—*Geophysical Journal of the Royal Astronomical Society*, 48, 131-3.
26 Cull, 1978—*Bureau of Mineral Resources, Australia, Record*, 1978/66 (unpublished).
27 Lilley, Sloane, & Sass, 1978—*Journal of the Geological Society of Australia*, 24, 439-45.
28 Cull & Denham, 1979—*BMR Journal of Australian Geology & Geophysics*, 4, 1-13.
29 Cull, 1979—*BMR Journal of Australian Geology & Geophysics*, 4, 303-7.
30 Cull, 1979—*Search*, 10, 429-33.
31 Cull, 1980—*Search*, 11, 201-3.
32 Facer, Hutton, & Frost, 1980—*Proceedings of the Linnaean Society of New South Wales*, 104, 95-109.

Table 3. Descriptive codes characterising measurement techniques.

(A) Geothermal gradient (mK m^{-1}): column 46

Indicator	*Depth of determination*
1	indirect
2	0-100 m
3	100-300
4	300-500
5	> 500 m

(B) Thermal conductivity (W m^{-1} K^{-1}): column 47

Indicator	*Technique*
1	estimated
2	external samples
3	cuttings in cell or transient reduction
4	divided bar/partial core
5	divided bar/full core

(C) Hole condition: column 48

Additive indicator	*Condition*
+1	long standing (> 6 mths)
+1	fluid fill
+1	stable groundwater
+1	minimal topography
+1	uniform stratigraphy
Sum for final indicator	

for extended intervals (sometimes using all data, including the surface temperature), the depth of determination is assumed to be mid-range. Weights are reduced by one for detrimental features such as groundwater migration or thermal refraction.

(b) thermal conductivity. Thermal conductivities are normally well determined using variations of the divided bar apparatus, with core samples for each borehole in which gradients have been determined. Standard designs have evolved for divided bar apparatus, and the precision of the results can be readily verified (Beck, 1965). In addition, the use of steady-state conditions allows high resolutions with total error less than 5 per cent. Consequently, a maximum weight of 5 is assigned where conductivity data are available at close intervals in uniform core. Weights are reduced for any other determination. For example, transient techniques are usually considered to be less accurate than the divided bar, with errors of ± 10% caused by uncertain boundary conditions (Scott & others, 1973). Cell techniques can be used where drill cuttings are the only

Table 2. Heat-flow data-file format.

Item	*Description*	*Units*	*Characters*	*Card columns*
1	Data number:			
	(a) reference number		2 digits	1-2
	(b) year of determination		2 digits	4-5
	(c) chronological sequence		3 digits	7-9
2	Name of site		12 characters	11-22
3	Latitude (S)	Deg.	2 digits & 2 decimal	25-29
4	Longitude (E)	Deg.	3 digits & 2 decimal	31-36
5	Elevation of collar	m	4 digits	38-41
6	Measurement depth	m	4 digits	42-45
7	Heat flow (Q)	mW m^{-2}	3 digits	48-50
8	Quality codes (Table 3):			
	(a) gradient		3 digits	54-56
	(b) conductivity			
	(c) condition			
9	Precision estimate		2 digits	58-59
10	Auxiliary codes (Table 4):			
	(a) geology (G)		1 digit	61
	(b) tectonics (T)		1 digit	62
	(c) heat production (A)	μW m^{-3}	1 digit & 1 decimal	64-66
	(d) no. of determinations (N)		2 digits	68-69
11	Other references (Table 1)		3 × 2 digits	75-80

Table 4. Auxiliary codes for local environment.

1	Archaean
2	Proterozoic
3	Phanerozoic non-orogenic
4	Early Paleozoic
5	Late Paleozoic
6	Mesozoic
7	Cainozoic orogeny or volcanic zone
8	Geothermal area/aquifer perturbation
9	Exothermic mineral deposit

samples available, but physical models must then be formulated for data reduction (Sass & others, 1971). Mathematical formulae have been derived consistent with experimental correlations to relate chip results to whole core data, but the accuracy of the results remains contentious. Data considered even less reliable are those obtained by any method using 'representative' core samples extracted from other boreholes or estimated from the known stratigraphy.

(c) borehole conditions. The remaining primary factor in assessing quality relates to borehole condition and physical environment. To some extent, this factor is a qualification of the preceding assessments of thermal gradient and thermal conductivity. A maximum value of 5 can be assigned. The attributes necessary for the highest rating include a long equilibration period ($>$ 6 months), the existence of a fluid medium, long-term stability (no flow), flat topography, and uniform stratigraphy. These conditions allow for well-determined thermal gradients with minimum sampling error for thermal conductivity. Rating of this factor is reduced by one for the absence of each attribute.

The quality of each heat flow value can be readily assessed in terms of the preceding primary factors of determination. Estimates of highest quality are rated 5, 5, 5, for the three separate criteria. However, some estimates of lower quality may be used, according to individual needs for accuracy in correlation, structural analysis, regional control, exploration etc. Values rated less than 333 must be used with caution, in spite of the quoted estimates of precision, which are based on internal statistics of data reduction. However, such estimates may indicate broad support for any assigned quality factors.

Auxiliary codes

Anomalies in heat flow may be attributed to several conflicting factors in the geological environment; corrections may be required for lateral changes in chemical components, differentiation, age, erosion, subsidence, etc. The codes noted in Table 4 are intended to provide sufficient information for selecting representative data for each environment. The primary item is intended to denote geological age; this is followed by a code indicating the last thermo-tectonic disturbance that may have affected the site. Such qualifications may be required for modelling thermal transients, which are not necessarily related to the age of the present surface rocks. Many authors have not included this information, and codes assigned have been based on current tectonic maps. Tectonic history in some areas is still subject to argument, and some entries in this core are correspondingly tentative.

Values of heat production (μW m^{-3}) are rarely available using core extracted from the relevant borehole, but special studies have been conducted, generally by regional surface sampling (Sass & others, 1976). Figures quoted from such a source are indicated by '0' in the number of determinations and a reference is given in the following item. Lateral extrapolation of such estimates can be justified from airborne radiometric surveys, which indicate count-rate spectra for U-K-Th, but there has been no attempt at calibration. Where a value was chosen by the original author as characteristic, this figure is quoted with an indication of the number of samples examined. In some locations there is no reasonable estimate, and this item remains blank.

The final item for each entry provides a listing of references. Where there are numerous determinations at one location, some reports may be superseded, but cross references may be used for estimates of precision. Other related work, such as the determination of heat production or estimates of age, may also be included as a complement to the primary publication.

Presentation of data

All heat-flow values obtained in Australia are noted in Table 5 according to the adopted format. A visual presentation of these values may result in the identification of regional trends. However, as the number of measurements continues to increase, the individual notations adopted by Sass & others (1976) and Lilley & others (1978) become more difficult to interpret. In general, maps are more readily assessed with contours, which reveal regional trends, causing partial suppression of anomalous data.

The computer techniques developed by Murray (1977) were used to produce the contour maps in Figures 1 & 2. Equal weights were first assigned to all data with a grid spacing of one degree in an attempt to preserve the integrity of individual determinations. There is no obvious discontinuity between marine and land values, and contours are generally smooth. Local variations are evident only in the Northern Territory and in the southeast highlands.

The contour map in Figure 2 was produced using a 3° grid together with the better quality measurements ($>$ 333). Marine data were accepted on face value and all were assigned the same weight as land-based data. The previously noted local anomalies are significantly reduced in number, but the general character of the contour map is unchanged.

Although some dubious values can be identified from a comparison of regional and local contours, the criteria for estimates of error remain subjective. Random errors related to data-reduction techniques can be specified from the statistics of each determination, but the principal source of error relates to conditions described in the assigned quality factors. In general, these result in systematic error rather than random error, and are not reflected in published estimates of precision. To calculate absolute accuracy in determinations of heat flow it is necessary to introduce external controls. In effect, a calibration is required to assess the assigned quality ratings in terms of error.

To demonstrate the validity of the quality factors, it is necessary to adopt statistical approximations. A 'true'

Table 5. Australian heat-flow data file (see Table 2 for details of file items).

Heat-flow data-file item													
1		2	3	4	5	6	7	8	9	10			11
Ref.	Yr.	No. Name	Lat.	Long.	Elev.	Depth	Q	Qual	P	GT	A	N	Lit.
1	53	1 G LAKE/DEE	41.97	146.60	1000	318	83	354	5	67			
1	53	2 ROSEBERRY	41.77	145.57	197	272	104	352	6	57			
4	62	3 COBAR	31.43	145.80	830	260	83	444	13	5			24
5	63	4 STOREY CK	41.67	147.75	830	182	159	213	2	57			
6	63	5 BROKEN HIL	31.95	141.47	3001028		80	534	1	2	4.6	56	08
8	64	6 TENNANT CK	19.67	134.22	328	250	89	444	8	2	3.9	7	2408
8	64	7 COOLGARDIE	30.95	121.17	420	250	33	334	3	1			09
8	64	8 KALGOORLIE	30.68	121.43	3801000		34	534	2	1			1609
8	64	9 NORSEMAN	32.33	121.62	300	350	37	434	4	1			09
8	64	10 RAVENSTHORPE	33.67	120.00	180	300	39	444	2	1			
8	64	11 MT MAGNET	28.00	118.00	460	470	54	333	8	1	6.8	7	24
8	64	12 CUE	27.45	117.87	450	400	39	334	1	1			
8	64	13 BULLFINCH	31.23	119.32	360	600	50	333	8	1			
8	64	14 RUM JUNGLE	13.00	131.00	60	500	84	433	7	29	6.3	33	24
8	64	15 RADIUM HILL	32.50	140.50	300	300	75	344	4	29	3.8	4	24
10	64	16 MOONIE	27.73	150.22	3002200		41	323	1	63			
10	64	17 CABAWIN	27.50	150.20	3003000		50	333	1	63			
10	64	18 KANMANTOO	35.08	139.25	150	250	88	333	3	47			
10	64	19 WHYALLA	33.17	137.50	60	185	91	343	2	27	8.4	2	
10	64	20 STAWELL	37.05	142.78	250	300	119	344	12	47	3.1	1	
10	64	21 CASTLEMAINE	37.05	144.22	280	165	121	233	11	47	3.4	1	
10	64	22 STROMLO	35.28	149.00	560	225	86	443	1	47	2.7	14	
12	66	23 BLOCKADE	20.58	140.00	360	350	74	344	4	2	3.1	2	
12	66	24 MT ISA	20.74	139.45	350	750	82	554	4	2	3.9	8	322408
13	67	25 A SPRINGS	23.92	133.97	600	700	62	434	2	43			
13	67	26 MCARTHUR	16.47	136.05	150	440	70	433	1	23			
13	67	27 FREWEENA	19.27	135.10	240	311	75	123	11	48			
13	67	28 BARALBA	24.15	149.85	180	382	57	243	1	53			
13	67	29 COLLINSVILLE	20.57	147.82	180	364	53	243	1	53			
13	67	30 CRACOW	25.28	150.28	300	265	56	344	3	58			
13	67	31 MT MORGAN	23.70	150.40	270	150	34	244	1	58			
13	67	32 CATTLE CK	20.02	137.83	300	238	48	332	2	43			
13	67	33 IPSWICH	27.42	152.75	180	282	63	243	4	68			
14	67	34 SNOWY MTS	36.40	148.30	1000	850	84	242	8	47	2.6	99	2408
18	69	35 NAROOMA	36.25	150.10	5	300	54	343	2	47	1.5	3	32
18	69	36 DROMEDARY 1	36.30	150.10	2	200	47	132	1	48	1.1	3	24
18	69	37 DROMEDARY 2	36.30	150.10	100	220	43	343	1	47	1.1	3	24
19	70	38 DOODLAKINE	31.63	117.82	300	300	54	454	1	1	8.9	36	24
19	70	39 FRASER RNG	32.00	122.95	300	300	29	454	1	1	0.5	60	24
19	70	40 NORTHAM	31.57	116.67	300	300	36	454	1	1	2.1	84	24
19	70	41 WOOLGANGIE	31.25	120.50	300	300	41	454	1	1	3.2	54	24
24	76	42 APSLEY	33.57	149.57	884	137	63	153	1	47	2.5	3	32
24	76	43 CPT FLAT	35.60	149.45	914	263	101	444	4	47	2.2	5	
24	76	44 MORUYA	35.90	150.12	7	168	54	244	1	47	1.5	12	32
24	76	45 SCONE	32.08	150.82	208	366	50	354	1	67	2.0	0	32
24	76	46 LODDON	34.23	150.77	707	365	88	333	2	67	2.9	0	32
24	76	47 NEBO	34.42	150.75	52	287	80	333	4	67	2.9	0	32
24	76	48 WALLANDOOL	34.32	150.73	309	374	88	333	5	67	2.9	0	32
24	76	49 CAPE BANKS	34.00	151.25	5	427	71	433	1	67	2.9	0	32
24	76	50 TARAGO	35.07	149.57	790	285	80	354	4	57	1.9	0	32
24	76	51 WARREGO	19.45	133.82	330	650	113	554	5	2			
24	76	52 BATCHELOR	13.03	131.08	150	242	80	344	4	29			
24	76	53 BENDIGO ST	33.20	139.47	229	310	64	344	1	47	3.8	12	
24	76	54 CARRIETON	32.55	138.48	520	376	92	343	4	27			
24	76	55 BUTE	33.87	138.02	116	218	88	243	2	27			

value is required so that the magnitude of systematic error can be detected for each quality group. It is assumed for this purpose that the sources of systematic error (i.e. the quality factors) are random in relation to geographical location. Reliable estimates for heat flow (a group mean) can then be generated for regions of similar geology, according to the Central Limit Theorem; the published estimates of heat flow are considered to constitute a single population with normal distribution.

Regional heat-flow groups were identified for several geological environments in Western Australia (near 30°S, 120°E), South Australia (33°S, 139°E), New South Wales (35°S, 150°E), and northwest Queensland (21°S, 138°E). Values were concentrated in grid spacings of about 6° near each centre. Two sub-groups were then generated in each region according to quality. The better quality estimates are readily distinguished in terms of standard deviation. Values rated better than 333 are associated with average error of

Table 5. Australian heat-flow data file (see Table 2 for details of file items).

Heat-flow data-file item														
1			2	3	4	5	6	7	8	9	10			11
Ref.	Yr.	No.	Name	Lat.	Long.	Elev.	Depth	Q	Qual.	P	GT	A	N	Lit.
24	76	56	EDIACARA	30.60	138.12	290	213	96	222	8	47			
24	76	57	IRON KNOB	32.72	137.13	180	305	109	220	10	27	7.5	6	
24	76	58	KADINA	33.97	137.75	46	476	101	444	4	27			
24	76	59	MARALINGA	30.17	131.60	180	252	54	322	4	23			
24	76	60	MOOTOOROO	32.25	140.93	220	589	68	544	2	27	3.1	11	
24	76	61	MT MCTAGGA	30.45	139.30	147	175	101	232	8	27			
24	76	62	PARABARANA	29.98	139.72	275	320	126	332	8	28	7.9	4	
24	76	63	STOCKYARD	34.77	138.80	300	185	88	243	8	27			
24	76	64	WUDINNA	32.98	135.55	240	303	58	344	8	23	4.9	17	
24	76	65	TARCOOLA	30.62	134.50	150	304	49	334	4	23	2.7	20	
24	76	66	BRANXEHOLM	37.87	141.80	160	158	55	242	1	67			
24	76	67	HEYWOOD	38.13	141.53	49	540	50	443	3	77			
24	76	68	PORTLAND	38.38	141.58	461	050	50	522	1	77			
24	76	69	SORRENTO	38.35	144.73	25	427	55	333	10	57			
24	76	70	TIMBOON	38.47	142.98	115	243	71	232	5	77			
24	76	71	KAMBALDA	31.20	121.68	310	1059	31	555	2	13	1.3	13	16
24	76	72	MT GOODE	27.62	120.57	488	79	34	132	8	13	1.9	6	
24	76	73	YACKABINDI	27.42	120.57	536	235	35	233	1	13	1.9	6	
24	76	74	MT NEWMAN	23.37	119.67	660	332	46	332	5	13			
24	76	75	MT WINDARA	28.50	122.23	445	318	40	333	4	13	1.2	5	
24	76	76	WANAWAY	31.63	121.53	371	513	34	454	1	13	1.2	4	
24	76	77	WIDGIEMOOL	31.52	121.58	317	110	32	330	3	13	1.2	4	
25	77	78	GLENORCHY	42.83	147.25	200	500	87	343	8	57			
25	77	79	OLGA RIDGE	42.77	145.78	200	330	57	322	11	57			
27	77	80	WOKURNA	33.72	138.12	300	300	91	555	4	27			
27	77	81	ROVER	20.08	133.67	400	550	100	443	4	2			
27	77	82	BUTE	33.93	137.97	300	350	87	434	8	27			
27	77	83	WARREGO	19.45	133.82	400	650	161	122	28	28			
27	77	84	EXPLORER	19.68	134.23	400	550	100	444	8	2			
28	79	85	BILILUNA	19.51	127.64	450	70	52	122	2	43			
28	79	86	NOONKANBAH	18.11	124.82	120	140	67	333	4	43			
28	79	87	HALLS CK	18.23	127.70	510	95	26	122	2	2			
28	79	88	TANAMI	19.97	129.70	450	80	34	122	6	2			
28	79	89	YUENDUMU	22.33	131.73	750	220	56	333	3	2			
28	79	90	ST GEORGE	18.69	125.14	2104	400	65	333	4	43			
28	79	91	WITTENOOM	22.33	118.23	720	330	39	334	3	2			
28	79	92	MILLSTREAM	21.65	117.02	320	230	43	344	1	2			
28	79	93	TOM PRICE	22.75	117.77	950	190	45	233	2	2			
28	79	94	MT MORGAN	23.63	150.37	350	140	57	233	1	57			
28	79	95	MT CHALMER	23.29	150.65	100	230	62	334	1	57	2.8	2	33
28	79	96	PEAK DOWNS	22.28	148.22	200	280	76	344	2	53			
28	79	97	BALFES CK	20.33	145.85	300	174	77	443	4	4			
28	79	98	DUGALD RIV	20.31	140.20	300	283	72	334	3	2	2.7	2	33
28	79	99	MT DORE	21.81	140.60	360	185	98	333	4	2	9.3	2	33
28	79	100	WOODLAWN	34.98	149.52	833	262	60	454	2	47	1.4	2	33
28	79	101	CANBERRA	35.30	149.15	605	260	73	454	3	47			
28	79	102	ARDLETHAN	34.34	146.85	220	200	99	333	5	47	2.3	8	33
28	79	103	MT GAMBIER	37.75	140.86	65	243	92	444	3	67			
31	80	104	BERRIGAN	35.70	145.80	187	180	73	444	1	47	7.0	2	
33	81	105	HALL	35.08	149.03	697	220	69	344	3	47	2.7	0	
33	81	106	MT WHELAN	23.32	138.87	145	600	80	444	3	63	10.7	3	
33	81	107	ARBOUIN	17.33	145.27	757	230	100	333	5	57	3.9	1	
33	81	108	GEORGETOWN	17.95	143.42	227	250	77	233	4	57	6.6	1	
33	81	109	JABILUKA	12.05	132.89	125	460	86	444	3	29	5.8	4	

14.5 per cent (one standard deviation), whereas other values may be in error by 26.6 per cent (Table 6).

Adequate sampling of each population should result in identical mean values for each group in each region, and, in view of the number of estimates available, the agreement is considered to be satisfactory. However, it must be emphasised that most regions used for statistical analysis probably do contain real variations in heat flow that can be attributed to changes in local geology. Consequently, heat-flow values are not truly random measurements of a single parameter, and any estimates of error remain contentious. Geological conditions are most uniform in Western Australia, and minimum values have been obtained for the standard deviations of each quality group; the results for this region should, therefore, be adopted when the error is being estimated for single determinations of heat flow elsewhere in Australia.

Table 6. Estimates of error associated with data of different quality.

Region	*R*	*N*	*Qm*	σ	σ_m
Western Australia	>333	9	36.92	3.75	1.25
(30S, 120E)	≤333	8	42.08	8.24	2.91
South Australia	>333	9	78.13	14.23	4.74
(33S, 139E)	≤333	10	85.42	25.29	8.00
New South Wales	>333	7	77.27	13.23	5.00
(35S, 150E)	≤333	6	66.68	20.50	8.37
NW Queensland	>333	7	86.06	10.67	4.03
(21S, 138E)	≤333	4	95.71	(48.10)	(24.05)

R—Quality rating factor
N—Number of heat-flow data
Qm—Mean value for heat flow
σ—Standard deviation
σ_m—Standard error of mean

References

ANDERSON, R. N., LANGSETH, M. G., & SCLATER, J. G., 1977—The mechanisms of heat transfer through the floor of the Indian Ocean. *Journal of Geophysical Research*, 82, 3391-409.

BAIN, J. H. C., 1977—Uranium mineralisation associated with late Palaeozoic acid magmatism in northeast Queensland. *BMR Journal of Australian Geology & Geophysics*, 2, 137-47.

BECK, A. E., 1965—Techniques of measuring heat flow on land. In LEE, W. H. K. (editor), Terrestrial heat flow. *American Geophysical Union, Monograph* 8.

BECK, A. E., 1976—The use of thermal resistivity logs in stratigraphic correlation. *Geophysics* 41, 300-9.

BOWLER, J. M., HOPE, G. S., JENNINGS, J. N., SINGH, G., & WALKER, D., 1976—Late Quaternary climates of Australia and New Guinea. *Quaternary Research*, 6, 359-94.

BULLARD, E. C., 1939—Heat flow in South Africa. *Proceedings of the Royal Society of London*, A, 173, 474-502.

BUNKER, C. M., BUSH, C. A., MUNROE, R. J., & SASS, J. H., 1975—Abundances of uranium, thorium, and potassium for some Australian crystalline rocks. *United States Geological Survey, Open File Report* 75-393.

BURNE, R. V., & KANTSLER, A. J., 1977—Geothermal constraints on the hydrocarbon potential of the Canning Basin, Western Australia. *BMR Journal of Australian Geology & Geophysics*, 2, 271-88.

CULL, J. P., 1979—Climatic corrections to Australian heat flow data. *BMR Journal of Australian Geology & Geophysics*, 4, 303-7.

CULL, J. P., 1981—Heat flow at standard depth. *Journal of Volcanology and Geothermal Research* 9, 77-85.

CULL, J. P., & DENHAM, D., 1979—Regional variations in Australian heat flow. *BMR Journal of Australian Geology & Geophysics*, 4, 1-13.

ERIKSON, A. J., VON HERZEN, R. P., SCLATER, J. G., GIRDLER, R. W., MARSHALL, B. V., & HYNDMAN, R., 1975—Geothermal measurements in deep-sea drill holes. *Journal of Geophysical Research*, 80, 2515-28.

FACER, R. A., HUTTON, A. C., & FROST, D. J., 1980—Heat generation of siliceous igneous rocks of the basement and its possible influence on coal rank in the Sydney Basin, New South Wales. *Proceedings of the Linnean Society of New South Wales*, 104, 95-109.

HOWARD, L. E., & SASS, J. H., 1964—Terrestrial heat flow in Australia. *Journal of Geophysical Research*, 69, 1617-26.

HYNDMAN, R. D., & SASS, J. H., 1966—Geothermal measurements at Mount Isa, Queensland. *Journal of Geophysical Research*, 71, 587-601.

JESSOP, A. M., HOBART, M. A., & SCLATER, J. G., 1976—The world heat flow data collection—1975. *Geothermal Series*, 5, *Ottawa, Canada.*

JONGSMA, D., 1976—Vema cruise 33 leg 2, in the southeast Indian Ocean, 21 December, 1975 to 17 January, 1976; observer's report. *Bureau of Mineral Resources Australia, Record* 1976/85 (unpublished).

KRCMAR, B., & MASIN, J., 1970—Prospecting by the geothermic method. *Geophysical Prospecting*, 18, 255-60.

LACHENBRUCH, A. H., & SASS, J. H., 1977—Heat flow in the United States and the thermal regime of the crust. *In* HEACOCK, J. G. (Editor), The Earth's crust. *American Geophysical Union Monograph* 20.

LILLEY, F. E. M., SLOANE, M. N., & SASS, J. H., 1978—A compilation of Australian heat flow measurements. *Journal of the Geological Society of Australia*, 24, 439-45.

MACDONALD, K. C., LYENDYK, B. P., & VON HERZEN, P., 1973—Heat flow and plate boundaries in Melanesia. *Journal of Geophysical Research*, 78, 2537-46.

MURRAY, A. S., 1977—A guide to use and operation of program CONTOR. *Bureau of Mineral Resources, Australia, Record* 1977/17 (unpublished).

NEWSTEAD, G., & BECK, A., 1953—Borehole temperature measuring equipment and the geothermal flux in Tasmania. *Australian Journal of Physics*, 6, 480-9.

POLEY, J. PH., & VAN STEVENINCK, J., 1970—Geothermal prospecting. *Geophysical Prospecting*, 18, 666-700.

ROY, R. F., BLACKWELL, D. D., & DECKER, E. R., 1968—Heat generation of plutonic rocks and continental heat flow provinces. *Earth and Planetary Science Letters*, 5, 1-12.

SASS, J. H., LACHENBRUCH, A. H., & MUNROE, R. J., 1971—Thermal conductivity of rocks from measurements of fragments and its application to heat flow determinations. *Journal of Geophysical Research*, 76, 3391-401.

SASS, J. H., JAEGER, J. C., & MUNROE, R. J., 1976—Heat flow and near surface radioactivity in the Australian continental crust. *United States Geological Survey, Open File Report* 76-250.

SCLATER, J. C., RITTER, U. G., & DIXON, F. S., 1972—Heat flow in the southwestern Pacific. *Journal of Geophysical Research*, 77, 5697-704.

SCOTT, R. W., FOUNTAIN, J. A., & WEST, E. A., 1973—A comparison of two transient methods of measuring thermal conductivity of particulate samples. *Review of Scientific Instruments*, 44, 1058-63.

SHERATON, J. W., & LABONNE, B., 1977—Petrology and geochemistry of acid igneous rocks of northeast Queensland. *Bureau of Mineral Resources, Australian, Bulletin* 169.

TURCOTTE, D. L., & OXBURGH, E. R., 1969—Convection in a mantle with variable physical properties. *Journal of Geophysical Research*, 74, 1458-74.

Appendix 1: New determinations of heat flow for Australia, with estimates of quality.

GSQ Mount Whelan No. 1 (23.318°S, 138.865°E, 145 m)

Stratigraphic drilling at GSQ Mount Whelan No. 1 was completed by the Geological Survey of Queensland in September 1977. PVC casing was immediately inserted by BMR to prevent collapse prior to thermal equilibration. The temperatures were last measured one year after completion of the hole. Data were obtained through the entire sedimentary sequence and into the granitic basement. Cores extracted for thermal conductivity measurements represent the major sequences encountered during drilling. A granitic core was chemically analysed to allow estimates of basement heat production.

Heat flow was calculated using two standard techniques. For intervals of uniform stratigraphy it can be assumed that thermal conductivity is well determined; consequently, heat flow can be calculated directly from the product of thermal conductivity and the thermal gradient measured over a corresponding 10-m interval of depth. The data, summarised in Figure A1, indicate with standard error a heat flow of 79.7 ± 3.1 mW m^{-2} from 8 determinations. The second method of data reduction is known as the Bullard plot. Observed temperatures are plotted as a function of cumulative thermal resistance from the surface to successive points of observation (Fig. A2). A linear relation is generated, in which the gradient is a function of the heat flow. Data from all sections of the hole are incorporated with appropriate weights for the thickness of each sequence. Data from GSQ Mount Whelan No. 1 reduced in this manner indicate a heat flow of 76.5 ± 1.8 mW m^{-2}, in close agreement with the previous determination.

Thermal conductivities were determined from 8 samples of granitic basement, giving values of 3.63 ± 0.02 W m^{-1} K^{-1}. Such consistency indicates a highly uniform composition and negligible sampling error. Rates of heat production within the basement were calculated from determinations of the average concentrations of K, U, and Th: 6.04%, 8 ppm, and 115 ppm, respectively. The conversion factors adopted by Roy & others (1968) have been used extensively for estimates of heat production. The relevant factors are expressed by Bunker & others (1975) in the relationship:

$$A\ (\mu W\ m^{-3}) = (0.27\ K_2O\% + 0.02\ Th\ ppm + 0.73\ U\ ppm) \times density/7.55 \quad \ldots (1)$$

Two core samples were submitted for analysis and a rate of 10.78 ± 1.0 μW m^{-3} is indicated for basement heat production at Mount Whelan.

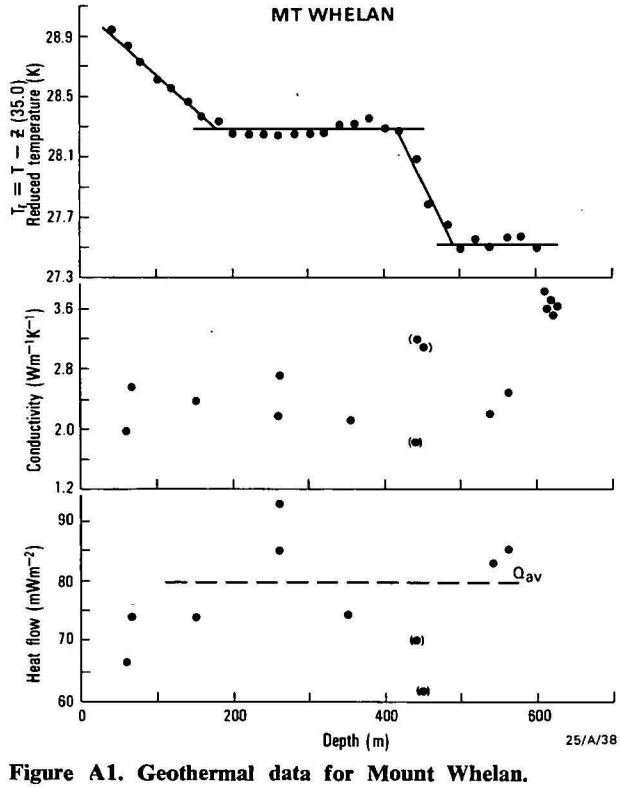

Figure A1. Geothermal data for Mount Whelan.

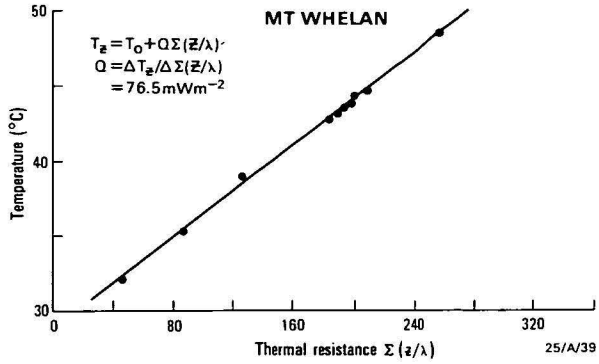

Figure A2. Bullard plot of cumulative resistance for Mount Whelan.

Georgetown (17.95°S, 143.42°E, 227 m)

The Georgetown Inlier contains significant deposits of uranium-fluorine-molybdenum, which are closely associated with the distribution of rhyolitic volcanics. The mineralisation is considered to be of hydrothermal origin, and there are active hot springs in the region (e.g. at Innot). Water circulation may result in anomalous temperatures at shallow depth.

Major prospects have been extensively drilled, but most holes are subject to caving. Consequently, equilibrium temperatures are not generally available. Calculations of heat flow are based on observations in one bore hole penetrating a granitoid to 260 m, but numerous data to depths of 120 m were obtained elsewhere for support. The geothermal gradient has a single linear segment, 100-260 m, with a magnitude of 25.81°C/km (Fig. A3). Closer to the surface, there is a change in gradient to 22.35°C/km, but some of these data may result from reduced equilibration rates in air.

Five core samples were available from depths near 100 m for determination of thermal conductivity. Consistent with the observation of a linear gradient, they were found to yield similar values of 2.99 ± 0.14 W m^{-1}K^{-1}. In view of the uniform stratigraphy, it is concluded that heat flow at greater depth can be calculated as a simple product (linear gradient x average conductivity) resulting in a value of 77.2 ± 3.6 mW m^{-2}.

Estimates of basement heat production are complicated by the proximity of the uranium ore deposits. Analysis of one fluoritised breccia deposit indicates 135 ppm U and 300 ppm Th. An estimate of the regional heat production is, therefore, based on values for the extensive granitoids (Bain, 1977). These are highly fractionated with concentrations of 11 ppm U, 46 ppm Th, and 4.74% K_2O (Sheraton & Labonne, 1977). Adoption of an average density of 2.7 t/m^3 in equation (1) gives a regional heat production of 6.6 ± 0.2 μW m^{-3}.

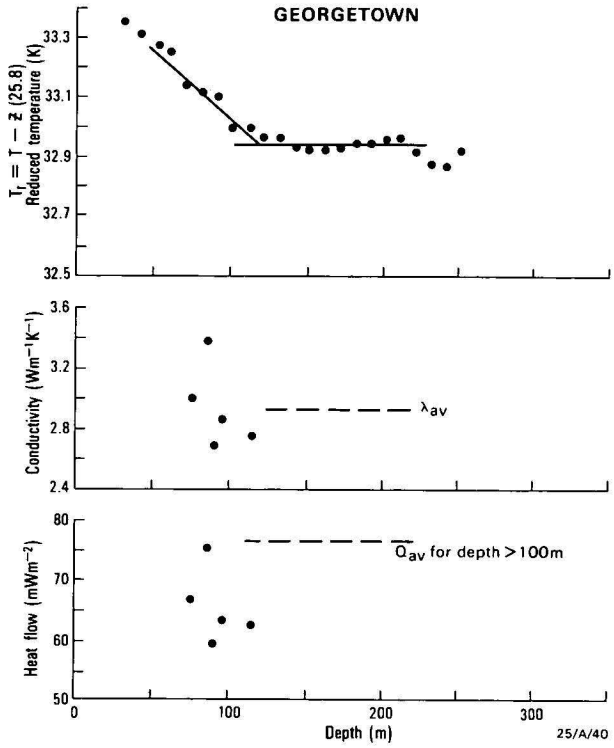

Figure A3. Geothermal data for Georgetown.

Arbouin (17.33°S, 145.27°E, 757 m)

Temperatures were measured to a vertical depth of 230 m in an exploration borehole testing a tin prospect. The equilibration period of approximately 1 year between drilling and logging is considered sufficient to ensure adequate resolution in uniform rock of high diffusivity. Although the hole is located in an elevated region, there are no significant variations in local topographic relief, and no corrections have been made to the data.

The geothermal gradient has 3 segments that are essentially linear (Fig. A4). However, actual values of gradient are similar in each segment and there is no apparent correlation with changes in stratigraphy. Core samples were available from each segment and values of thermal conductivity were found to be in the range 3.4 to 5.1 W m^{-1} K^{-1}. Individual determinations of thermal conductivity were combined with the apparent thermal gradient over corresponding intervals of depth to give estimates of heat flow. The mean of 10 determinations was found to be 99.8 ± 4.9 mW m^{-2}, with no consistent variation with depth.

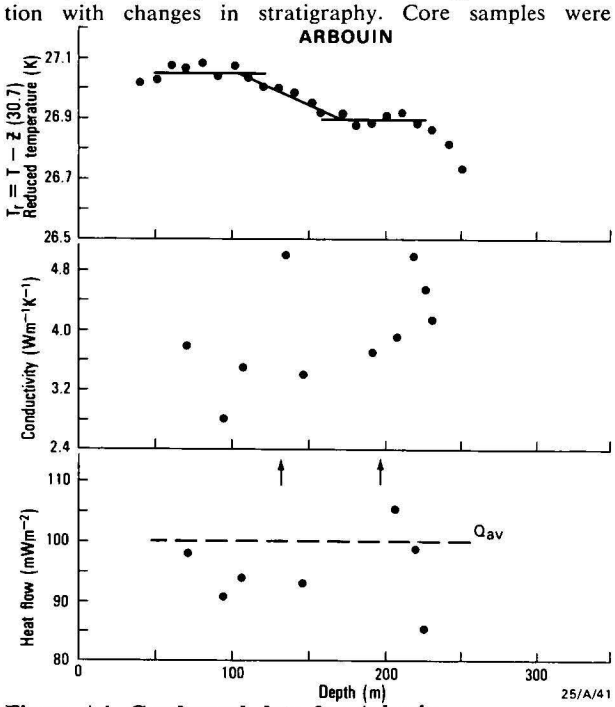

Figure A4. Geothermal data for Arbouin.

Estimates of heat production can be based on the analysis of regional granitoids (Bain, 1977). In the Herbert River region, Sheraton & Labonne (1977) have indicated values of 5 ppm, 30 ppm, and 4.18% for the concentrations of U, Th, and K_2O, respectively. Adoption of a density of 2.7 t/m^3 in equation (1) gives a heat production of 3.85 ± 0.25 μW m^{-3}.

Jabiluka (12.05°S, 132.89°E, 125 m)

In July 1979, Pancontinental Mining requested that BMR conduct a geothermal survey at the site of the Jabiluka uranium mine. Five boreholes were selected for survey; all had been drilled at least 6 months prior to survey and thermal equilibrium was, therefore, likely. All boreholes were vertical and uncased except for a surface collar. Core samples were available from each borehole, allowing determinations of thermal conductivity.

Temperature gradients were generally near 24.7°C/km, with extrapolated surface temperatures of 31.2°C compared to mean annual air temperatures near 29°C (Fig. A5). Howard & Sass (1964) noted previously that ground temperatures consistently exceed mean annual air temperatures by 1-3°C, possibly because of variable albedo and ground/air coupling. This effect is observed throughout the continent, and ground surface temperatures at Mt Isa, Tennant Creek, and Rum Jungle are also greater than mean annual air temperatures.

Variations in geothermal gradient for individual boreholes reflect changes in thermal conductivity with the types of rock encountered at each depth. Consequently, changes in stratigraphy may be detected within each borehole. However, such simple correlations may not be applicable for steeply dipping structures associated with the ore body. Some heat may be refracted to highly conductive zones, causing lateral perturbations in gradient unrelated to

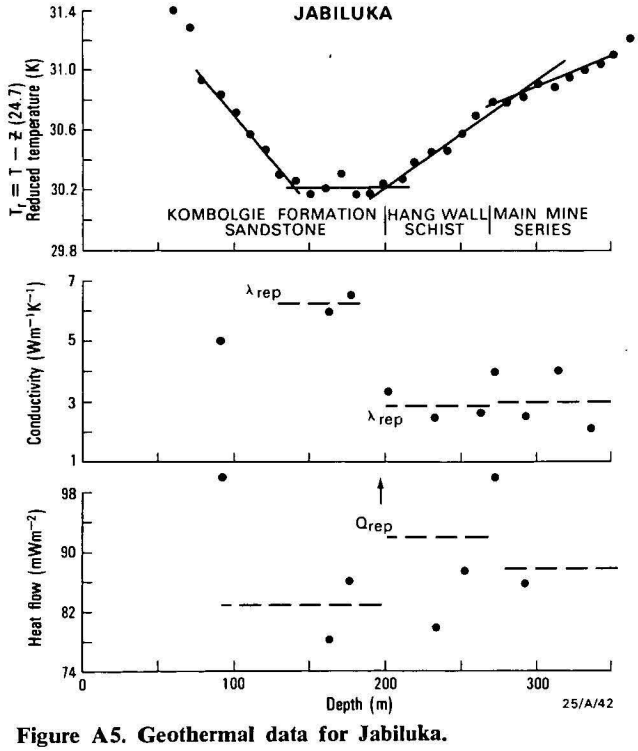

Figure A5. Geothermal data for Jabiluka.

regional heat flow values. Furthermore, it is possible that thermal gradients within the Main Mine Series will decrease with depth to reflect decreasing concentrations of radioactive heat sources.

The highest values of thermal conductivity (5.5 W $m^{-1}K^{-1}$) are associated with sandstones at shallow depth and with schists in the lower foot wall. The sandstone values are caused by the high silica content, and the data are considered to be representative of the Kombolgie Formation. The samples of schist are more variable, so their thermal conductivities are subject to sampling errors, and estimates of a representative value have a high uncertainty. Average values are near 2.9 W $m^{-1}K^{-1}$. The Main Mine Series has similar sample variability, with measurements ranging from 2.2-4.1 W $m^{-1}K^{-1}$. However, most of this unit appears to have a uniform composition, and a mid-range value of 3.0 W $m^{-1}K^{-1}$ can be assumed for the bulk of the Main Mine Series. Results for the Lower Mine Series are reasonably constant, and values of 3.5 ± 0.4 W $m^{-1}K^{-1}$ are considered to be representative of the full unit.

Representative thermal conductivities were specified in the above manner for four major stratigraphic units: the Kombolgie Formation, the Hanging Wall Schist, the Main Mine Series, and the Lower Mine Series. The temperature gradients in each of these units, determined by linear regression, were 13.2, 31.6, 29.4, and 23.6°C/km, respectively. Corresponding values of heat flow are 83.2, 91.6, 88.2, and 82.6 mW m^{-2}, with an average value of 86.4 mW m^{-2}. This result is consistent with regional trends described by Cull & Denham (1979), and is similar to the values of 83.6, 96.1, and 81.9 mW m^{-2} obtained for Rum Jungle, Tennant Creek, and Mount Isa, respectively.

Estimates of heat production are complicated by the proximity of the uranium ore body. A chemical analysis conducted on 12 core samples indicated average concentrations of 2.31%, 15.5 ppm, and 22 ppm for K_2O, U, and Th, respectively. Very high values associated with concentrations of ore were observed in two other samples. A value more representative of the region is determined from surface samples of granite from 30 km south. Concentrations of 4.23%, 10 ppm, and 70 ppm were determined from K_2O, U, and Th, respectively. Adoption of these values in equation (1), gives rates of heat production as 5.8 ± 2.1 μW m^{-3} at the mine site, and 8.0 ± 1.0 μW m^{-3} for the regional basement.

Mount Isa (20.74°S, 139.45°E, 350 m)

Geothermal gradients at Mount Isa have been reported in detail by Hyndman & Sass (1966). Data were obtained in 14 boreholes in the mine. Rock types were sampled at the 13 level, and thermal conductivities were measured using divided bar techniques. Values of heat flow ranged from 74 to 108 mW m^{-2} with a mean of 82 mW m^{-2}.

New data have now been obtained by BMR from the 19 level in borehole Z 72 E Dec No. 2, penetrating a further 160 m to a total depth of 1100 m. Core samples have been extracted from the borehole, allowing more detailed measurements of thermal conductivity. As a result, heat-flow values can be determined with greater precision than previously.

A pronounced curvature was observed in the geothermal gradient close to collar level. This curvature is unrelated to changes in thermal conductivity and is attributed to thermal perturbations caused by mine ventilation. At greater depths the gradient is nearly linear, indicating uniform thermal conductivity. Data in the linear section can be approximated with a gradient of 19.75°C/km. This is consistent with the results of Hyndman & Sass (1966), which indicate a range of 18.2-25.5°C/km, with an average of 19.82°C/km.

Thermal conductivities were determined for 14 core samples. The results were assumed to be well sampled, with a direct relationship to the geothermal gradient over corresponding 5-m intervals. A heat-flow measurement of 75.3 ± 2.4 mW m^{-2} was calculated from the average product. This result is within the range obtained by Hyndman & Sass (1966), but is significantly less than the mean value of 81.9 mW m^{-2}. Hyndman & Sass atribute such discrepancies to refraction of heat in steeply dipping structures with contrasting thermal conductivities.

Hall (35.08°S, 149.03°E, 697 m)

Temperatures were measured in an uncased stratigraphic borehole, CAN 155, that penetrates Silurian limestone to a depth of 240 m. Although the geothermal gradient is essentially linear, there are several perturbations causing a scatter of observations, which can be related to changes in thermal conductivity (Fig. A6). An accurate mean value for thermal conductivity cannot be readily determined, because of possible sampling errors. However, conductivity values for 10-15-m intervals range from 1.7-4.7 W $m^{-1}K^{1-}$, giving a weighted average of 2.78 W $m^{-1}K^{-1}$.

When combined with the best-fit linear gradient of 25.8°C/km, the average conductivity indicates a heat flow of 71.7 mW m^{-2}. Greater precision is obtained by combining individual determinatons of thermal conductivity with the apparent gradient for the corresponding 10-m intervals of depth. The results are consistent with climatic trends noted elsewhere in the region of the Snowy Mountains (Cull, 1979). Values of heat flow appear to be increasing with depth, but the degree of curvature is difficult to resolve. Uncorrected values indicate a heat flow of 68.9 ± 2.9 mW m^{-2} from 14 determinations. This result is consistent with values of 72.5 ± 2.5 mW m^{-2} at Canberra (Cull & Denham, 1979), where climatic corrections of up to 30 per cent were suggested (Cull, 1979).

Estimates of heat production can be based on the compilation of Heier & Lambert, summarised by Sass & others (1976). Regional studies of surface samples from the Snowy Mountains area indicate heat-production rates of 2.9 ± 0.1 μW m^{-3} for granitic basement. Samples from the Canberra region are marginally less active and indicate a rate of 2.7 ± 0.2 μW m^{-3}.

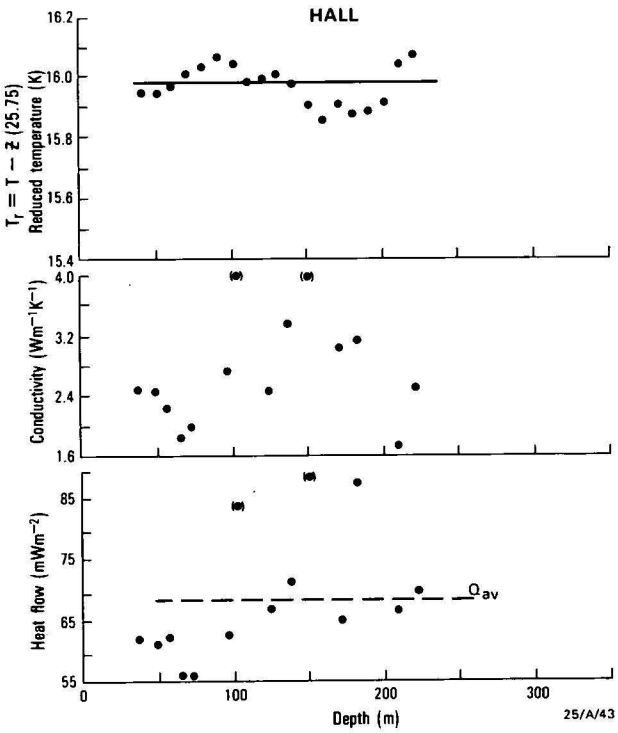

Figure A6. Geothermal data for Hall.

BMR Journal of Australian Geology & Geophysics, 7, 23-33.

SOURCE ROCK POTENTIAL AND HYDROCARBON PROSPECTIVITY OF THE DARLING BASIN, NSW

C. M. Brown*, K. S. Jackson, K. L. Lockwood, & V. L. Passmore

Available geological and geophysical data for the dominantly Devonian Darling Basin of western New South Wales indicate a high risk for petroleum exploration. Hydrocarbon prospectivity is confined to the concealed western Darling Basin, where block-faulted, graben-like troughs contain a generally thick sequence of Middle Devonian to Lower Carboniferous continental sediments, underlain by Lower Devonian marine sediments. Geochemical data for cores from BMR Ivanhoe No. 1 and from thirteen petroleum exploration wells held on open file at BMR are used to evaluate source rock potential and organic maturation levels. The continental sediments have no source potential. The marine Lower Devonian Amphitheatre Formation has a generally low organic carbon content, is thought to be gas prone, and is thermally mature to overmature for oil generation. The geochemical data support the hypothesis that trough flanks and margins, where sediments have not been too deeply buried or thermally altered, offer the best prospects for preservation of source and reservoir rocks. On the basis of the limited data available, the eastern flank of the Lake Wintlow High-Wilcannia High is considered the most prospective region of the Darling Basin.

Introduction

The Darling Basin is a poorly defined intracratonic basin of thick, predominantly Devonian, sedimentary rocks that underlie some 150 000 km^2 of western New South Wales between Broken Hill and Cobar (Fig. 1). In this paper we present the results of an organic geochemical study of Devonian samples from subsidised petroleum exploration wells and shallow BMR drilling, undertaken to assess the petroleum potential of the basin. In addition, the distribution of potential hydrocarbon source rocks is reviewed and exploration potential discussed.

The hydrocarbon potential of the basin has been regarded as poor (Smith, 1977). However, the proximity of the basin to the Moomba-Sydney gas pipeline has stimulated hydrocarbon exploration activity and active promotion of the basin by the New South Wales Department of Mineral Resources (Longworth & others, 1979). In a comprehensive appraisal of the petroleum geology of western New South Wales, Evans (1977) suggested that hydrocarbons may occur within regressive Lower Devonian sandstone reservoirs of shallow-marine or deltaic facies, and may have been generated from and sealed by Lower Devonian marine shales now preserved in concealed graben-like troughs of the western Darling Basin. His assessment, however, was not supported by quantitative geochemical data and organic maturation indicators.

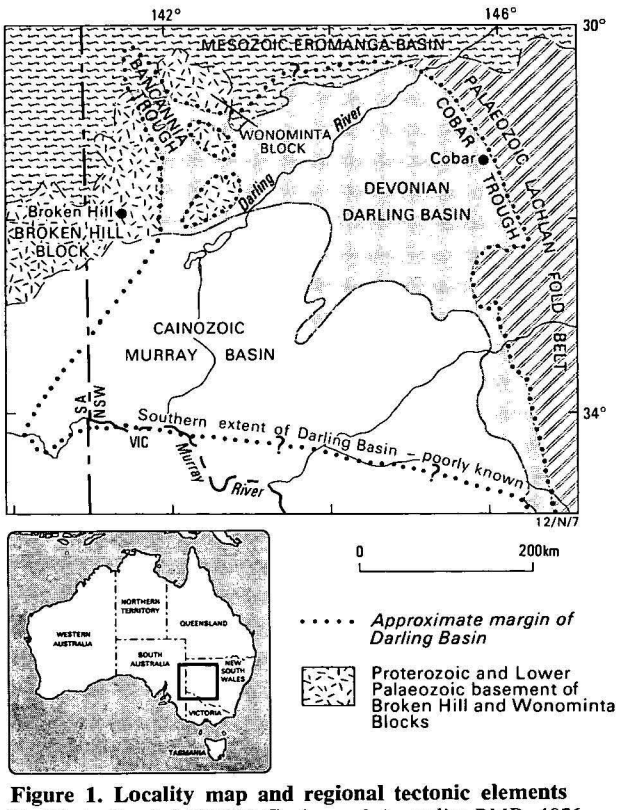

Figure 1. Locality map and regional tectonic elements
Modified after 1:2 500 000 Geology of Australia; BMR, 1976.

Regional framework

The present-day Darling Basin consists of up to 7000 m of Late Silurian to Early Carboniferous sedimentary rocks with those of Devonian age predominating (Packham, 1969; Bembrick, 1976a; Evans, 1977). In the west, the basin unconformably overlies Proterozoic and Lower Palaeozoic rocks of the Broken Hill and Wonominta basement blocks, and in the east onlaps folded, faulted, and metamorphosed older Palaeozoic rocks of the Lachlan Belt (Fig. 1). We include in the basin the Bancannia Trough in the west (Bembrick, 1976b) and the Cobar Trough in the east. To the north, the Devonian Sequence extends beneath the Mesozoic Eromanga Basin; in the west and south, the basin is concealed beneath a thin veneer of Upper Carboniferous, Permian, Cretaceous, and Cainozoic sediments of the Murray Basin and associated infrabasins (Fig, 2; Thornton, 1974, 1976). The nature, age, and extent of the basement beneath the Darling Basin is largely unknown, but geophysical evidence (Wyatt & others, 1980) and limited borehole data suggest the basin may be underlain by lower Palaeozoic basement rocks (Doutch & Nicholas, 1978) of the Kanmantoo Fold Belt and possibly, rifted segments of Proterozoic crust (Scheibner, 1976).

The structure of the basin is characterised by trends inherited from the underlying and adjacent basement areas. In the east, the Devonian sediments of the Cobar Trough are strongly folded, faulted, and metamorphosed. Westwards, deformation diminishes and in the adjacent parts of the Darling Basin, unmetamorphosed but indurated sediments (Fig. 2) crop out in a series

*authors listed in alphabetical order

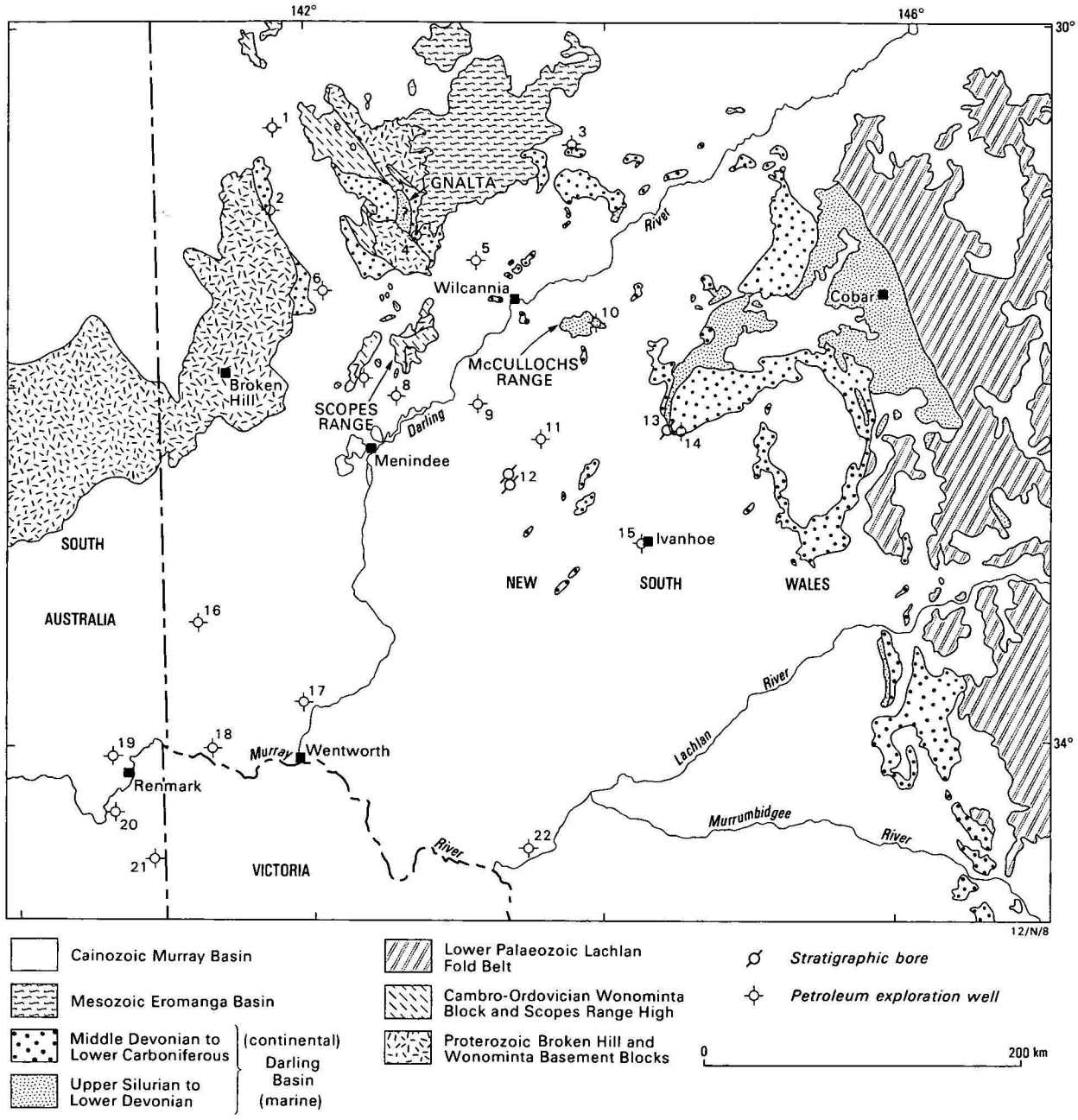

Figure 2. Generalised geology and location of petroleum exploration wells
Modified after 1:1 000 000 Geological Map of New South Wales; Pogson, 1972.

Petroleum exploration wells and stratigraphic bores

1. Bancannia North No. 1
2. Bancannia South No. 1
3. Mount Jack No. 1
4. Gnalta No. 1
5. Pondie Range No. 1
6. Jupiter No. 1
7. Byrndale No. 1
8. Blackgate No. 1
9. Blantyre No. 1
10. Poopelloe Lake No. 1
11. Mount Emu No. 1
12. BMR Manara Nos. 1, 2
13. BMR Ivanhoe No. 1
14. Berangabah No. 1
15. Ivanhoe No. 1
16. Tarrara No. 1
17. Wentworth No. 1
18. Lake Victoria No. 1
19. North Renmark No. 1
20. Berri South No. 1
21. Nadda No. 1
22. Balranald No. 1

of northeasterly trending anticlines and synclines. Seismic data indicate that the Devonian sequence of the western Darling Basin, beneath the Murray Basin, is block-faulted in a series of graben-like troughs, which contain up to 7 km of sedimentary rocks (Figs. 3, 4; Planet Oil Company, 1966, 1968; Alliance Oil Development Australia, 1968a; Beaver, 1973; Bauer & others, 1979).

Petroleum exploration

The metamorphism of rocks of the Cobar Trough and degree of induration of the folded sediments of the adjacent eastern parts of the basin suggest that the block-faulted but relatively undeformed sedimentary rocks in the west are more prospective for hydrocarbons, and hence, exploration activity has mainly been undertaken in the western Darling Basin, approximately west of longitude 145°E.

Exploration drilling commenced in 1963 with the sinking of Mount Jack No. 1, and has continued intermittently with the drilling of a further twelve exploration wells in previously untested areas of the western Darling Basin (Fig. 2). In the northwest, the principal targets were poorly defined structural traps in the

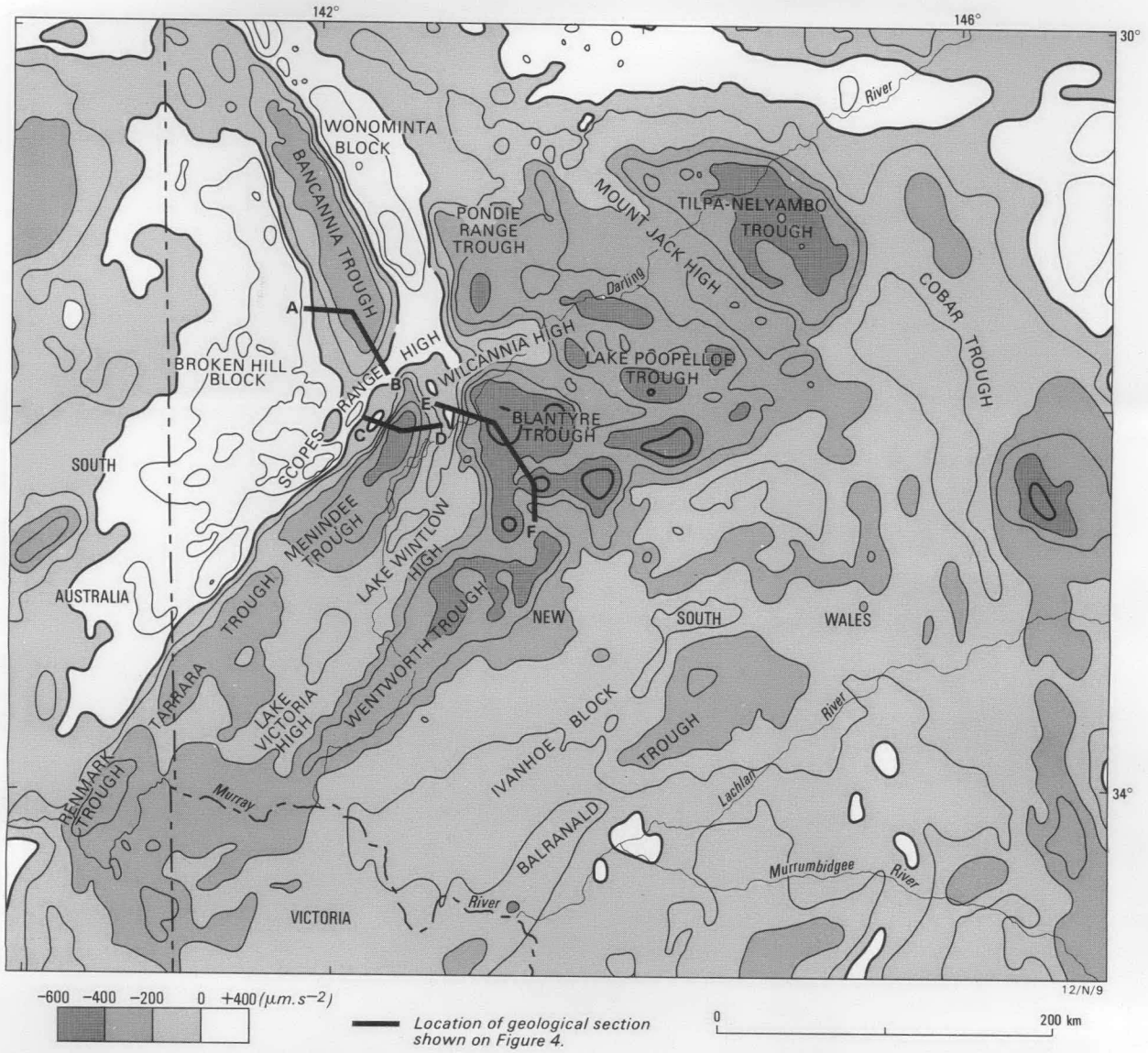

Figure 3. Bouguer gravity anomalies and structural elements. Correction: the value, on the legend, of the positive anomalies should read +200 μm.s^{-2} (not 400).

Based on BMR gravity data bank, and Anfiloff & others, 1976.

Lower Devonian marine sequences and underlying Lower Palaeozoic basement rocks (Bembrick, 1976a, 1976b). Farther south, several wells intersected Middle to Upper Devonian non-marine clastics (Bembrick, 1974; Thornton, 1974, 1976). The most recent company activity has been the drilling of Blackgate No. 1 and Byrndale No. 1 on the flanks of the Menindee Trough by Comserv Pty Ltd in 1980/81. The results of these are not yet known to the authors. In addition to the reviews undertaken by Evans (1977), and Longworth & others (1979), geophysical exploration activity has been reviewed by Bauer & others (1979).

None of the petroleum exploration wells tested the Lower Devonian play proposed by Evans (1977), and only four of the wells referred to above penetrated sediments of Early Devonian age: three of these encountered marine sediments. Drilling results have generally been discouraging with no significant hydrocarbon shows in any of the wells, although minor gas shows were recorded in non-marine Devonian sandstones in Jupiter No. 1 (Wiltshire, 1970), Bancannia South No. 1 (Baarda, 1968a), and Bancannia North No. 1 (Baarda, 1968b). Traces of bitumen were observed in Middle to Upper Devonian sandstone in Bancannia South No. 1.

BMR drilling

A paucity of available samples of possible hydrocarbon source rocks in the marine Lower Devonian necessitated extra material being collected by BMR. This operation was, however, limited by: a maximum drilling capability of 300 m; the apparent absence of Lower Devonian marine facies around the western margins of the basin; and the structural deformation and incipient metamorphism of much of the Lower Devonian sequence cropping out in the east. Only one of three holes drilled, BMR Ivanhoe No. 1 (Fig. 2), obtained samples from this interval. It was located on the eroded core of an anticline on the southeastern flank of the Lake Poopelloe Trough (Fig. 2), near the site of Berangabah No. 1, from which only sparse cuttings samples were available. Two other drill holes, BMR Manara Nos. 1 and 2 had, for technical reasons, to be abandoned at 175 m and 210 m and failed to penetrate beneath the Murray sequence.

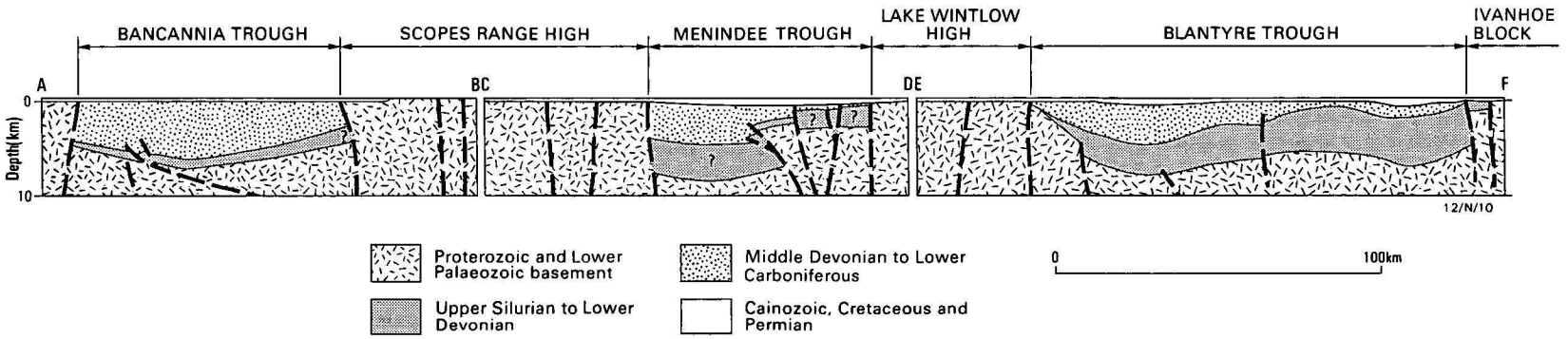

Figure 4. Geologic section, western Darling Basin
After Evans, 1977; based on seismic data from Alliance, 1968a; Planet, 1968; Beaver, 1973.

Table 1. Source rock data for Lower Devonian Amphitheatre Formation cores from BMR Ivanhoe No. 1

Sample no.	*Depth (m)*	*TOC %*	*EOM ppm*	*SATS ppm*	*AROM ppm*	*POLAR ppm*	*ASPH ppm*	*Pr/n.C$_{17}$*	*Ph/n.C$_{18}$*	*Pr/Ph*	*Lithology*	*Source rating*
1	29.1	0.46	95	5.6	1.1	29.1	55.9	0.17	0.09	1.57	gy/Sltst	lean-barren
2	61.8	0.98	939	72.3	96.7	228.2	403.8	0.93	0.29	3.29	gy/bk Sltst	fair
3	90.0	0.12	70	3.8	1.0	19.9	35.0	0.50	0.41	1.25	gy/bk Sltst	barren
4	117.0	0.02	63	3.8	3.8	20.0	19.1	0.50	0.39	1.03	slt Sh	barren
5	133.0	0.16	104	12.9	11.0	36.8	30.4	0.32	0.12	2.93	slt Sh	lean-barren
6	170.0	0.81	762	31.2	35.8	270.5	302.5	0.35	0.14	2.64	bk/Sh	fair
7	200.7	0.12	165	17.8	9.6	56.9	26.1	0.38	0.32	0.78	bk/Sh	lean-barren
8	215.4	0.15	135	17.7	13.2	39.8	37.7	0.54	0.37	1.03	slt Sh	lean-barren
9	224.9	0.14	110	9.1	5.5	43.1	45.9	0.41	0.24	1.78	slt Sh	lean-barren
10	240.0	0.15	72	3.8	2.9	19.2	43.2	naphthenic			bk Sltst	barren
11	250.4	0.08	46	5.3	3.8	8.3	26.4	naphthenic			bk Sh	barren
12	269.7	0.15	68	7.0	4.7	18.8	34.0	naphthenic			slt Sh	barren
13	282.6	0.29	115	5.2	4.4	41.9	47.0	0.48	0.29	1.37	bk Sltst	barren
14	300.9	0.09	59	6.7	4.8	10.4	34.3	naphthenic			slt Sh	barren

Structural and stratigraphic framework: western Darling Basin

Structure

The western part of the Darling Basin has been subdivided into a number of structural divisions (Fig. 3). We recognise the same features in the northwest as Evans (1977) with some modifications resulting from the Bouguer gravity anomaly contours (Fig. 3) derived from the BMR Gravity Data Bank (Anfiloff & others, 1976).

Stratigraphy

Pre-Devonian basement. Proterozoic metamorphics and sediments, and Cambro-Ordovician sediments and volcanics crop out around the western margin of the basin, and are thought to underlie the Devonian sequence in the Bancannia and Menindee Troughs (Bembrick, 1976b). They are also exposed in the Scopes Range High (Fig. 2), where Lower Ordovician quartz sandstone and conglomerate unconformably overlie Proterozoic schist, phyllite, and quartzite.

Devonian. The Devonian sediments in the western Darling Basin (Fig. 5) can be divided into two major sequences, a lower unit of predominantly fine-grained Lower Devonian marine rocks and an upper unit of extremely thick, molasse-like, coarse-grained Mid-Devonian to Lower Carboniferous, fluviatile sediments. The lower sequence generally consists of up to 4000 m of marine siltstone and shale, which, in the upper few hundred metres, grade upwards into regressive shallow-marine sandstone bodies (Amphitheatre Formation of Baker & others, 1975; Baker, 1978; Pogson & Felton, 1978). Elsewhere, around the western margins of the basin, several hundred metres of coarse-grained continental redbeds, of possible Early Devonian age, occur in the Gnalta area (Rose, 1974) and in Bancannia South No. 1. well (Baarda, 1968a). The upper depositional sequence consists of up to 6000 m of fluviatile sandstone, conglomerate, and minor red shale, generally referred to as the Mulga Downs Group (Packham, 1969; Webby, 1972; Glen, 1979a, 1979b).

Post Early Carboniferous. Relatively thin sequences of Upper Carboniferous to Lower Permian and Lower Cretaceous sediments have been encountered in wells within the graben-like troughs, below the Cainozoic Murray Basin sequence. The Lower Permian is generally only a few hundred metres thick, but in the fault-bounded Renmark Trough (Fig. 3), and possibly in other troughs, consists of up to 1000 m of marine argillaceous diamictite, soft grey mudstone, minor siltstone, and sandstone (Thornton, 1974, 1976). The Lower Cretaceous consists of several hundred metres of poorly consolidated marine and non-marine sandstone, siltstone, and shale.

Potential source rock facies

Pre-Devonian basement

Twelve shallow sample holes were drilled in the structurally high Scopes Range area (Fig. 2) by Alliance Oil Development (1968b), to determine the source potential of Cambro-Ordovician basement rocks. Minor, weakly metamorphosed shales were encountered, and total organic carbon content for three samples analysed was no better than 0.4 percent. Evans (1977) considered the Lower Palaeozoic to have negligible source potential

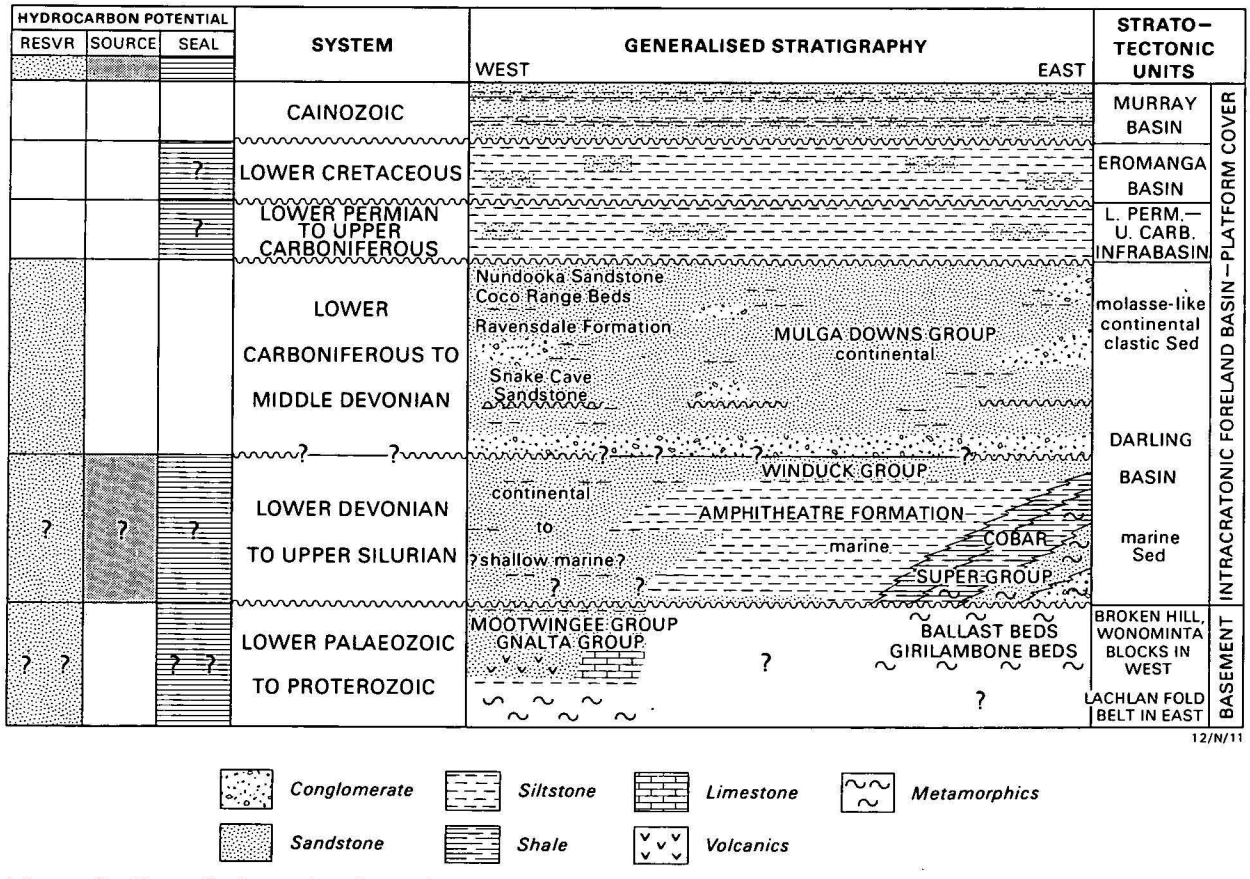

Figure 5. Generalised stratigraphy and summary of hydrocarbon prospectivity.

because of its deep burial below the Devonian, although Bembrick (1976b) suggested that source rocks may occur in unmetamorphosed Lower Palaeozoic marine sediments underlying the Bancannia Trough.

Lower Devonian

The continental character of the redbed sequence in the Gnalta area, at the western margin of the basin, indicates negligible source potential, although Strusz (1966) reported the occurrence of possible worm and trilobite tracks towards the top of the sequence, suggesting the presence of marine and, therefore, potential source rocks in adjacent concealed troughs. Further east, outcrops of the shallow-marine sandstones that occur towards the top of the Lower Devonian sequence contain little or no carbonaceous matter and only minor intercalated shale, and are thus throught to have little or no source rock potential. The underlying fine-grained Lower Devonian marine sequence, thought to be the most likely potential source of hydrocarbons, is rarely exposed, but was intersected by Poopelloe Lake No. 1, Berangabah No. 1, BMR Ivanhoe No. 1, and Mount Emu No. 1.

Poopelloe Lake No. 1 is located on an up-faulted segment of the central Lake Poopelloe Trough, at McCullochs Range. A thick sequence of grey shale, siltstone, and minor sandstone was encountered, but petrographic analysis of core showed mineral and fabric alteration associated with deep burial (Wiltshire, 1970), implying thermal destruction of source potential. It seems likely that source rocks occurring at depth elsewhere within the trough systems have been subject to similar excessive maturation (Evans, 1977) and hence, present day potential source rocks are likely to be preserved only at relatively shallow depths on the flanks of the troughs.

Berangabah No. 1, on the southeastern flank of the Lake Poopelloe Trough, intersected shaly siltstone, with carbonaceous matter consituting up to six per cent of samples (Ranneft, 1968). Spores and acritarchs in one core showed no signs of undue carbonisation and the core showed no evidence of the incipient metamorphism present at Poopelloe Lake No. 1.

BMR Ivanhoe No. 1 continuously cored 305 m of grey marine siltstone, with increasing amounts of interbedded black shale toward the base (Passmore, 1981). No evidence of incipient metamorphism was encountered, but some of the shale laminae were slickensided, and fracturing is common. Visual estimates of colour alteration of spore and condont samples show the sequence to be thermally mature to overmature; details are given below.

The sequence penetrated by Mount Emu No. 1, in the central Blantyre Trough, consists mainly of marine Lower Devonian siltstone with minor sandstone and limestone and contains little fine-grained sediment and no carbonaceous material, and hence has poor source rock potential.

The play proposed by Evans (1977) assumes that in the deeper parts of the Bancannia and Menindee Troughs, marine or deltaic source rocks could occur. However, the presence of marine rocks in the Bancannia Trough was interpreted from the occurrence of poorly preserved, possible marine or brackish water, algal microfloras, of possible Early Devonian age, in the basal Devonian section in Bancannia South No. 1 (Baarda, 1968a; Evans, 1977). In addition, seismic profiles in the Bancannia Trough suggest the presence of a large prograding delta (Evans, 1977), presumably grading laterally into marine sediments, or, alternatively, large alluvial fans (Evans, personal communication, 1981). The presence of marine Lower Devonian in the Menindee Trough was postulated on the basis of seismic character correlation with the Bancannia Trough sequence. We believe the basal section in Bancannia South No. 1 is entirely a continental redbed sequence (Baarda, 1968a) and, although the redbed character may in part reflect poor development of land plants in the Early Devonian, and the Lower Devonian sequence probably includes fluviodeltaic sediments in both the Bancannia and Menindee Troughs, the presence or absence of marine potential source rocks has not yet been established in either trough.

In addition, the graben-like troughs and intervening structural highs of the western Darling Basin are thought to have developed during late Devonian and mid-Carboniferous periods of wrench faulting (Evans, 1977). However, the section across the eastern flank of the Lake Wintlow High (Fig. 4) as interpreted by Evans (1977), indicates that faulting here occurred in the Early Devonian, and that the Lower Devonian pinches out against the basement high beneath Middle Devonian to Lower Carboniferous sediments.

Interpretation of the section therefore suggests that in the Early Devonian the Lake Wintlow High-Wilcannia High was an emergent basement high, and formed a western shoreline during deposition of marine sediments. Elsewhere, the high may not have been entirely emergent in the Early Devonian and Lower Devonian marine sediments may have been deposited over the high and subsequently removed by erosion. From the limited available evidence, the presence of marine potential source rocks has been unequivocally established only in areas east of the Lake Wintlow High-Wilcannia High.

Mid-Devonian to Lower Carboniferous

The thick coarse-grained fluviatile sediments of Middle Devonian to Early Carboniferous age appear to have negligible source potential, owing to their continental affinities and the redbed character of associated fine-grained clastics.

Post Early Carboniferous

A small number of samples from the thin Carboniferous-Permian, Cretaceous, and Cainozoic sediments encountered during drilling of the Murray Basin sequence were analysed for BMR during the course of a continuing Australia-wide BMR source rock evaluation program. Tertiary and Cretaceous samples are generally immature, with the Permian reaching maturity for oil generation; however, most samples have low organic carbon contents and are considered poor potential source rocks.

Petroleum geochemistry

Source rock potential of the Devonian sediments in the Darling Basin was evaluated by geochemical analysis and vitrinite reflectance determinations on core and

cuttings from BMR Ivanhoe No. 1 and six petroleum exploration wells (Tables 1, 2, 3). The analyses were carried out by the BMR Petroleum Technology Laboratory, and by CSIRO Fuel Geoscience Unit and AMDEL under contract to BMR.

Source rock richness

The following chemical analyses were performed in order to evaluate source rock richness: total organic carbon (TOC); total solvent extractable organic matter (EOM); and liquid chromatographic fractionation of the EOM into saturated hydrocarbons (SATS), aromatic hydrocarbons (AROM), and polar or nitrogen, oxygen, sulphur-containing organic compounds (POLAR). Separation of asphaltenes (ASPH) from the EOM, prior to liquid chromatography, was carried out on some of the samples. Mean maximum vitrinite reflectance values R_0 max and the ratios of pristane to nC_{17} ($Pr/n.C_{17}$) and phytane to $n.C_{18}$ ($Ph/n.C_{18}$) are also shown in the data tabulations.

Data from the petroleum exploration wells (Table 2) indicate generally poor source potential: only two samples, from the Lower Devonian Amphitheatre Formation in Berangabah No. 1, have significant TOC values—0.57 and 0.42 per cent. As to be expected, the organic matter extract values are also low and typical of poor source potential.

Three of the 14 core samples of Amphitheatre Formation from BMR Ivanhoe No. 1 gave significant TOC values of 0.46, 0.81 and 0.98 per cent (Table 1), although these are still below average for good quality shale source rock. The source rock ratings in Table 1 were obtained by plotting total hydrocarbons (SATS plus AROM) against TOC (modified after the technique used by Jackson & others, 1980). Based on this plot, two cores are thought to be fair source rocks and the remainder are rated lean to barren.

The age of a rock is important in determining its likely organic content, given the variation of biologic conditions with time, particularly in the Devonian. However, the criterion of significant TOC (>0.5% for clastic rocks) for a rock to be considered a potential generator of hydrocarbons is generally applied irrespective of rock age, but not irrespective of the level of organic maturation, because thermal maturation leads to decreasing total organic carbon content.

The type of organic matter preserved in a sediment is, similarly, partly a function of rock age or the biota prevalent at the time of deposition. Current convention is to use the macerals present (inertinite, exinite, etc) to interpret the nature of the sedimentary kerogen and hydrocarbons (gas or liquid) likely to be generated, again regardless of age. Certainly for Devonian samples, one cannot expect much in the way of woody tissue (i.e. vitrinite) and our results show abundance of inertinite or non-source organic matter.

The saturated hydrocarbons isolated from cores from BMR Ivanhoe No. 1 are, in general, highly paraffinic as indicated by gas chromatographic analyses. Extracts from core samples at depths of 240 m, 250.4 m, 269.7 m, and 300.9 m were lowest in paraffins and richer in naphthenic compounds. This may be due to a significant variation in the type of organic matter or partial biodegradation of the saturated hydrocarbons, preferentially destroying the n-paraffins. Types of organic matter (Table 3) will be discussed in more detail, but examination of the data has shown no obvious relation between the content of n-paraffins in the extract and the type of insoluble organic matter in the core. Bimodal gas chromatograms were obtained for extracts from core samples at 177 m and 200.7 m, implying that the rocks are either marginally mature or immature, but contain mixed kerogen types. However, this conclusion is in conflict with the maturation data to be discussed, which imply relatively high maturation levels.

Organic maturation

It proved difficult to evaluate maturation using the vitrinite reflectance technique, owing to the paucity of organic matter and problems in recognising true vitrinite macerals. Some reflectance data are given in Table 2; those values placed in bracket are considered doubtful, owing to the low number of counts used to calculate the R_0 mean maximum value (R_0 max). The R_0 max values for the Devonian sediments vary from 0.7 per cent to 1.45 per cent, the majority being around 0.9 per cent. Using R_0 max range of 0.7-1.3 per cent as indicative of oil mature sediments, the Upper Devonian, as sampled in Table 2, would appear to be mature for oil and certainly not highly overmature.

Reflectance data for vitrinite in core from BMR Ivanhoe No. 1 are considered very doubtful, owing mainly to the difficulty in recognising true vitrinite macerals, because significant amounts of vitrinite cannot be expected in rocks of this age. Our interpretation shows a reflectance range from 0.85 to 1.8 percent (Table 3) suggesting that the Lower Devonian Amphitheatre Formation at the Ivanhoe location is mature to overmature.

$Pr/n.C_{17}$ and $Ph/n.C_{18}$ ratios from Ivanhoe No. 1 are plotted in Figure 6 and from the work of Connan & Cassou (1980), would appear to imply a mature and possibly overmature section.

Further evidence of possible overmaturity in BMR Ivanhoe No. 1 is given by spore coloration. A few recognisable spores of medium to dark brown colour were noted at a depth of 50 m, but no spores were recognised below this depth (E. Truswell, BMR, personal communication). The colour is considered equivalent to a thermal alteration index of 4, indicative of overmature sediments. A conodont colour alteration index was determined for 15 of 147 conodont elements or fragments recovered from 31 samples from BMR Ivanhoe No. 1 (Jones & others, 1981). It was concluded that the sediments had been subjected to a temperature no greater than 140°C and possibly less than this. This would place the sediments at the upper temperature end of the oil window, generally thought to be in the range 70°-140°C.

Types of organic matter

The type of organic matter in cores from BMR Ivanhoe No. 1 was determined visually (Table 3) after concentration of the organic matter by flotation. Little organic material was obtained in the concentrates, and much of this occurred as irregular structureless grains, either vitrinite or inertodetrinite. Very little exinitic

Table 2. Source rock chemistry of samples from petroleum exploration wells.

Well	*Depth (m)*	*Unit sampled*	*TOC %*	*EOM ppm*	*SATS ppm*	*AROM ppm*	*POLAR ppm*	*ASPH ppm*	R_0 %
Blantyre No. 1[1]	275.8	Permian	0.10	97	9	45	44	—	0.71
	587.9	U. Dev.	0.10	78	16	24	36	—	—
	1425.9	U. Dev. unit 3	0.15	50	11	10	25	—	1.45
Mount Emu No. 1[2]	664.0	M. Dev.	0.17	157	32	10	42	58	—
	928.0	M/L Dev.	0.15	75	3	10	3	36	—
Pondie Range No. 1[1]	265.1	U. Dev. unit 1	0.05	151	0	1	37	—	0.70
	450.8	U. Dev. unit 2	0.10	209	11	14	74	—	(0.78)
	693.5	U. Dev. unit 3	<0.05	36	0	0	30	—	(0.72)
	2110.5	U. Dev. unit 6	<0.05	34	1	2	90	—	(0.90)
	2343.7	U. Dev. unit 7	<0.05	27	0	0	10	—	(0.92)
Bancannia North No. 1[1]	420.8		<0.05	182	8	2	49	—	(0.92)
	1477.6		<0.05	39	1	0	19	—	(0.93)
Berangabah No. 1[3]	33.5-36.6	L. Dev. Ampthitheatre Formation	0.57						
	35.1-36.6	L. Dev. Ampthitheatre Formation	0.42						
	189.0-192.0	L. Dev. Ampthitheatre Formation	0.07						
	243.8-246.9	L. Dev. Ampthitheatre Formation	0.09						
	335.3-338.3	L. Dev. Ampthitheatre Formation	0.15						
	387.1-390.1	L. Dev. Ampthitheatre Formation	0.11						
	408.4-411.5	L. Dev. Ampthitheatre Formation	0.06						
	448.0-451.1	L. Dev. Ampthitheatre Formation	0.17						
Poopelloe Lake No. 1[1]	529.7	Dev. siltstone	0.10	117	0	8	96	—	—
Balranald No. 1[1]	186.3	Tertiary	0.08	1197	34	119	119	—	—
Berri South No. 1[1]	589.0	Tertiary	1.00	1137	197	45	781	—	0.54
Lake Victoria No. 1[4]	553	Cretaceous	0.40	140	—	—	—	—	0.48
	643	Cretaceous	0.17	—	—	—	—	—	0.56
Nadda No. 1[1]	233	Tertiary	0.15	48	11	12	20	—	0.51
	292	Tertiary	0.10	65	2	32	20	—	—
North Renmark No. 1[4]	738	Cretaecous	0.96	1933	—	—	—	—	—
	1096	Permian	0.19	—	—	—	—	—	0.73
	1184	Permian	0.09	—	—	—	—	—	0.74
Tararra No. 1[1]	191	Tertiary	0.15	188	22	42	124	—	0.61
	249	Tertiary	1.05	427	49	60	366	—	0.71
	570	Cretaceous	0.05	94	7	41	46	—	0.96
Wentworth No. 1[1]	550.8	Permian	0.15	126	35	21	37	—	—
	614.5	Permian	0.20	173	22	7	39	—	—

R_0 Values in parentheses are uncertain.
[1] Core, analysed for BMR by CSIRO, Division of Fossil Fuels.
[2] Core, analysed for BMR by Australian Mineral Development Laboratories.
[3] Cuttings, analysed by BMR.
[4] Analysed for BMR by Robertson Research Limited.

Table 3. Organic matter descriptions for Lower Devonian Amphitheatre Formation from BMR Ivanhoe No. 1.

Sample no.	(m)	Organic matter[1] Vitrinite %	Inertinite %	Exinite %	Type of Exinite[2]	TOC %	Vitr refl, R_0 % mean max.
1	29.1	90	—	10	R,S,C	0.46	—
2	61.8	4	95	7	R,S	0.98	1.61
3	90.0	—	100	0	—	0.12	1.25[3]
4	117.0	—	90	10	R	0.02	1.49[3]
5	133.0	—	98	2	R	0.16	1.27[3]
6	170.0	—	97	3	R	0.81	1.11[3], 1.32[3]
7	200.7	—	99	1	R	0.12	1.44[3]
8	215.4	78	19	3	R	0.15	—
9	224.9	51	46	3	R	0.14	1.60
10	240.0	50	50	0	—	0.15	—
11	250.4	56	44	<1	LD	0.08	0.85
12	269.7	64	36	<1	C	0.15	1.57
13	282.6	8	85	5	R	0.29	1.63
14	300.9	30	70	0	—	0.09	1.81

1 Organic matter was concentrated by flotation and then prepared as a polished briquette.
2 R—resinite, S—sporinite, C—cutinite, LD—liptodetrinite.
3 Reflectance measured for 'vitrinite-like' organic macerals.

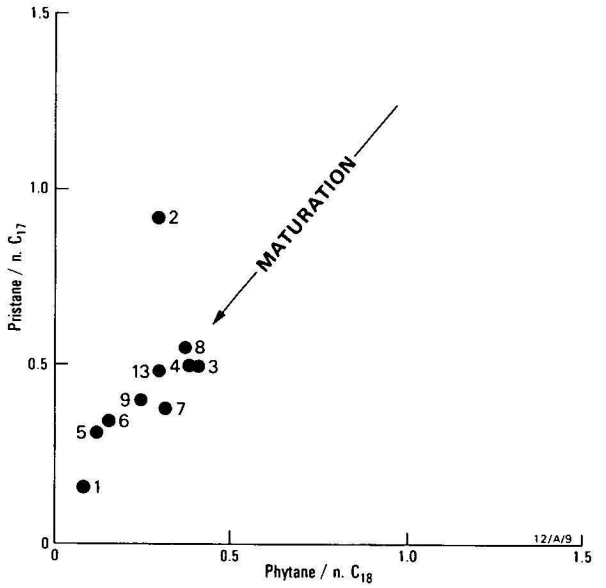

Figure 6. Source rock maturation plot, Amphitheatre Formation, BMR Ivanhoe No. 1.

material (the oil source organic maceral) was recognised. The high inertinite contents recorded dramatically downgrade any source potential, as inertinite is considered incapable of generating hydrocarbons. Those concentrates with significant vitrinite contents (>50 per cent) may be gas sources; however, the generally low TOC values of the samples indicate a low source potential.

Finely disseminated organic matter, concentrated from core from BMR Ivanhoe No. 1 was also examined at BMR (E. Truswell, BMR, personal communication). The organic matter is mostly herbaceous and woody debris, no algal debris is present, and the material is predominantly a gas source.

Hydrocarbon exploration potential

The available, but admittedly limited, geochemical data indicate that the Devonian rocks of the Darling Basin, as we see them today, have low hydrocarbon source potential. However, it is possible that the overmature rocks were a source of hydrocarbons at some time past, but this potential has now been partly thermally destroyed, leading to the low organic carbon and extract values observed. The basin appears to lack oil prone source rocks, and the Lower Devonian sediments were probably a source for gas.

Organic maturation levels could not be interpreted with precision, but the Lower Devonian encountered in BMR Ivanhoe No. 1 on the southeastern flank of the Poopelloe Trough appears to be mature to overmature and the sediments encountered in Poopelloe Lake No. 1, on an up-faulted segment of the central Lake Poopelloe Trough, show incipient metamorphism. Extrapolation of these results suggests that the Lower Devonian approaches metamorphic grade and is overmature in deeply buried parts of the troughs, and is probably mature to overmature on the margins of the troughs. It therefore seems unlikely that any hydrocarbons trapped at depth in Lower Devonian reservoirs could have survived within the troughs. Moreover, mild metamorphism of the eastern Darling Basin, and wrench faulting, rifting, and deep burial of the western Darling Basin during the Devonian to mid-Carboniferous may have contributed to an early generation, early migration, and hence, protracted maturation of hydrocarbons. Therefore, the most prospective areas appear to be the flanks of the troughs, where hydrocarbons (probably gas) may be generated and held in mature to overmature Lower Devonian sediments.

In addition, if marine source rocks are absent from the Bancannia and Menindee Troughs, the Lower Devonian marginal marine play proposed by Evans (1977) is confined to the eastern flank of the Lake Wintlow High-Wilcannia High, where sandstone reservoirs are likely to be suitably juxtaposed to marine source rocks of moderate maturity on the western margins of the Blantyre, Wentworth, and Lake Poopelloe Trough systems. The potential play assumes that suitable sandstone bodies were deposited on the eastern flank of the Lake Wintlow High-Wilcannia High and that they have retained porosity and permeability. Elsewhere, both in outcrop and in the subsurface, Lower Devonian sandstones are usually well-cemented, hard

and tight, and original porosity has largely been destroyed by deep burial. Hence, even if marine source rocks are present in the deeply buried Lower Devonian of the Menindee Trough, we would expect these to be overmature, and porosity and permeability in Lower Devonian reservoirs to have been destroyed. If Lower Devonian marine source rocks occur in the Bancannia Trough, stratigraphic traps in marginal deltaic complexes of the type suggested by Evans (1977) could prove prospective at shallow depths.

Elsewhere, in certain areas of the Darling Basin, such as the Tilpa-Nelyambo Trough, little is known about the stratigraphic and structural development of the Devonian sediments and, hence, the above generalised conclusions regarding hydrocarbon prospectivity may not apply.

The overlying Middle Devonian to Lower Carboniferous continental clastic sequence contains excellent reservoir rocks, but despite the formation of suitable structures during graben formation, the sequence contains no suitable seals. In addition, early generation and migration of hydrocarbons may have resulted in their subsequent escape before deposition of the overlying thin Permian sediments.

Lower Palaeozoic sediments flanking and partly underlying the western Darling Basin are thought to have negligible source potential, and have generally been considered non-prospective for hydrocarbons. Surface outcrops, however, include carbonate and sandstone units (Packham, 1969; Rose & Brunker, 1969; Wilson, 1967) and, although little is known of their subsurface distribution or porosity and permeability characteristics, it is conceivable that reservoirs within Lower Palaeozoic rocks, flanking the Devonian troughs at shallow depths, could host gas generated from the Lower Devonian.

Conclusions

- The Lower Devonian marine sequence of the Darling Basin has a low organic carbon content, is probably gas prone, is thermally mature to overmature within the troughs, and is downgraded as a potential hydrocarbon source rock.
- Potential source and reservoir rocks are only likely to be preserved on trough flanks and margins that have not been deeply buried or tectonically deformed during the Devonian-Carboniferous periods of folding, faulting, and rifting.
- From the limited currently available geochemical and geological data, the most prospective part of the basin appears to be the eastern flank of the Lake Wintlow High-Wilcannia High, where potential reservoir rocks, at relatively shallow depths, are likely to be suitably juxtaposed to potential source rocks.
- The currently available data also suggest that the Mid-Devonian to Lower Carboniferous, Permian, and Cretaceous sequences are non-prospective for hydrocarbons, but potential within the block-faulted Lower Palaeozoic rocks flanking the Devonian troughs cannot be entirely eliminated.
- The results of the study give little encouragement to hopes for adequate source potential in the Devonian rocks of the Darling Basin, and tend to confirm previous assessments of poor hydrocarbon prospectivity. However, caution should be exercised in extrapolating the results to other parts of the basin, and they need to be viewed in the context of a limited sample base in an inadequately explored basin.

Acknowledgements

The authors gratefully acknowledge the contribution of BMR colleagues in all phases of the Darling Basin project: C. Simpson for the interpretation of ERTS imagery, BMR drilling staff for support during field operations, E. Truswell for microscopic examination of samples, R. Nicoll for conodont examination, Z. Horvath for laboratory determinations of carbon abundances, and E. Nicholas and D. Forman for suggestions and criticisms of drafts of this manuscript. We are also grateful to P. R. Evans for helpful comments on the manuscript. The NSW Department of Mineral Resources and Development contributed cuttings from the Berangabah No. 1 well for inclusion in this study.

References

ALLIANCE OIL DEVELOPMENT AUSTRALIA, 1968a—Lake Wintlow seismic survey, P.E.L. 52, New South Wales, by Geophysical Associates Pty Ltd. *Bureau of Mineral Resources, Australia, Petroleum Search Subsidy Acts File* 68/3031 (unpublished).

ALLIANCE OIL DEVELOPMENT AUSTRALIA, 1968b—Evaluation of the Cambro-Ordovician prospects of the Scopes Range Area, P.E.L. 52, New South Wales. *Internal company report* (unpublished).

ANFILOFF, W., BARLOW, B. C., MURRAY, A. S., DENHAM, D., & SANFORD, R., 1976—Compilation and production of the 1976 Gravity Map of Australia. *BMR Journal of Australia Geology & Geophysics*, 1(4), 273-6.

BAARDA, F. D., 1968a—Planet Bancannia South No. 1 well completion report for Planet Exploration Co. Pty Ltd, by Cundill Myers and Associates Pty Ltd. *Bureau of Mineral Resources, Australia, Petroleum Search Subsidy Acts File* 67/4268 (unpublished).

BAARDA, F. D., 1968b—Planet Bancannia North No. 1 well completion report for Planet Exploration Co. Pty Ltd. *Bureau of Mineral Resources, Australia, Petroleum Search Subsidy Acts File* 67/4277 (unpublished).

BAKER, C. J., 1978—Geology of the Cobar 1:100 000 sheet. *Geological Survey of New South Wales, Sydney.*

BAKER, C. J., SCHMIDT, B. L., & SHERWIN, L., 1975—Revised stratigraphy of the Cobar-Gunderbooka area. *Geological Survey of New South Wales, Quarterly Notes*, 20, 1-14.

BAUER, J. A., MATHUR, S. P., STAGG, H. M. J., HARRISON, P. L., 1979—A proposal for a seismic survey in the western Darling Basin, New South Wales. *Bureau of Mineral Resources, Australia, Record* 1979/25 (unpublished).

BEAVER (Exploration Australia, N.L.), 1973—Menindee regional seismic survey, P.E.L.'s 193,197, New South Wales, by G.E.S. Pty Ltd. *Bureau of Mineral Resources Australia, Petroleum Search Subsidy Acts File* 73/250 (unpublished).

BEMBRICK, C. S., 1974—Murray Basin. *In* MARKHAM, N. L. & BASDEN, H., (editors), The mineral deposits of New South Wales. *Geological Survey of New South Wales, Sydney.* 555-68.

BEMBRICK, C. S., 1976a—Darling Depression. *In* LESLIE, R. B., EVANS, H. J., & KNIGHT, C L., (editors), Economic geology of Australia and Papua New Guinea, Vol. 3—Petroleum. *Australasian Institute of Mining and Metallurgy, Monograph* 7, 398-400

BEMBRICK, C. S., 1976b—Bancannia "Trough". *In* LESLIE, R. B., EVANS, H. J., & KNIGHT, C L., (editors), Economic geology of Australia and Papua New Guinea, Vol. 3—Petroleum. *Australasian Institute of Mining and Metallurgy, Monograph* 7, 254-8.

BMR, 1976—Geology of Australia, 1:2 500 000 scale geological map. *Bureau of Mineral Resources, Australia, Canberra.*

CONNAN, J., & CASSOU, A. M., 1980—Properties of gases and petroleum liquids derived from terrestrial kerogen at various maturation levels. *Geochimica et Cosmochimica Acta*, 44, 1-23.

DOUTCH, H. F., & NICHOLAS, E., 1978—The Phanerozoic sedimentary basins of Australia and their tectonic implications. *Tectonophysics*, 48, 365-88.

EVANS, P. R., 1977—Petroleum geology of western New South Wales. *The APEA Journal*, 17(1), 42-9.

GLEN, R. A., 1979a—The Mulga Downs Group and its relation to the Amphitheatre Group southwest of Cobar. *Geological Survey of New South Wales, Quarterly Notes*, 36, 1-10.

GLEN, R. A., 1979b—Relations between the Amphitheatre and Mulga Downs Groups, in the Buckambool area, southwest of Cobar. *Geological Survey of New South Wales, Report* GS 1979/070 (unpublished).

JACKSON, K. S., HAWKINS, P. J., & BENNETT, A. J. R., 1980—Regional facies and geochemical evaluation of the southern Denison Trough, Queensland. *The APEA Journal*, 20(1), 143-58.

JONES, P. J., STRUSZ, D. L., & NICOLL, R. S., 1981—A short note on an Early Devonian marine fauna from BMR Ivanhoe No. 1 Bore. *Bureau of Mineral Resources, Australia, Professional Opinion* GEOL 1981/002 (unpublished).

LONGWORTH & MCKENZIE PTY LTD & WONGELA GEOPHYSICAL PTY LTD, 1979—Petroleum exploration of the Darling Depression. *Report for New South Wales Department of Mineral Resources and Development* (unpublished).

PACKHAM, G. H., (Editor), 1969—The geology of New South Wales. *Journal of the Geological Society of Australia*, 16(1).

PASSMORE, V. L., 1981—BMR Ivanhoe No. 1 well completion report. *Bureau of Mineral Resources, Australia, Record* 1981/26 (unpublished).

PLANET OIL COMPANY, 1966—Bancannia seismic survey, P.E.L. 114, New South Wales, by Namco Geophysical Company. *Bureau of Mineral Resources, Australia, Petroleum Search Subsidy Acts File* 66/11094 (unpublished).

PLANET OIL COMPANY, 1968—Nucha seismic survey, P.E.L. 114, New South Wales, by Planet Management and Research Pty Ltd. *Bureau of Mineral Resources, Australia, Petroleum Search Subsidy Acts File* 68/3021 (unpublished).

POGSON, D. J., 1972—Geological Map of New South Wales, scale 1:1 000 000. *Geological Survey of New South Wales, Sydney.*

POGSON, D. J., & FELTON, E. A., 1978—Reappraisal of geology, Cobar-Canbelego-Mineral Hill region, Central Western New South Wales. *Geological Survey of New South Wales, Quarterly Notes*, 33, 1-14.

RANNEFT, T. S. M., 1968—Berangabah No. 1 well completion report. *Texam Oil Corporation internal company report* (unpublished).

ROSE, G., 1974—White Cliffs 1:250 000 Geological Series Explanatory Notes. *Geological Survey of New South Wales, Sydney.*

ROSE, G., & BRUNKER, R. L., 1969—The upper Proterozoic and Phanerozoic geology of northwestern New South Wales. *Proceedings of the Australasian Institute of Mining and Metallurgy*, 229, 105-20.

SCHNEIBNER, E., 1976—Explanatory notes on the Tectonic Map of New South Wales, scale 1:1 000 000. *Department of Mines, Geological Survey of New South Wales, Sydney.*

SMITH, E. R., 1977—Australia's onshore basins: their petroleum prospects and future exploration programs. *The APEA Journal*, 17(2), 17-23.

STRUSZ, D. L., 1966—Report on specimens of possible Devonian age, submitted by American Overseas Petroleum Ltd. *Bureau of Mineral Resources, Australia, Technical File* N/SH/ 54-16, Wilcannia (unpublished).

THORNTON, R. C. N., 1974—Hydrocarbon potential of western Murray Basin and infrabasins. *Geological Survey of South Australia, Report of Investigations*, 41.

THORNTON, R. C. N., 1976—Murray Basin and associated infrabasins. *In* LESLIE, R. D., EVANS, M. J., & KNIGHT, C. L., (editors), Economic geology of Australia and Papua New Guinea, Vol. 3—Petroleum. *Australasian Institute of Mining and Metallurgy Monograph* 7, 91-4.

WEBBY, B. D., 1972—Devonian geological history of the Lachlan Geosyncline. *Journal of the Geological Society of Australia*, 19(1), 99-123.

WILSON, R. B., 1967—Geological appraisal of the Mootwingee area, New South Wales, *The APEA Journal*, 7(2), 103-14.

WILTSHIRE, M. J., 1970—Poopelloe Lake No. 1, well completion report, N.S.W. Oil and Gas Company N.L. *Bureau of Mineral Resources, Australia, Petroleum Search Subsidy Acts File* 69/2014 (unpublished).

WYATT, B. W., YEATES, A. N., & TUCKER, D. H., 1980—A regional review of the geological sources of magnetic and gravity anomaly fields in the Lachlan Fold Belt of NSW. *BMR Journal of Australian Geology & Geophysics*, 5, 289-300.

BMR Journal of Australian Geology & Geophysics, 7, 35-45.

RELATIVE FALL OF HOLOCENE SEA LEVEL AND COASTAL PROGRADATION, NORTHEASTERN SPENCER GULF, SOUTH AUSTRALIA

R. V. Burne*

The levels of intertidal environments of prograding Holocene coastal complexes of northeast Spencer Gulf have been precisely measured and their relation with the tidal range determined. Beach ridges and the top of subtidal *Posidonia* sea-grass deposits are the best indicators of relative sea level. Bases of active beach ridges range from +1.1 m to +1.8 m A.H.D. (Australian Height Datum) and the upper limit of *Posidonia* growth is <—2 m A.H.D. The elevation of old preserved examples of these facies has been established along transects across intertidal and supratidal plains. ^{14}C dating has been carried out on unaltered mollusc shells recovered from beach ridges and the base of the regressive intertidal facies above the subtidal sea-grass facies. Sea-grass root fibres and shell hash from the top of the buried subtidal facies have also been dated. A Holocene sea-level history has been constructed for northeast Spencer Gulf, and shows the following events: 6000-4000 years B.P.—probable construction of a shingle ridge at +3–4 m at the peak of the Holocene transgression, followed by about 1 m fall of sea level, but little progradation, owing to low rates of carbonate production; 4000-3000 years B.P.—formation of regressive carbonate shorelines with fall of relative sea level from about +2 m to about +1.5 m, and the construction of beach ridges; 3000-2000 years B.P.—no beach ridge construction along surveyed transects, but continued progradation of shorelines with a further 1.0 m fall in relative sea level; 2000 years B.P. to Present—construction of beach ridges accompanied shore-line progradation, and a fall in relative sea level of 0.5-1.0 m. A contributing cause of relative movement of sea level in the region may be continuing tectonic uplift, as evidenced by the high seismicity of the adjacent Flinders Ranges.

Introduction

Prograding coastal complexes have accumulated along the northeastern margin of Spencer Gulf during the Holocene (Fig. 1). They are composed of calcareous, terrigenous, evaporitic, and algal sediments, which preserve a depositional record of marine transgression and subsequent regression. Evidence of former intertidal environments within the complexes provides a basis for the study of Holocene shoreline evolution and relative sea level described in this paper.

Intertidal environments and sea level indicators

Mean tidal range for northern Spencer Gulf is about 1.5 m, with spring tides commonly having a range of over 3.0 m. Meteorological effects may add as much as 1 m to predicted tides (Radok, 1978; Radok & Raupach, 1977). These short term variations in sea level give rise to a broad intertidal zone up to 3.5 km wide at the seaward margin of the coastal complexes. Environmental subdivisions have been recognised in the intertidal zone, reflecting variation in the frequency and duration of tidal inundation and exposure to wave action (Burne & Colwell, in press). On exposed shores the sediments are dominantly sandy, with shell beaches forming high in the intertidal zone. Protected shores are characterised by muddy sediment, much of which is laid down in relatively tranquil intertidal environments in the lee of mangroves that colonise the mid-intertidal zone. On both types of shore a major distinction exists between a bioturbated homogenised facies low in the intertidal zone and a laminated facies high in the intertidal zone.

The elevation ranges of environmental sub-divisions of the intertidal zone have been precisely determined along surveyed transects, selected after examination of aerial photographs and field study. Elevations were determined by a field party from the Australian Survey Office, led by Mr P. Rumbold. Levels along the transects were connected to existing bench marks that had been tied to Australian Height Datum (A.H.D.), which represents a point a little higher than the mid-point of the tidal range at Port Pirie (Fig. 2). Rumbold (personal communication, 1978) has estimated the accuracy of transect levels relative to the datum of the Port Pirie tide gauge (zero of which has been determined at −1.907 m A.H.D.). At the most distant site, north of Red Cliff Point, the transect levels are accurate to within 0.1 m compared with the tide gauge, and at the closest site, north of Wood Point, to within 0.06 m.

The elevations have been related to tidal inundation data derived from Port Pirie tide records, which have been kept continuously since 1917. The data presented in Figure 2 give, for each elevation across the tidal range, the percentage of time inundated by the tide. These data were computed from tidal records for the year 1974, with the extremes of the range being the maximum and minimum heights recorded over the period 1917-1978.

The inundation ranges of the environments in which sedimentary facies form that could be used as sea-level indicators are also given in Figure 2. Their relations demonstrate that beach ridges and mangrove stands are not really precise indicators of sea level in areas of moderate tidal range, such as Spencer Gulf. Bases of active beach ridges range from +1.1 m to +1.8 m (A.H.D.) and the seaward margin of mangrove colonisation varies from −0.4 m to + 1.0 m (A.H.D.).

Deposits of sea grass areas may have some use as indicators of sea level. Most sea grasses are subtidal, although *Zostera* extends into the low intertidal zone. *Posidonia* is entirely subtidal in occurrence, and has a characteristic fibrous root-system, which is preserved in a distinctive sedimentary facies of grey, poorly-sorted carbonate sand, often containing articulated bivalves and gastropod shells. The top of this facies, preserved beneath the intertidal flat, may be taken as having formed at or below a former minimum tide level.

* Baas Becking Geobiological Laboratory, P.O. Box 378, Canberra City, ACT 2601

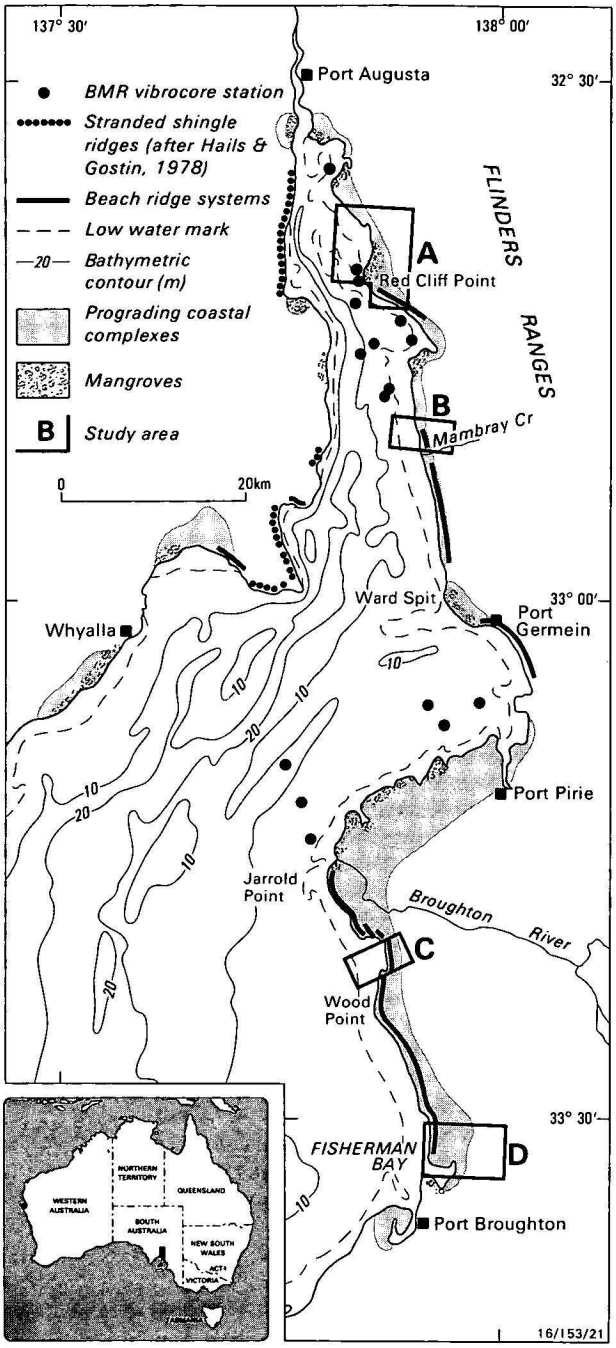

Figure 1. Location and exent of Holocene prograding coastal complexes, northern Spencer Gulf.

Evidence for altered shore lines

The coastal complexes show evidence of shoreline progradation and marine regression. Successive shell beach ridges form seaward-accreting systems; stranded shell beach ridges occur in inland areas of the coastal complexes; and tidal creeks between Port Pire and Jarrold Point pass landwards into areas that are now cultivated fields, but in which traces of filled creeks are visible from the air.

A sedimentary sequence that preserves a record of Holocene marine regression has been found in cores through the coastal complexes. It consists of a facies of subtidal sands, rich in sea-grass fibre, overlain by intertidal shelly sands, and either a thin supratidal clay facies or beach-ridge shell grit at the surface (Fig. 3).

Evidence for sea-level change during the Holocene

Evidence for changed sea level in Spencer Gulf has been described by Hails & Gostin (1978). Stranded shingle beach deposits, composed largely of terrigenous material, have been identified between Whyalla and Port Augusta, along the northwestern shore of the Gulf (Fig. 1). They form well-preserved ridges, 3-5 m above present mean sea level, which are thought to have formed when sea level stood some 3 m higher than at present. However, although shells from the seaward margin of this ridge system have yielded a Holocene ^{14}C age, the ridges are thought to have formed during the Late Pleistocene (Hails & Gostin, 1978; Gostin & others, 1981). Gostin & others (1981) concluded from a study of the Holocene beach ridge system on the northeastern shore of Spencer Gulf that sea level has been within about 1 m of its present elevation for the past 5000-6000 years.

In order to see if the shell beach ridges observed in our study contained evidence of changed sea level, the transects surveyed across the intertidal zones were extended across the width of the coastal complexes (Fig. 4) and the elevation of any stranded beach ridge intersected was measured precisely. Seven of the transects crossed stranded shell ridges. Some ridges have been considerably modified by deflation or floodwaters, but nevertheless, all show an increase in elevation landward from the present shore (Fig. 5).

The upper boundary of the subtidal sea-grass facies at the base of the regressive sequence has been traced in cores and pits along two transects (Fig. 5, transects F-F′ & G-G′), and, along both, rises gradually and consistently landwards. Unfortunately, these transects end low in the intertidal zone and do not continue to the present subtidal zone of living *Posidonia.*

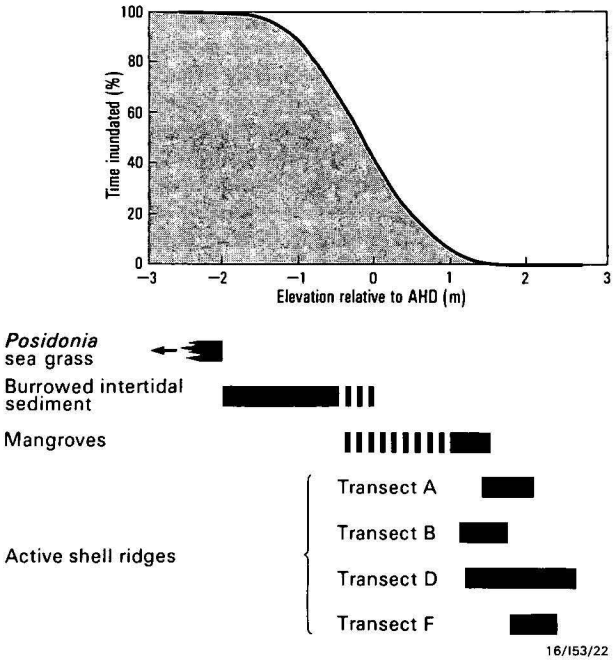

Figure 2. Elevation range of intertidal environments and their relative tidal inundation periods.

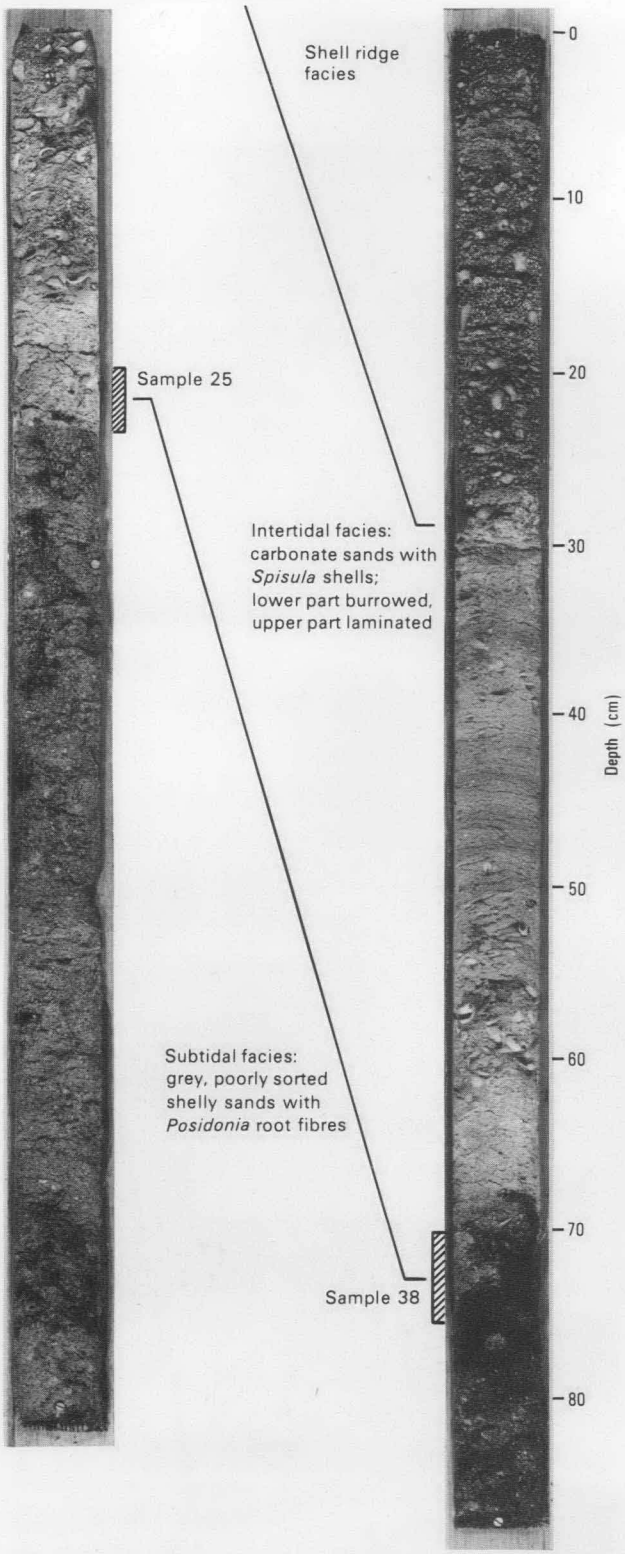

Figure 3. Regressive sequences shown in cores from transect G-G′, Fisherman Bay.

^{14}C dating

^{14}C dating has been used to establish a time scale for shoreline progradation and relative sea-level fall.

Analysis and reporting

35 samples were analysed in the laboratories of the University of New South Wales by Mr Djohadze, and 5 samples at Beta Analytic, Florida, by Dr Stipp. The sample data and results are presented, in accordance with the recommendations of Stuiver & Polach (1977), in Table 1. An environmental correction of -450 ± 35 years has been applied to the Holocene carbonate and fibre samples results to allow for the sea-water reservoir origin of the dated carbon. This correction was determined by Gillespie & Polach (1980) from analyses of molluscs taken alive from south-east Australian waters prior to the detonation of nuclear devices in the atmosphere. No such correction has been applied to the *Anadara* dates, δ^{13}C corrections have been made using estimated δ^{13}C values of $0 \pm 2‰$ for shell samples (Hudson, 1977; Stuiver & Polach, 1977) and $-5 \pm 2‰$ for fibre samples (Polach, personal communication, 1982).

Material selected

Samples for dating were selected from four situations; shell beach ridges; the base of the intertidal facies of the regressive sequence underlying the coastal complexes; the top of the subtidal sea-grass facies in the regressive sequence; and shells of *Anadara* found lying on the intertidal flat. Sample locations are given in Figure 4.

Beach ridges. These morphologically distinct features are constructed mainly from shells of subtidal and intertidal molluscs, which have been transported landwards by wave action during the rising tide. Cores through the ridges show that they rest on sediments of the intertidal flat.

24 samples were dated. Most samples were composed entirely of *Spisula* shells, a bivalve which inhabits the low intertidal zones. Shortages of apparently fresh material in some of the older ridges necessitated samples of other kinds of molluscs. The ages obtained date the death of the organisms forming the shells, which, obviously, predates their addition to the ridges. Ridges considered to be active yielded corrected ages of 220 ± 87 years and -137 ± 78 years (samples NSW 273 and NSW 354).

Base of the intertidal facies. 10 samples were collected from pits dug in the intertidal and supratidal plain at a horizon immediately above the top of the grey, subtidal sea-grass facies of the regressive sequence. The samples, *Spisula*, are not noticeably present in the subtidal sea-grass facies and are taken to have formed almost in situ during the earliest colonisation of the low intertidal zone during regression. However, articulated specimens have not been observed, and all shells have undergone some reworking.

Top of the subtidal sea grass facies. The top of this facies, representing the end of subtidal conditions, was sampled from three cores, one taken from the intertidal flat at Wood Point, and two from the supratidal plain at Fisherman Bay. Each sample was divided into a fibre sub-sample and a shell-hash sub-sample. The sea-grass fibres are assumed to have formed in place, and probably give a date closer to the end of subtidal conditions than does the shell hash, which may have been derived from elsewhere. Two sample pairs of shell hash and fibre were dated. One pair gave good age agreement, the other gave a shell-hash date some 2000 years older than the fibre date. A third sample did not contain enough fibre for analysis, and the shell hash alone was dated.

Figure 4. Aerial photographs of study areas, showing surveyed lines of transects and location of ^{14}C samples.

4a. Red Cliff Point.

Note: former shoreline with stranded beach ridges between A and B; supratidal plain; mangroves and tidal creeks on protected northwest-facing coast; and beach-ridge accumulation on exposed south-facing coast. Dark areas offshore are colonised by sea grass.

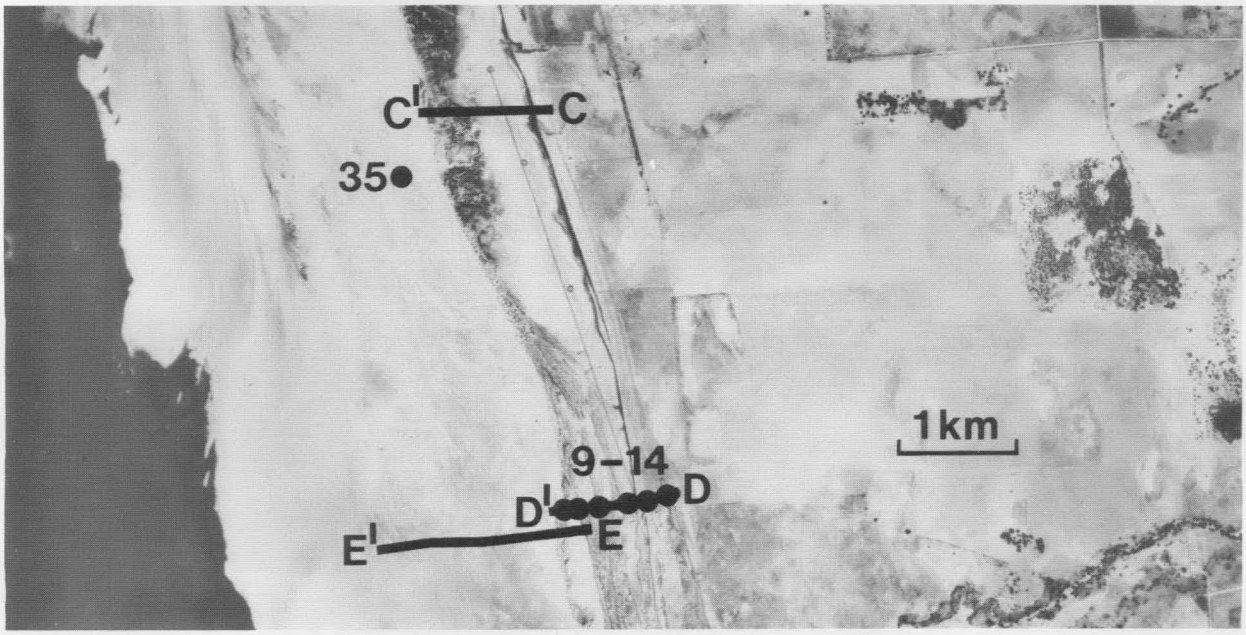

4b. Mambray Creek.

Note: stranded beach ridge between C and D; beach ridge system truncated to the north (similar truncation occurs to the south of the area shown); broad intertidal flat; and location from which *Anadara* (sample 35) was collected. Dark subtidal areas to left are colonised by sea grass.

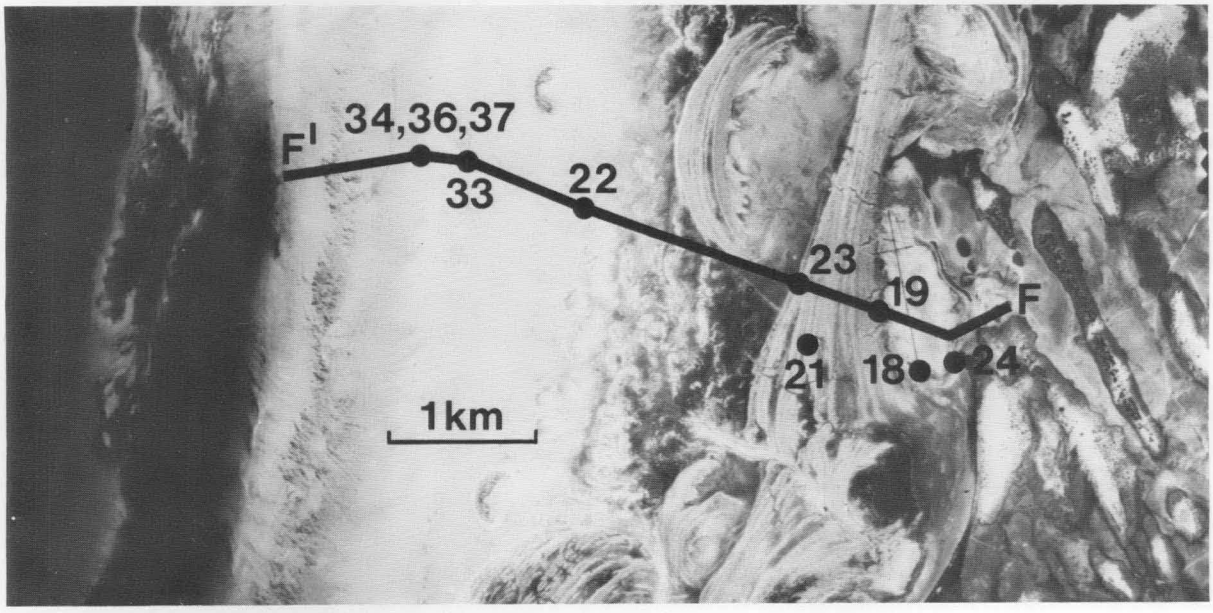

4c. North of Wood Point.

Note: gypsum lakes fed by continental groundwater springs landward of beach ridges; old Pleistocene linear dunes at extreme right; beach ridge systems; broad intertidal flat; and area of subtidal colonisation at right.

Anadara from the tidal flat. The bivalve *Anadara trapezia* is not thought to have lived in Spencer Gulf since the last interglacial (Gill, 1972; 1977; Gostin & others, 1981). Its presence in the shingle ridges described by Hails & Gostin (1978) has been taken to indicate a Pleistocene age for that deposit.

Apparently fresh, unabraded *Anadara* shells are scattered over the modern intertidal flat, north of Mambray Creek, and incorporated into sediments of the Holocene tidal flat. One sample of these shells (NSW 357, Fig. 4b) was dated to test the interpretation that they represent reworked Pleistocene material. The resulting age of 23 600 ± 600 years is suspect and may reflect some diagenetic alteration of the sample, but it precludes a Holocene origin for the shells.

Sample purity

Samples of shell hash were crushed and analysed without further preparation, owing to the small size of the available sample. Separated sea-grass fibres were washed in acid, rinsed, and dried. The mollusc shell samples were cleaned with a wire brush, leached in

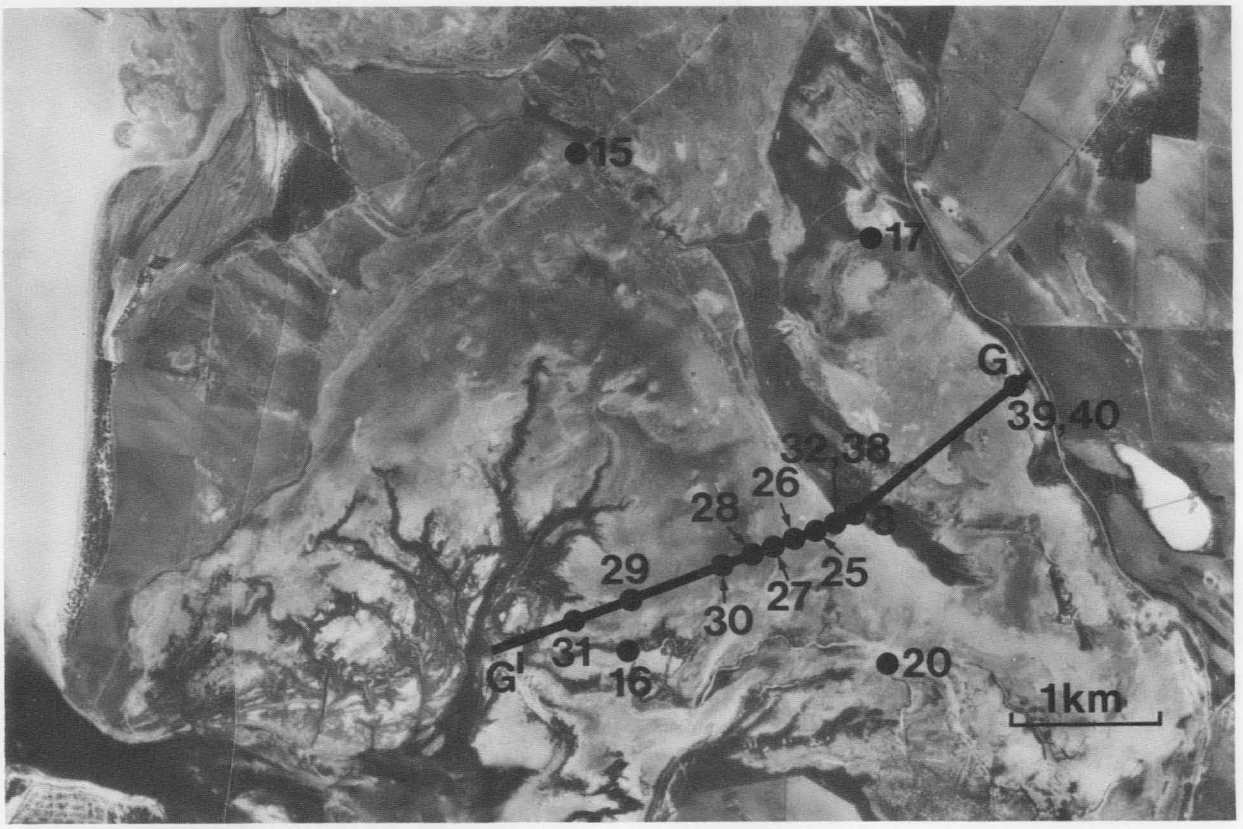

4d. Fisherman Bay.
This is a restricted embayment. Open gulf waters are to the left, mouth of the bay is at bottom left. Note: beach ridges accumulating around cores of old Pleistocene linear dunes; tidal creek systems; and broad supratidal plain.

acid, and then powdered. Aliquots were then examined by XRD. The *Anadara* sample was composed of aragonite with traces of calcite, which suggests the possibility of diagenetic alteration in this sample, which might give rise to an artificially young age for the shells. All other analyses showed aragonite alone, and the samples are assumed to have been unaltered.

^{14}C ages and evidence for rates of sea level change

Three indicators of former sea level have been dated: stranded shell ridges; the base of the intertidal facies of the regressive sequence; and the top of the underlying subtidal sea-grass facies in the regressive sequence. The relation between these features and former sea level may be estimated by comparing the position of currently forming similar features with present-day sea level.

Beach ridges

The level of the crest and seaward base of the stranded ridges are generally both well-marked features, although they may have undergone some modification. Ridge crests may be lowered by deflation or erosion by surface water runoff; seaward bases may be buried by the accretion of younger ridges, or modified by later flood waters. The apparently unmodified examples of seaward bases of ridges have been taken to be more reliable indicators of former sea level. As noted in the introduction, the seaward bases of active ridges range from 3.2 m to 3.7 m above normal low tide level (i.e. +1.1 m to +1.8 m A.H.D., Fig. 2).

The range of ages obtained and the elevation of both crest and seaward base for the sampled shell ridges are presented in Table 1. Ridges considered to have experienced appreciable morphological modification are indicated.

Base of the intertidal facies

This is identified by the lowest *Spisula*-bearing sediments overlying the top of the sea-grass facies. To allow for the effects of burrowing, it is assumed that these sediments are equivalent to those forming about −0.5 m relative to A.H.D. in the present intertidal zone (Fig. 2). Age ranges for this horizon and the elevation of the samples are given in Table 1 (Samples 25-34).

Top of the subtidal facies

The top of the grey fibre-bearing facies is readily identified, and is assumed to have formed below former minimum tide level, although it is possible that, despite there being now no evidence of appreciable erosion, the surface formed by erosion of older subtidal deposits during regression. Age ranges and present elevation of sample locations are given in Table 1.

Results

Rates of shore line progradation

Red Cliff Point area (Fig. 4a). The oldest date reported for the Red Cliff Point area is a reservoir-corrected age of 5020 ± 105 B.P., quoted by Gostin & others (1981), who suggested that shoreline progradation of

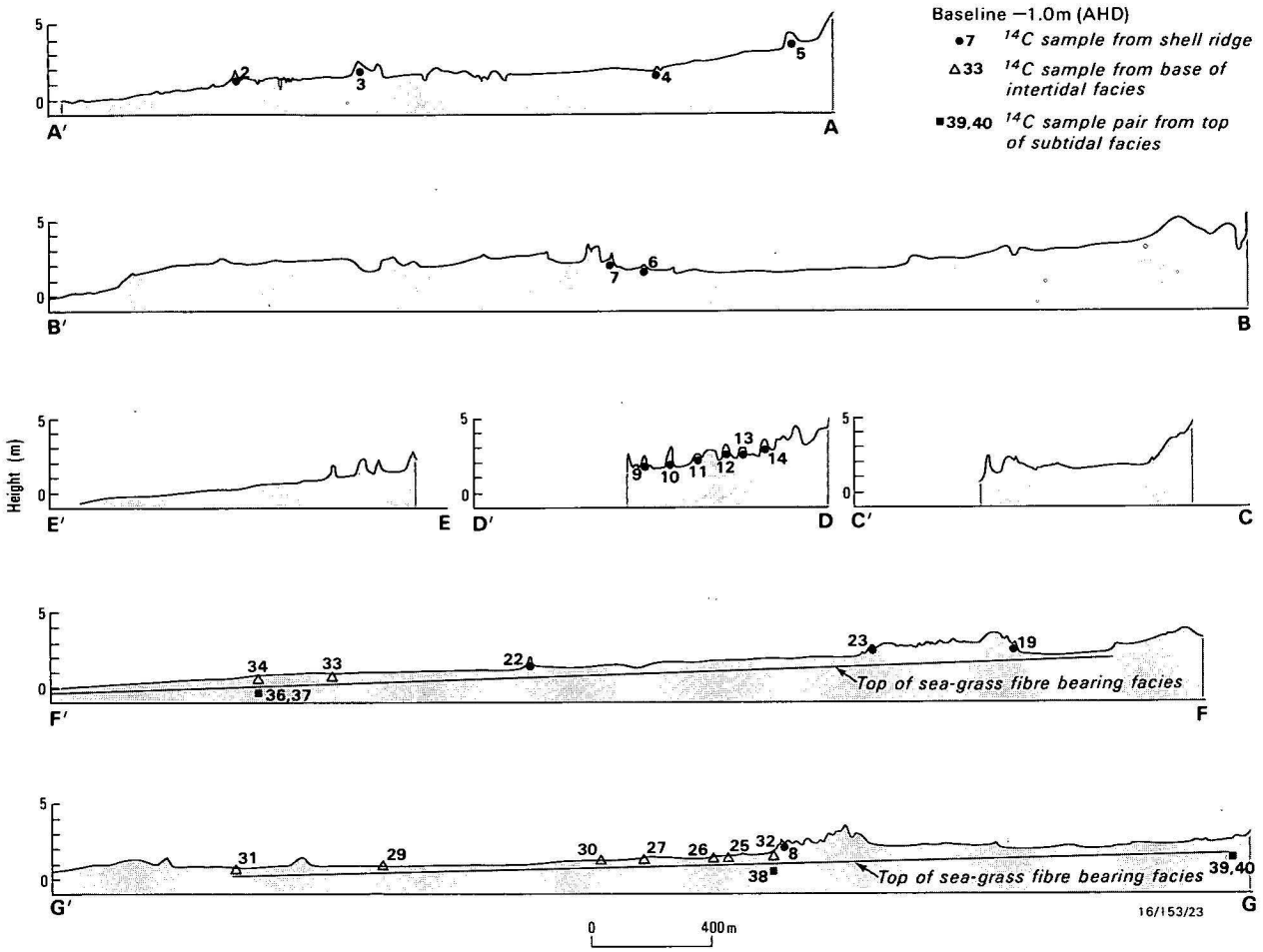

Figure 5. Sections along transects through beach ridge systems, showing sample locations and facies boundaries.

8.4 km had occurred in the area over the last 5000-6000 years. Our results show evidence for gradual accretion of the shore, to a maximum of 3.6 km perpendicular to the old shoreline, over the past 4060 years (Table 1). During progradation, the nature of the shore north of Red Cliff Point has evolved from an exposed shell-ridge coast to a protected mangrove-colonised coast.

Mambray Creek area (Fig. 4b). Unfortunately the landward shell-ridge sample (NSW 283) provided a young ^{14}C date, which is unacceptable for dating the origin of the ridge. Dates on the ridges seaward of this ridge suggest that 0.5 km of progradation has taken place over the past 1560 years ,Table 1). The similarity in age of the seaward shell ridges may be explained by the redistribution, by longshore drift, of shells from slightly older ridges undergoing erosion to the south into presently active ridges (Fig. 4b).

South of Mambray Creek the growth of Ward Spit has sheltered the shore to the north, and has transformed the prograding shoreline from an exposed area of beach ridge accumulation to a protected mangrove-colonised coast (Fig. 1).

Wood Point (Fig. 4c). A transect across the embayment between Jarrold Point and Wood Point indicates progradation of about 2.6 km over the past 4400 years (Table 1). The sheltering effect of the seaward advance of adjacent promontories may account for the decrease in numbers of shell ridges accumulating with time along this transect.

Fisherman Bay (Fig. 4d). The oldest shell-ridge date obtained in this area is 3970 ± 106 years B.P. (NSW 358). The inferred rates of progradation vary from 1 km to 4 km over the past 4000 years (Table 2). Some reversals occur in the age of shells from the base of the intertidal facies along a transect landwards across the intertidal plain. These probably reflect local redistribution of old shell material. Dates from the top of the sub-tidal facies suggest 5 km of progradation in the last 4000 years.

Variations in sea level

Rates of sea-level fall, obtained by computing regression lines for age and elevation data for apparently unaltered seaward bases of stranded ridges, are shown for the various areas in Table 2. The results range from a rate of sea-level fall of 0.3 m/1000 years for the Wood Point area to 0.7 m/1000 years for Mambray Creek.

The gradual and consistent increase in elevation of the top of the subtidal facies of the regressive sequence in the Wood Point and Fisherman Bay areas indicates maximum sea levels up to 5 m higher than present. The horizon has not been extensively dated, but in the Fisherman Bay area rates of sea-level fall of 0.7-1.1 m/1000 years are indicated (Table 2). Rates of sea-level fall indicated by dates on this surface at Wood

Table 1. ^{14}C sample data, including height ranges, suggested former sea levels, and progradation rates.

BMR sample no.	Lab. code & no.	Transect	Location[1]	Environment[2]	Material[3]	Mineralogy[4]	$D^{14}C‰$[5]	Conventional age (yrs. B.P.)	Corrected age[6] (yrs. B.P.)	Sample (%)	Sample elevation (metres AHD) A[7]	Sample elevation (metres AHD) B[8]	Former sea level H[9]	Former sea level R[10]	Progradation D[11]	Progradation ΔD[12]
1	NSW 272	—	R	SR	M	1	—429.4± 7.9	4510±110	4060±115	100	2.4	2.8	0.9	X	3.6	0.9
2	NSW 273	A	NR	SR	M	1	— 80.1± 9.1	670± 80	220± 87	100	1.4	2.1	—	X	0.0	0.0
3	NSW 284	A	NR	SR	S	1	—206.7± 8.8	1860± 90	1410± 97	100	1.7	2.6	0.3	X	0.5	0.3
4	NSW 285	A	NR	SR	S	1	—258.3±10.1	2400±110	1950±115	60.34	2.0	2.3	0.6	X	1.3	0.6
5	NSW 286	A	NR	SR	S	1	—384.7±15.0	3900±200	3450±203	49.53	3.2	4.2	1.8	X	2.0	0.6
6	NSW 275	B	R	SR	M	1	—421.0± 7.8	4390±110	3940±115	100	2.0	3.1	0.5	X	2.0	0.5
7	NSW 276	B	R	SR	M	1	—404.1± 8.1	4160±110	3710±115	100	1.7	2.1	0.3	X	1.8	0.5
8	NSW 277	G	FB	SR	M	1	—176.3± 8.3	1560± 80	1110± 87	100	1.7	2.7	0.3	O	2.6	2.3
9	NSW 278	D	M	SR	S	1	—146.2± 9.5	1270± 90	820± 97	100	1.2	2.4	—	X	—	0.0
10	NSW 279	D	M	SR	S	1	—133.9±10.2	1160± 90	710± 97	100	1.6	3.0	0.2	X	0.2	0.3
11	NSW 280	D	M	SR	S	1	—144.7±10.0	1260± 90	810± 97	100	1.8	2.6	0.4	X	0.4	0.5
12	NSW 281	D	M	SR	S	1	—210.8± 8.6	1900± 90	1450± 97	100	2.1	3.0	0.7	X	0.6	0.4
13	NSW 282	D	M	SR	M	1	—211.7± 8.3	2010± 90	1560± 97	100	2.3	3.0	0.9	X	0.8	0.5
14	NSW 283	D	M	SR	M	1	— 96.6± 8.3	810± 80	360± 87	100	2.3	3.5	0.9	O	1.1	—
15	NSW 349	—	FB	SR	S	1	—247.6± 8.8	2290± 90	1840± 97	100	?	?	—	O	3.6	1.9
16	NSW 350	—	FB	SR	S	1	—308.2± 7.7	2960± 90	2510± 97	100	?	?	—	O	1.1	0.4
17	NSW 358	—	FB	SR	S	1	—423.1± 7.1	4420±100	3970±106	100	?	?	—	O	3.9	1.0
18	NSW 351	—	W	SR	M	1	—452.9± 7.7	4850±110	4400±115	100	?	?	—	O	2.6	0.6
19	NSW 352	F	W	SR	M	1	—359.2± 7.5	3590± 90	3130± 97	100	2.7	3.0	1.3	X	2.2	0.7
20	NSW 359	—	FB	SR	M	1	—318.0± 8.0	3080± 90	2630± 97	100	?	?	—	O	2.8	1.1
21	NSW 353	—	W	SR	S	1	—245.2± 8.5	2260± 90	1810± 97	100	2.8	2.9	1.4	X	2.0	1.1
22	NSW 354	F	W	SR	S	1	— 40.6± 8.0	330± 70	—130± 78	100	1.8	2.4	0.4	X	0.0	0.0
23	NSW 355	F	W	SR	S	1	—151.2± 8.7	1320± 80	970± 87	100	2.4	3.0	1.1	X	1.5	1.5
24	NSW 356	—	W	SR	S	1	—396.2± 7.2	4050±100	3600±106	100	3.0	3.2	1.6	O	2.7	0.8
25	NSW 360	G	FB	BI	S	1	—261.2± 8.1	2430± 90	1980± 97	100	1.4	0.4	1.5	X	2.5	1.3
26	NSW 364	G	FB	BI	S	1	—366.7± 7.8	3670±100	3220±106	100	1.4	0.4	1.4	—	2.3	0.7
27	NSW 365	G	FB	BI	S	1	—232.5±15.4	2130±160	1680±164	42.4	1.3	0.4	1.3	X	2.1	1.3
28	NSW 366	G	FB	BI	S	1	—224.7± 8.2	2050± 80	1600± 87	100	1.1	0.3	1.3	X	1.9	1.2
29	NSW 361	G	FB	BI	S	1	—298.9± 7.2	2850± 90	2400± 97	100	0.8	0.4	0.9	—	1.3	0.5
30	NSW 367	G	FB	BI	S	1	—207.0±12.4	1860±130	1410±135	59.76	1.0	0.3	1.1	X	1.8	1.3
31	NSW 362	G	FB	BI	S	1	—317.0± 7.3	3060± 90	2610± 97	100	0.8	0.4	0.9	—	0.8	0.3
32	NSW 363	G	FB	BI	S	1	—329.0± 7.8	3210± 90	2760± 97	100	1.7	0.6	1.6	—	2.6	0.9
33	NSW 368	F	W	BI	S	1	—214.0± 9.2	1940± 90	1490± 97	100	1.1	0.3	1.2	X	1.5	1.0
34	NSW 369	F	W	BI	S	1	—189.8± 7.9	1690± 80	1240± 87	100	0.8	0.3	1.0	X	1.0	0.8
35	NSW 357	—	M	A	A	2	—946.6± 3.7	23600±600	n.a.	100	0.4	—	—	—	—	—
36	B 362	F	W	TG	F	3	—277.9±28.2	2620±320	2170±322	5.3	0.8	0.4	2.5	X	2.2	1.0
37	B 363	F	W	TG	H	4	—956.0±10.3	4890±150	4440±154	26.9	0.8	0.4	2.5	X	2.2	0.5
38	B 365	G	FB	TG	H	4	—426.5±21.8	4470±310	4020±193	11.0	1.7	0.7	3.1	X	3.3	0.8
39	B 366	G	FB	TG	H	4	—413.2±13.6	4280±190	3830±193	14.9	2.5	0.7	3.8	X	5.0	1.3
40	B367	G	FB	TG	F	3	—376.5±29.4	3800±390	3350±392	6.2	2.5	0.7	3.8	X	5.0	1.4

1 NR—North of Red Cliff Point; R—Red Cliff Point; M—North of Mambray Creek; W—North of Wood Point; FB—Fisherman Bay; see Figures 4 & 5 for precise locations.
2 SR—Shell ridge; BI—Base of intertidal facies: A—*Anadara* resting on intertidal flat; TG—Top of subtidal sea-grass fibre-bearing facies.
3 M—Mollusc shells; S—*Spisula* shells; A—*Anadara* shells; F—*Posidonia* root fibres; H—Shell hash.
4 1—Aragonite; 2—Aragonite with traces of calcite; 3—Organic matter; 4—Not analysed.
5 $D^{14}C‰$ W.R.T. 0.95 N.B.S. Oxalic Acid.
6 Ocean reservoir effect constant of 450±35 y subtracted (Gillespie & Polach, 1980); n.a.—correction inapplicable.
7 Shell ridge samples = elevation of seaward base of ridge; Other samples—elevation of intertidal or supratidal flat.
8 Shell ridge samples = elevation of ridge crest; other samples—depth beneath surface of sampled sediment (±0.05 m).
9 Suggested former sea level height relative to present (in metres); Shell-ridge heights ±0.5 m; Base of intertidal facies assumes formation at a position in the tidal range equivalent to a present elevation of —0.5 m A.H.D.; Top of subtidal facies assumes equivalent to present elevation of —2 m A.H.D.
10 X—sample used to determine rate of sea level fall (Table 2); O—evidence of later morphological modification; — date not suitable for assessing age of feature.
11 Distance in km of sampled feature from currently active equivalent environment, measured normal to former shore line.
12 Rates of progradation implied by D (km/1000 yrs).

Table 2. Rates of relative sea level fall determined for the study areas.

Area	*Sea level indicator*	*Rate (m/1000 y)*
North of Red Cliff Point (Transect A)	Shell ridge seaward bases	0.6
Red Cliff Point (Transect B)	Shell ridge seaward bases	0.3
North of Mambray Creek (Transect D)	Shell ridge seaward bases	0.7
North of Wood Point (Transect F)	Shell ridge seaward bases	0.3
North of Wood Point (Transect F)	Base of intertidal facies	0.7
Fisherman Bay (Transect G)	Base of intertidal facies	0.6
North of Wood Point (Transect F)	Top of subtidal facies	0.5-1.1
Fisherman Bay (Transect G)	Top of subtidal facies	0.7-1.1

Point vary from 0.5 m/1000 years to 1.1 m/years (Table 2).

Discussion

The imprecise indicators of age and sea level used in this study and the wide spread of the results prevents a detailed reconstruction of Late Holocene sea-level history in Spencer Gulf. However, the results are consistent with the conclusions that: (1) shorelines have prograded over the past 5000 years; and (2) the area had a higher relative sea level, somewhere between 1.5 m and 5.2 m above the present level, 5000 years ago.

There is no clear evidence for the cause of the Holocene fall in relative sea level in the area. The different rates of relative sea level fall shown by shell-beach ridge systems from the various areas (Table 2) suggest a possibility of differential uplift, but the data are insufficiently precise to confirm this, and it may simply reflect local variation in tidal range. Crawford (1963) regarded the gravels, later described by Hails & Gostin (1978), as offshore bars uplifted by tectonic changes. Spencer Gulf lies next to one of the most seismically active areas in Australia (McCue & Sutton, 1979) and it is possible that continuing tectonic uplift of the region may have contributed to Holocene relative sea-level fall in Spencer Gulf.

The rates of sea-level fall indicated by changes in elevation of the subtidal sea-grass horizon are generally higher than the rates derived from stranded shell-ridge systems, and this difference may reflect an increase in the tidal range in the area during the Holocene, as well as possibly less stormy conditions during the climatic optimum before 2000 years B.P.

No dates are available yet for the Holocene transgression in Spencer Gulf, though the transgressive surface can be traced in cores from the subtidal and intertidal zones (Gostin & others, 1981). Thom & Chappell (1975) concluded that, along the east coast of New South Wales, sea level stabilised at about its present level some 6000 years B.P., and Hails & Gostin (1978) suggested a similar date for the peak of the Holocene transgression in Spencer Gulf.

The oldest dates determined from the prograding sequences are about 5000 years B.P. This may mean that the peak of the Holocene transgression was attained later in Spencer Gulf, but it is also possible that as yet undated evidence of an earlier peak in the transgression exists, perhaps shorewards of the dated features.

The evidence of falling sea level over the past 4000 to 5000 years presented in this study could be extrapolated back a further 1000 years to a time that coincided with the peak of the Holocene transgression elsewhere in Australia. If a constant rate of sea level fall of 1 m/2000 years is assumed, a figure consistent with most of the data (Table 2), this would provide a high stand of relative sea level of 3 m at 6000 years B.P.

Evidence from sub-tidal cores shows Holocene sedimentation rates of 1-2 cm/100 years. Therefore, 6000 years ago the subtidal environments would have been 0.6-1.2 m deeper, relative to present sea level, and this, coupled with a 3 m higher sea level, would have provided an environment in which constructive waves could be generated, capable of building the shingle ridges described by Hails & Gostin (1978). These would be composed of cobbles reworked from Pleistocene alluvial fan deposits and *Anadara* reworked from outcrops of Pleistocene marine limestone by the transgressing sea. A late Pleistocene age for the shingle ridges was suggested by Gostin & others (1981) because of the presence in the ridges of *Anadara* shells that yielded Pleistocene amino acid racemisation dates, and because the elevation of the ridges appeared to be too high to have been constructed during the Holocene, for which period they (Gostin & others, 1981) assumed relative sea level to be no more than about 1 m above present level. It is suggested here that the dated *Anadara* shells are, in fact, reworked, and that the height of the ridges is compatible with their formation during a period of higher sea level in the early Holocene.

It would have been some time after the peak of the transgression was attained before the 'carbonate factory' of the subtidal sea-grass areas became fully established. The landward margin of the sea-grass facies of the regressive sequence buried beneath the prograding complex is, in fact, composed mainly of quartz sand. Although it is likely that sea level fell soon after the peak of the transgression, it was not until sediment had built up in the subtidal and intertidal zones that the shoreline could prograde. Thus, we find the 4000-year shoreline sediments occur next to a higher strandline, thought by Gostin & others (1981) to be Late Pleistocene, but which may, in fact, be the highest Holocene shoreline. Eventually, onshore transport of carbonate from the subtidal and intertidal zones became significant about 4000 years B.P., and shoreline progradation commenced.

The peritidal carbonate coastal complexes, with their broad supratidal plains, have similarities with the large supratidal embayments of Shark Bay and supratidal sabkhas of the Trucial Coast of the Persian Gulf, and it is relevant to note that both these areas are also places of relative sea level fall in the late Holocene (Logan & others, 1970; Evans & others, 1969). This suggests that deposits of extensive ancient supratidal zones might indicate relative sea-level fall as well as shoreline progradation.

Conclusion

The data for Spencer Gulf, presented above, are consistent with the following suggested sea-level history for the region:

6000-4000 years B.P.

The peak of the Holocene transgression may be assumed to have been reached at about the same time as it was on the east coast of Australia (Thom & Chappell, 1975), 6000 years B.P., although no material from the transgression surface has yet been dated. The elevation of the top of the subtidal sea-grass facies beneath the landward margin of the Holocene coastal complex at Wood Point suggests that sea level stood between 3 and 5 m higher than present levels in northern Spencer Gulf. Study of offshore cores from various localities has indicated that 1-2 m of sediment has accumulated since the Holocene transgression in the shallow subtidal areas of the Gulf. This, coupled with the higher sea level, indicates that water depth in these shallow areas was 4-7 m greater at the peak of the transgression. These conditions may have been suitable for the formation of the elevated shingle ridge described by Hails & Gostin (1978).

Immediately after the peak of the transgression was reached, shoreline progradation was restricted by a combination of deeper water near the shore and shortage of sediment. Carbonate production took some time to become established, and the oldest subtidal sediments preserved beneath the landward margins of the Holocene coastal complexes are quartz-rich rather than carbonate-rich. However, although little progradation occurred, it is likely that relative sea level fell, possibly by as much as 2 m, over this period.

4000-3000 years B.P.

The oldest dated beach ridges were formed during this period in the Red Cliff Point and Wood Point/Fisherman Bay areas. They reflect the onset of shoreline progradation in these areas as a result of shoreward transport of carbonates from areas of subtidal production, probably encouraged by shallower conditions offshore. Relative sea levels of +1 m to +2 m are indicated, and a fall of sea level of about 1.0 m over this period is suggested.

3000-2000 years B.P.

This period is marked by continued shoreline progradation in the Red Cliff Point, Wood Point, and Fisherman Bay areas. However, along the transects studied, no beach ridges were constructed. Episodic construction of beach ridges has been noted in the Gulf of Carpentaria by Rhodes (1980), who attributed it to variations of storminess. However, in Spencer Gulf it may be a local phenomenon caused by sheltering resulting from adjacent coastal accretion. A further 0.5 m fall in relative sea level is suggested for this period.

2000 years B.P.-Present

Further shoreline progradation was accompanied by shell ridge construction and a relative sea-level fall of 0.5-1.0 m. Between Port Germein and the area north of the mouth of Mambray Creek (Fig. 1), longshore reworking of beach ridges accompanied overall progradation, which apparently did not commence in this area until 1600-2000 years B.P.

Acknowledgements

I thank Mr J. Marshall, Mr H. Polach, Dr E. G. Rhodes, and the Dr M. R. Walter for discussions of this work, and Dr H. A. Jones and Prof. B. G. Thom, who reviewed the manuscript and suggested many improvements. Mr L. Pain and Mr M. Tratt provided technical assistance. The aerial photographs in Figure 4 are reproduced by courtesy of the Department of Lands, South Australia.

The Baas Becking Laboratory is supported by the Bureau of Mineral Resources, the Commonwealth Scientific and Industrial Research Organisation, and the Australian Mineral Industries Research Association Ltd.

References

BURNE, R. V. & COLWELL, J. B., 1982—Temperate carbonate sediments of northern Spencer Gulf, South Australia: A high salinity "Foramol" province. *Sedimentology*, 29.

CRAWFORD, A. R., 1963—Quaternary sedimentary breccias and emerged offshore bars near Point Lowly. *Quarterly Geological Notes of the Geological Survey of South Australia*, 5, 1-2.

EVANS, G., SCHMIDT, V., BUSH, P., & NELSON, H., 1969—Stratigraphy and geological history of the sabkha, Abu Dhabi, Persian Gulf. *Sedimentology*, 12, 145-59.

GILL, E. D., 1972—*Anadara* (Bivalvia) in the Indian and Pacific waters of Australia. *Journal of the Marine Biological Association of India*, 14, 726-31.

GILL, E. D., 1977—Time of migration of the mollusc *Anadara* to SE Australia. *Search*, 7, 40-1.

GILLESPIE, R., & POLACH, H. A., 1980. The suitability of marine shells for radiocarbon dating of Australian prehistory. *In* BERGER, R., RAINER, J., & SUESS, H. E. (editors), *Proceedings of the 9th International Conference on Radiocarbon Dating, University of California Press, Los Angeles*, 404-21.

GOSTIN, V. A., HAILS, J. R. & POLACH, H. A., 1981—Quaternary sea levels in upper Spencer Gulf, South Australia. *Search*, 12, 43-5.

HAILS, J. R., & GOSTIN, V. A., 1978—Stranded shingle beach ridges, upper Spencer Gulf, South Australia: Evidence for high wave energy dissipation during the Late Pleistocene. *Transactions of the Royal Society of South Australia*, 102, 169-73.

HUDSON, J. D., 1977—Stable isotopes and limestone lithification. *Journal of the Geological Society, London*, 133, 637-60.

LOGAN, B. W., READ, J. F., & DAVIES, G. R., 1970—History of carbonate sedimentation, Quaternary Epoch, Shark Bay, Western Australia. *In* Carbonate sedimentation and environments, Shark Bay, Western Australia. *American Association of Petroleum Geologists, Memoir* 13, 38-84.

MCCUE, K. F. & SUTTON, D. J., 1979—South Australian earthquakes during 1976 and 1977. *Journal of the Geological Society of Australia*, 26, 231-36.

RADOK, R., 1978—Oceanography of northern Spencer Gulf: A response to a brief by the South Australian Department for the Environment. *Horace Lamb Institute of Oceanography, Adelaide.*

RADOK, R., & RAUPACH, M., 1977—Sea level and transport phenomena in St. Vincent Gulf. *Institute of Engineers 3rd Australian Conference on Coastal and Ocean Engineering,* 103-9.

RHODES, E. G., 1980: Modes of Holocene coastal progradation Gulf of Carpentaria. *Ph.D. Thesis, Australian National University, Canberra* (unpublished).

STUIVER, M., & POLACH, H. A., 1977—Reporting of ^{14}C data. *Radiocarbon,* 19, 355-63.

THOM, B. G. & CHAPPELL, J., 1975—Holocene sea levels relative to Australia. *Search,* 6, 90-3.

BMR Journal of Australian Geology & Geophysics, 7, 47-54.

ELEVATION AND GRAVITY PROFILES ACROSS AUSTRALIA: SOME IMPLICATIONS FOR TECTONISM

Vadim Anfiloff

Twenty sets of elevation and gravity profiles across the Australian continent and its margins were prepared by computer from a data bank of 260 000 observations. Their concise and accurate presentation enables crustal blocks to be identified from their elevation and surface character The profiles indicate that the continent consists of rigid crustal blocks containing the cratonised remnants of ancient mobile belts. Some blocks have been eroded to great depth, others are blanketed by sediments and many are undergoing passive isostatic adjustment. Differential vertical movements between adjacent small blocks suggest that some are not in isostatic equilibrium, and differences in regional free-air anomaly level over distances of up to 6 degrees of arc confirm that complete isostasy does not prevail. Around the outer zone of the continent, the dominant direction of movement is downwards, presumably in response to erosion of the base of the crust. However, horizontal compression may be preventing some of the blocks from subsiding, resulting in topographic features, including the Australian Alps.

Introduction

During the production of the 1976 Gravity Map of Australia (Anfiloff & others, 1976), a special data bank of gravity observations was prepared as a preliminary to producing machine contours of Bouguer anomaly. After severe editing, about 260 000 observations were accepted for this data bank. Although the distribution of observations is variable, the coverage is very thorough over the continent and much of its margins.

The data bank made it possible to produce a set of elevation and gravity profiles across the continent along selected latitudes and longitudes. The profiles are not distributed regularly (Fig. 1) as they were sited so as to include the largest topographic features and gravity anomalies, but most parts of the continent are represented. Diagonal profiles were not produced, because of the increased difficulty this would have entailed. The task was made difficult by the large volume of data and the large number of steps involved, but the final product made the effort worthwhile.

This paper presents 9 sets of profiles along latitudes 17°S, 22°S, 24°S, 26°S, 29°S, 31°S, 34°S, 35°S, 36°S (Figs. 2-10), and 9 sets along longitudes 117°E, 120°E, 123°E, 129°E, 133°E, 137°E, 140°E, 144°E, 147°E (Figs. 11-19). As some profiles cut some features diagonally, they should be examined in conjunction with topographic and gravity maps of the continent. The method of producing the profiles is described here, and some of their implications for the crust and isostatic processes affecting it are discussed. The profile along 29°S (Fig. 6) is relevant to the study reported by Dooley (1979).

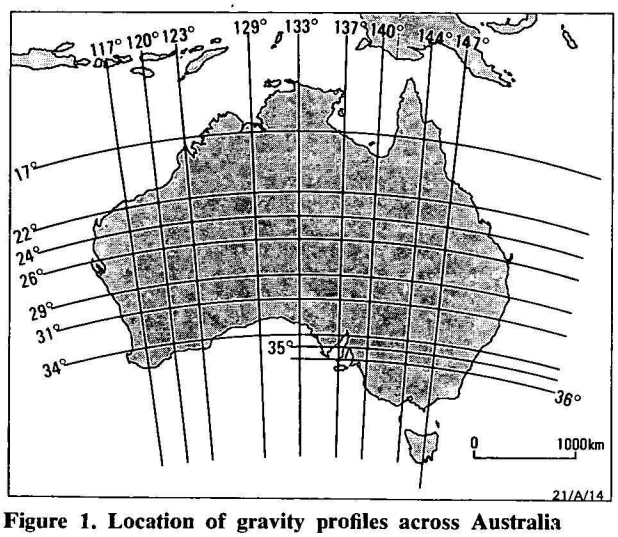

Figure 1. Location of gravity profiles across Australia

Production of elevation and gravity profiles

The profiles were produced with a standard processing package normally used for detailed gravity traverses. The main step was to manipulate data occurring within narrow, 0.1° wide, corridors to produce strings of principal facts along the selected parallels and meridians. This involved projecting stations and allocating artificial coordinates, while retaining the original latitude values for the purpose of computing Bouguer values. Projecting stations onto a median line made each profile more representative of the topographic surface, thereby facilitating the identification of crustal blocks.

The final elevation and gravity profiles were produced at a linear scale in degrees. Two elevation profiles were produced, one with a vertical scale common to all sets, and one with an expanded scale to emphasize the relief. The free-air and multiple-density Bouguer profiles were produced at a fixed vertical scale in all sets, and densities of 2.30, 2.67, and 2.90 t/m^3 were used to demonstrate the effect of topographic density on the Bouguer anomaly.

Effect of topographic density

Topographic effects are not particularly obvious in the current set of profiles, because in most areas, the station spacing is coarse in relation to the width and height of topographic features. For this reason, the shapes of the three Bouguer profiles shown are fairly constant in any given area. The highlands in eastern Australia are an exception, but, owing to the compactness of the profiles, topographic effects are difficult to observe in this area.

Figure 20 shows an analysis of topographic effects over the eastern highlands along 36°S. This area contains some of the largest and steepest topographic relief in the continent and consequently causes a considerable spread in a set of Bouguer profiles for topographic densities in the range 2.0-3.0 t/m^3. Terrain corrections are also large, reaching a maximum of 200 μm/s^2, and frequently exceeding 50 μm/s^2.

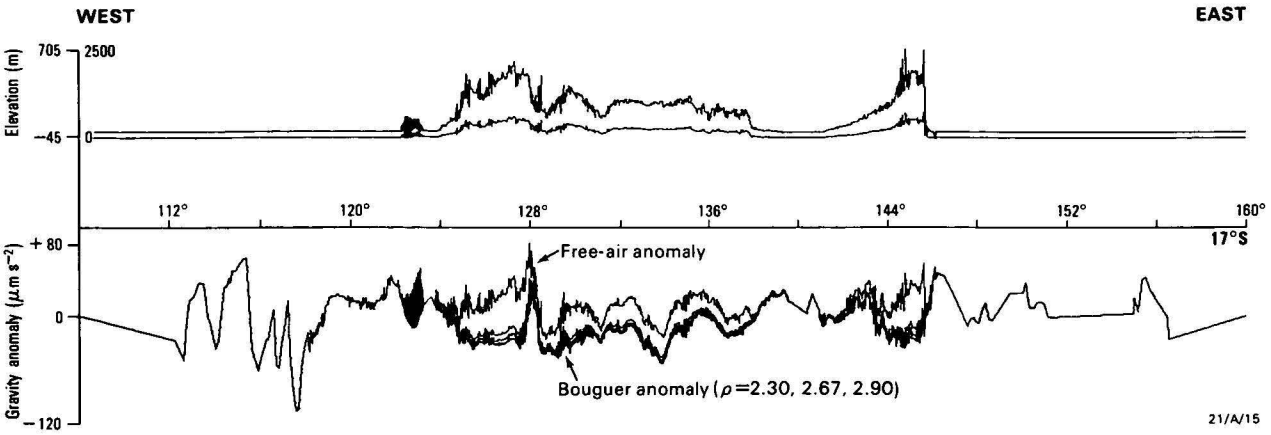

Figure 2. Elevation and gravity profiles along 17°S.

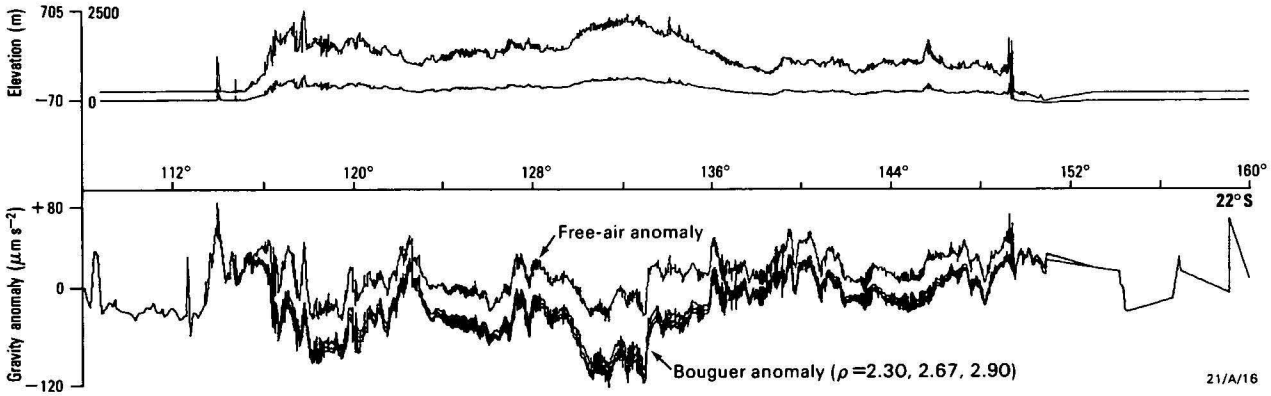

Figure 3. Elevation and gravity profiles along 22°S.

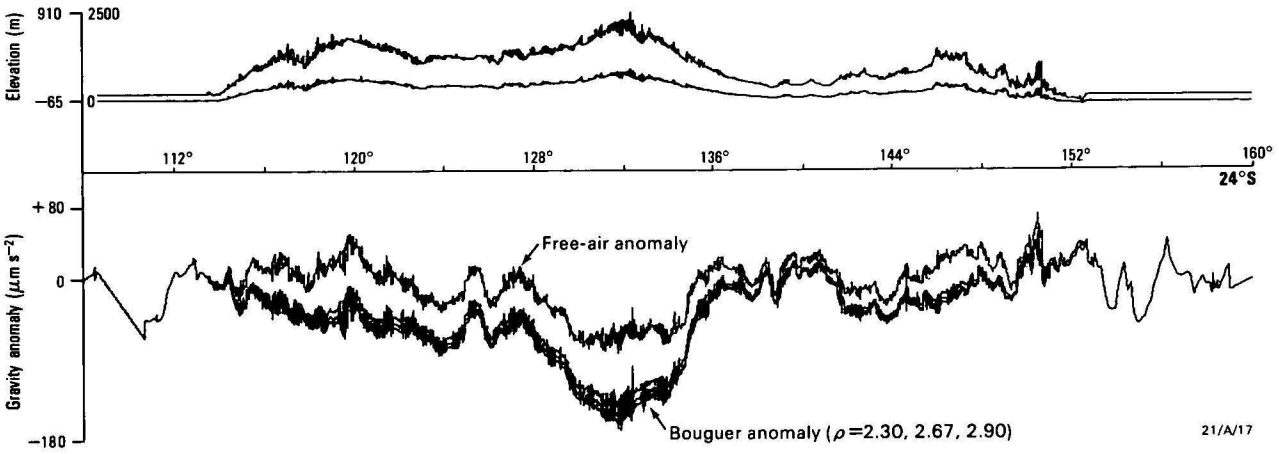

Figure 4. Elevation and gravity profiles along 24°S.

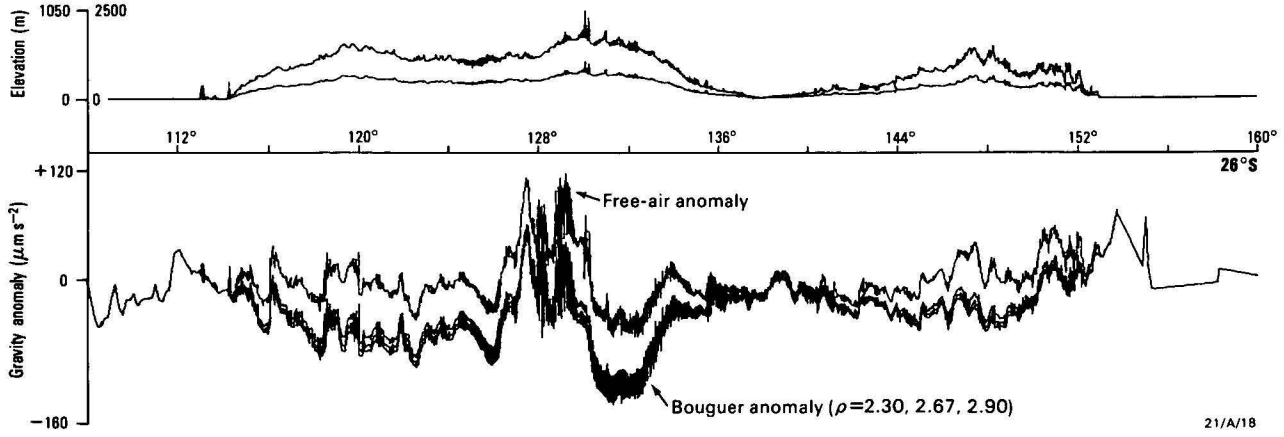

Figure 5. Elevation and gravity profiles along 26°S.

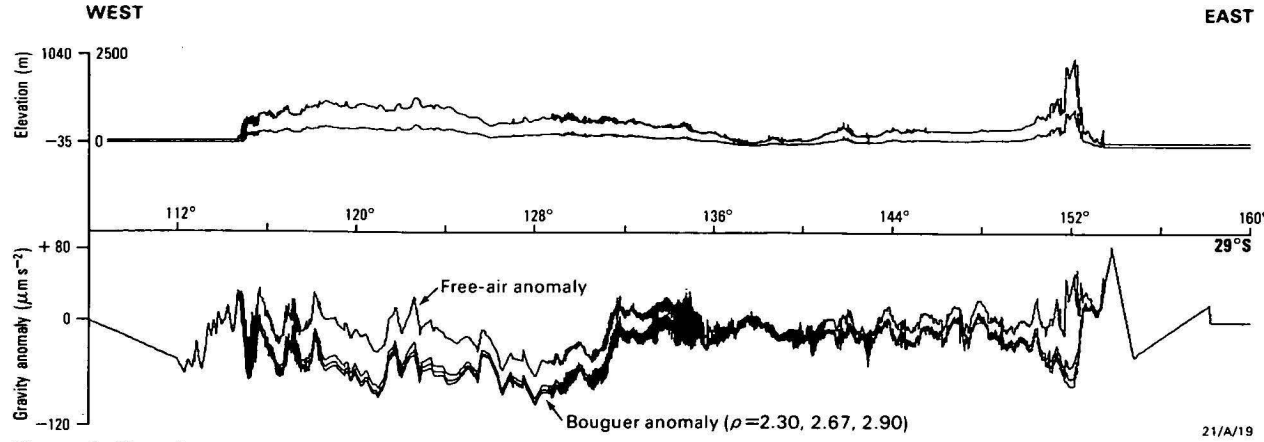

Figure 6. Elevation and gravity profiles along 29°S.

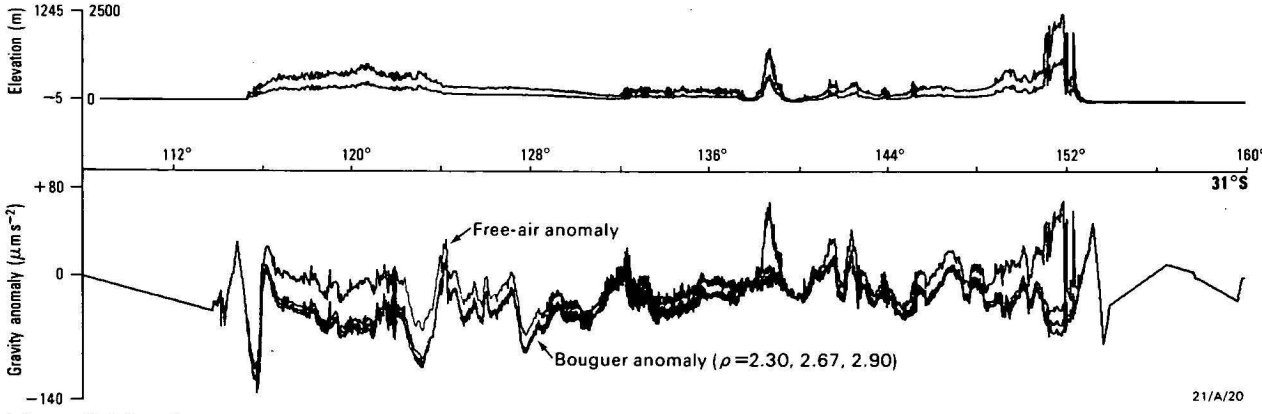

Figure 7. Elevation and gravity profiles along 31°S.

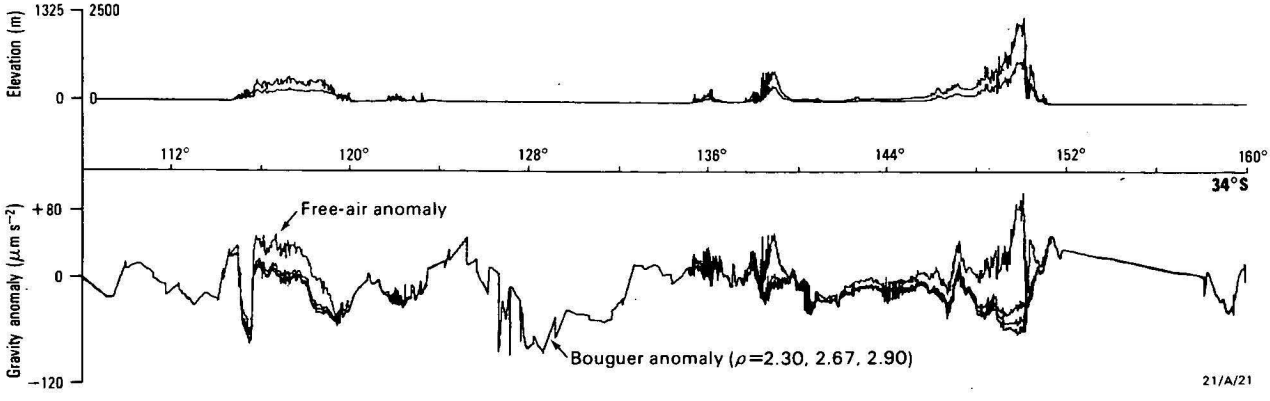

Figure 8. Elevation and gravity profiles along 34°S.

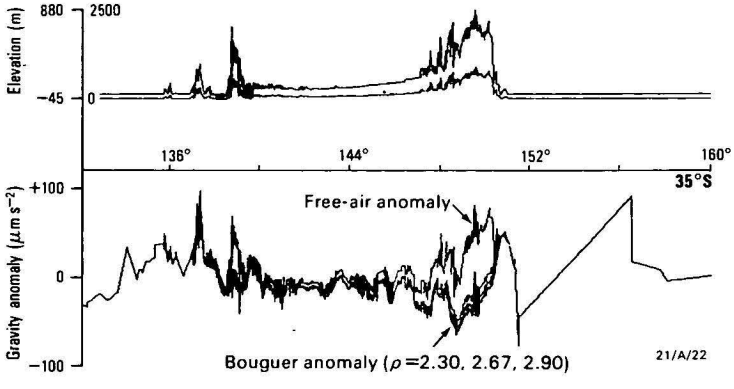

Figure 9. Elevation and gravity profiles along 35°S.

CORRECTION: In Figs. 2-19 the values on the gravity anomaly scale should be increased by a factor of 10 (to complete the conversion from Mgals to μms^{-2}).

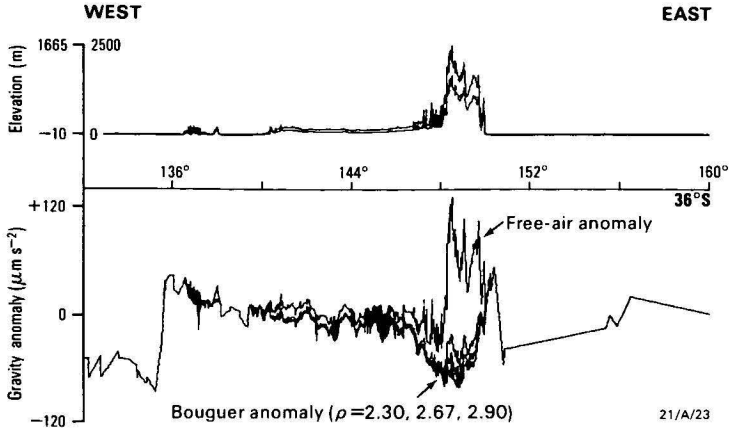

Figure 10. Elevation and gravity profiles along 36°S

Interpretation

The elevation and gravity profiles provide the basis for broad deductions concerning the nature of the Australian crust and tectonic processes acting on it. Some of the main deductions are discussed here.

Amplitude of Bouguer gravity anomalies

The largest gravity anomalies occur in central Australia (Fig. 15) where there is a maximum variation of 1800 μm/s^2. In this region, the gradients are very steep, but detailed surveys have not been carried out to determine the maximum gradients accurately with a view to establishing the maximum depth of the causative bodies. Current interpretations (Anifiloff & Shaw, 1973; Dooley, 1973; Mathur, 1976; Wellman, 1978) use maximum depths ranging from 20 km to 35 km. However, there is mounting geological and geophysical evidence that the majority of density irregularities can be adequately accounted for by bodies in the upper half of the crust. In my view, there are no large anomalies on the continent that necessarily require explanation in terms of bodies below a depth of about 20 km. The possible implications of this are beyond the scope of the present paper. However, one important implication is that during the Proterozoic, when most of the large anomalies were formed, the crust may have been thinner than it is at present. As mobile belts formed, their roots would not extend or be maintained below the depth of the first active discontinuity at a depth of about 20 km. Subsequently, the crust may have cooled and thickened, 'fossilising' the old discontinuity at a shallower depth than the present Mohorovicic discontinuity.

The smaller gravity anomalies associated with some of the large Proterozoic mobile belts are consistent with erosional stripping of as much as 10 km of the upper crust. This is particularly applicable to the Fraser Range Mobile Belt (120° to 128° on Fig. 7), where both granites and granulites are interpreted to bottom at about 12 km (Anfiloff & Shaw, 1973). Figure 7 suggests that part of this belt is cratonised and welded to the Yilgarn Block (120°E), which has an elevated dissected surface, suggesting erosional unloading. The other half is part of the 'Eucla block' (128°E), whose elevation has a distinct character up to the Fraser Fault (124°E), which separates the two blocks. Thus, the Fraser Range Mobile Belt has been bisected, and subjected to differential erosion and sedimentation.

Other crustal blocks are evident in Figure 7 and other figures. The profiles suggest that the crust consists of rigid blocks containing the cratonised remnants of mobile belts that have been eroded, blanketed by sediments, or both. They suggest that some blocks have moved up and down isostatically, and that differential vertical movements related to isostatic processes have produced much of the continent's morphology.

Amplitude of free-air anomalies

Where topographic relief is small, free-air anomalies have the same shape as Bouguer anomalies and indicate subsurface mass distributions. Where topography has a large relief, the free-air anomaly includes the effect of topographic mass and can, therefore, follow the shape of topography. In the simplest case, where there are no density changes below the ground surface, the free-air anomaly is produced entirely by topography, and has the same shape. Removing this anomaly (Anfiloff, 1976) is equivalent to applying an extended Bouguer correction to gravity observations. Free-air anomalies are complex where geological structures and topographic relief are both subject to change. In central Australia, (Fig. 15) large local free-air anomalies represent the cratonisation of the mobile belts there. Each separate belt is unable to adjust isostatically, but there is a correlation between an overall increase in elevation and a regional decrease in free-air anomaly, which suggests that the whole region is rising and may eventually reach equilibrium.

In Papua New Guinea and in the Australian Alps (Fig. 19 at 8°S and 37°S), large changes in free-air anomaly are caused by the mass of topography. If isostatic equilibrium is assumed, a strong positive correlation between elevation and free-air level implies that any buoyant material supporting the mass of topography must be located at a large depth rather than a shallow one. Thus, Wellman (1979) argued that the Australian Alps are being supported by a slab of underplated low-density material occurring at a depth of 50-60 km. However, given that crustal subsidence has occurred in the adjacent Murray, Surat, and Bass basins, the underplating would have to be exclusive to the Alpine block, requiring a special mechanism. If we consider Tasmania to be in an equivalent elevated position to the Alpine block, underplating becomes an untenable explanation for the chequer-board pattern of subsidence and non-subsidence. Uniform erosion of the base of

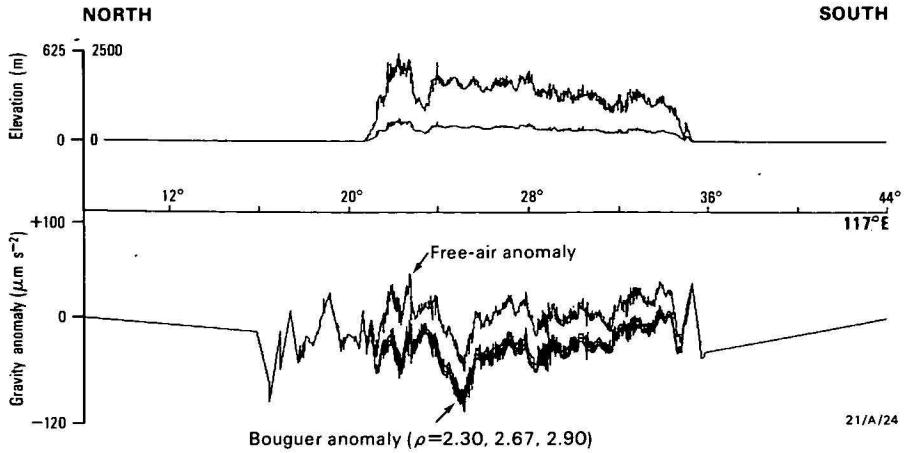

Figure 11. Elevation and gravity profiles along 117°E.

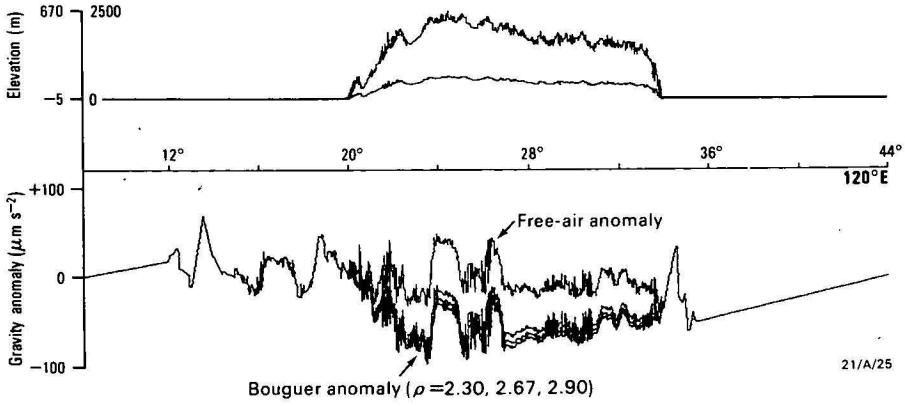

Figure 12. Elevation and gravity profiles along 120°E.

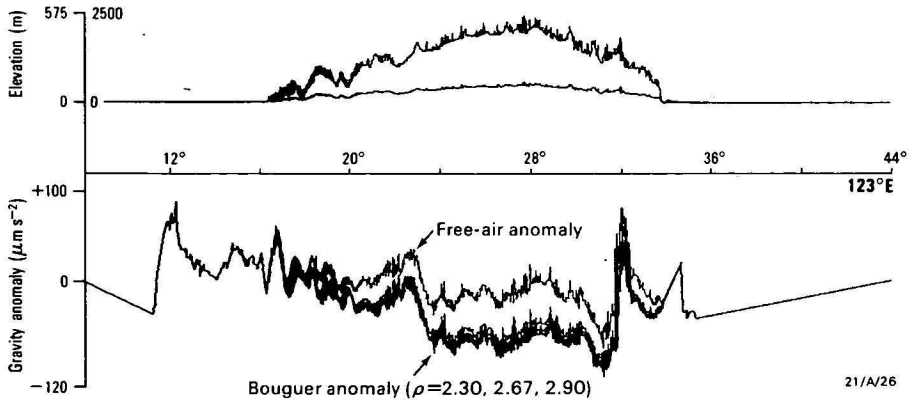

Figure 13. Elevation and gravity profiles along 123°E.

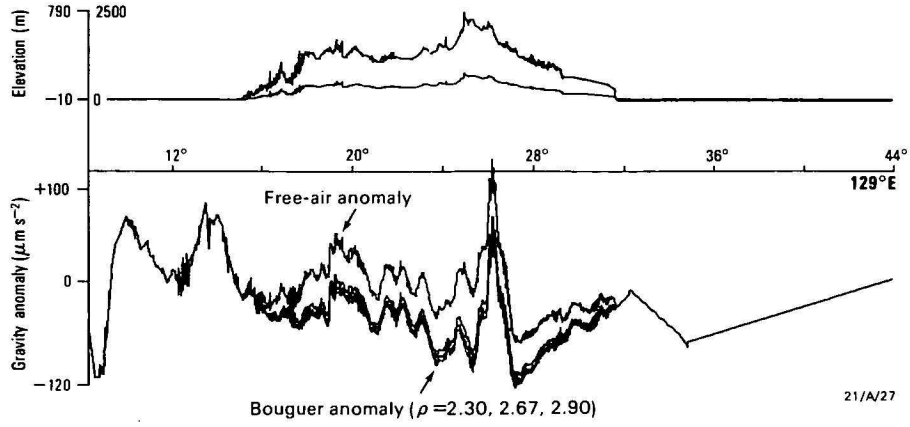

Figure 14. Elevation and gravity profiles along 129°E.

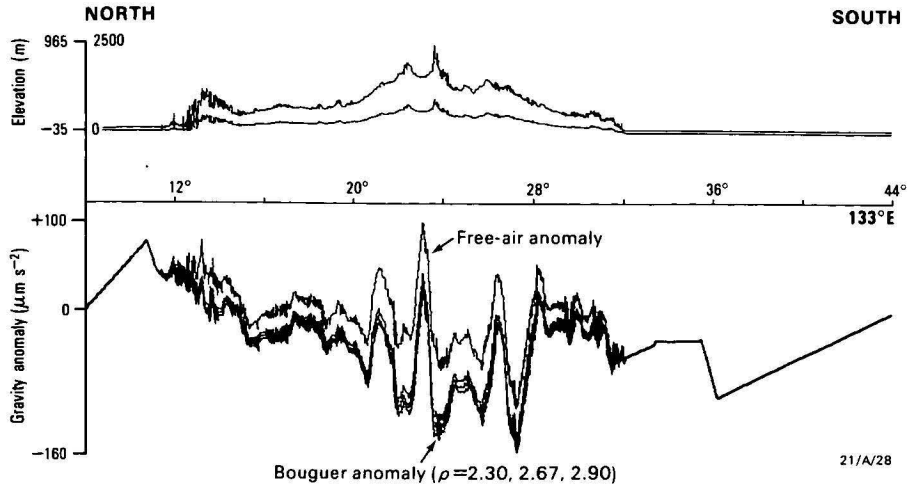

Figure 15. Elevation and gravity profiles along 133°E.

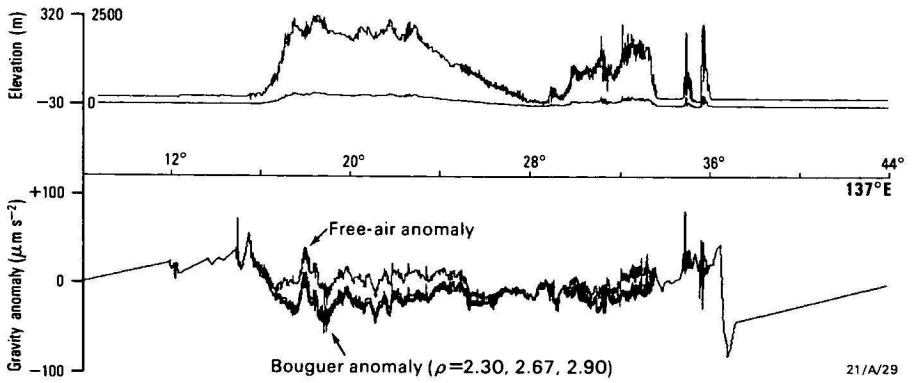

Figure 16. Elevation and gravity profiles along 137°E.

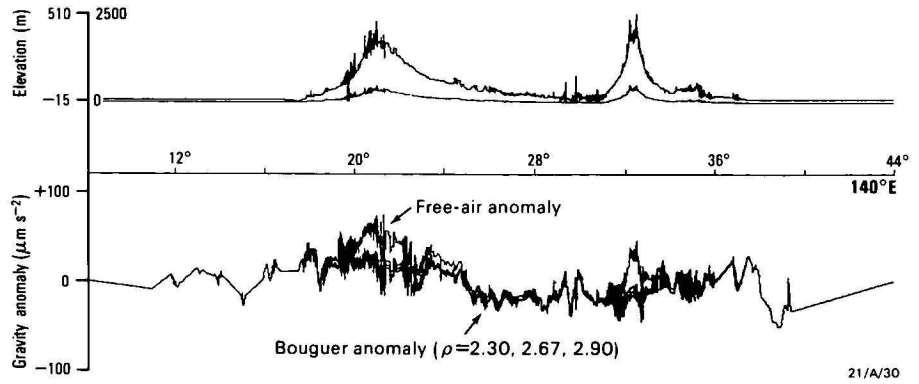

Figure 17. Elevation and gravity profiles along 140°E.

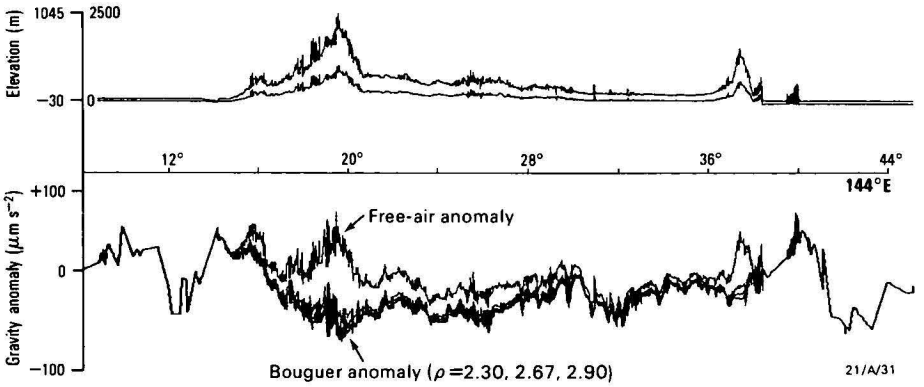

Figure 18. Elevation and gravity profiles along 144°E.

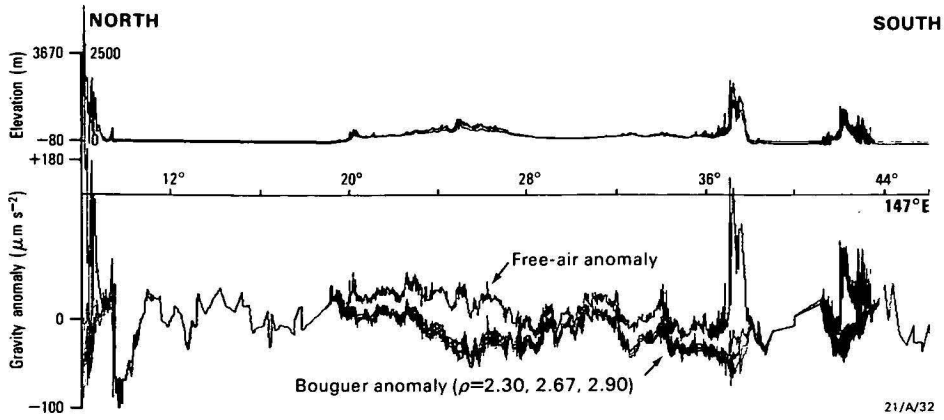

Figure 19. Elevation and gravity profiles along 147°E.

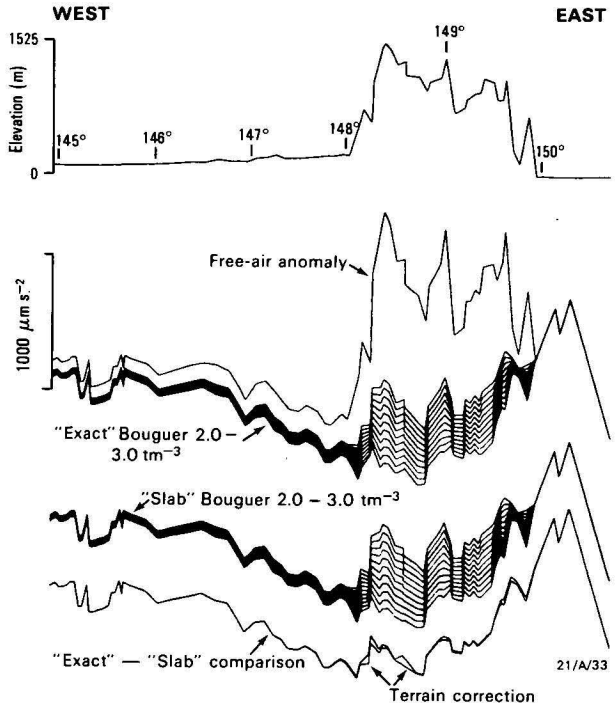

Figure 20. Analysis of gravity data over the Australian Alps at 36°S.
The 'exact' Bouguer profiles are produced using the automatic elevation inversion method of Anfiloff (1976). The amount of terrain correction is equal to the difference between 'exact' and 'slab' profiles.

the crust, caused by a hot substratum, in conjunction with a passive mechanism to arrest the subsidence of some blocks, is a more viable explanation.

Although the crust as a whole must float on the mantle, not every portion of it necessarily floats freely. The elevation and gravity profiles across Australia suggest that the continent consists of separate rigid crustal blocks that undergo differential vertical movements. In areas where the original geological content can be assumed to be uniform, these movements imply a variable response to uniform loading or unloading, thereby implying that some blocks are not in equilibrium. In numerous areas, there are indications that the regional level of free-air anomaly changes from one block to another. If isostasy prevails regional free-air levels must be the same over all crustal blocks, irrespective of their altitude, provided that the blocks are sufficiently wide to avoid edge effects. The complicating factors are that, on the one hand, edge effects are a function of the assumed depth of compensation, and on the other, free-air profiles are usually sufficiently irregular to make it difficult to determine the regional free-air level. Given these two factors, the question of isostasy cannot be resolved in many areas of Australia.

There is one area where the two complicating factors do not cloud the issue. Profiles along 137°E and 140°E, (Figs. 16 & 17) show that the Eromanga Basin (28°S) has a regionally lower elevation and free-air anomaly than the Mount Isa Block (20°S). The difference in free-air anomalies persists over about 6° of arc in the N-S direction and a similar distance in the E-W direction. Along 140°E (Fig. 17), the regional difference in anomaly is about 800 μm/s^2, and the change occurs across the Cork Fault at 25°S. A similar situation is apparent along 147°E (Fig. 19), where the Anakie Block (25°S) has higher elevation and free-air anomalies than the Surat Basin (29°S). These examples are strong evidence that significant isostatic imbalance occurs.

This finding is in agreement with Shirley (1979) who interpreted the Mount Isa Block as being out of isostatic equilibrium. The Eromanga Basin is likely to be in equilibrium, as the sediments indicate that it has been free to adjust a considerable distance vertically. The Mount Isa Block on the other hand, has remained in an elevated position. The data in eastern Australia suggest that, although subsidence is the dominant tendency, some blocks are prevented from subsidising, resulting in a chequer-board pattern of basins and morphological features. Koshtak (1971) demonstrated experimentally that horizontal compression applied externally to a mosaic of rigid blocks produces a chequer-board stress pattern. Thus, external compression in conjunction with widespread basal erosion can explain the passive isostatic movements in eastern Australia. Basal erosion of the crust could be caused by high mantle temperatures associated with the formation of the Tasman Sea.

Conclusions

The elevation and gravity profiles presented here are a primary source of information regarding the crust and tectonic processes. The crust in Australia appears to

behave as a mosaic of rigid blocks containing the cratonised remnants of ancient mobile belts. Individual blocks adjust isostatically in response to supracrustal processes, and these movements often rejuvenate ancient sutures along which ancient mobile belts formed. The new movements obscure these belts by causing erosion in the uplifted part and burying the downthrown part. Horizontal compression acting through the crust may be a major factor in explaining why some blocks do not adjust as quickly as others. The compression is associated with significant isostatic imbalance, and therefore has ramifications for the interpretation of long wavelength gravity anomalies.

References

ANFILOFF, W., & SHAW, R. D., 1973—The gravity effects of three large uplifted granulite blocks in separate Australian shield areas. *In* MATHER, R. S., & ANGUS-LEPPAN, P. V. (editors), *Proceedings: Symposium on Earth's Gravitational Field & Secular Variations in Position, Sydney, 1973*, 273-89.

ANFILOFF, W., 1976—Automated density profiling over elongate topographic features. *BMR Journal of Australian Geology & Geophysics*, 1, 57-61.

ANFILOFF, W., BARLOW, B. C., MURRAY, A. S., DENHAM, D., & SANDFORD, R., 1976—Compilation and production of the 1976 Gravity Map of Australia. *BMR Journal of Australian Geology & Geophysics*, 1, 173-6.

DOOLEY, J. C., 1973—The gravity anomalies of central Australia and their significance for long-term tectonic movements. *In* MATHER, R. S., & ANGUS-LEPPAN, P. V., (editors), *Proceedings: Symposium on Earth's Gravitational Field and Secular Variations in Position, Sydney, 1973*, 248-60.

DOOLEY, J. C., 1979—A geophysical profile across Australia at 29°S. *BMR Journal of Geology & Geophysics*, 4, 353-9.

KOSHTAK, B., 1971—Models of block systems. *Problems of Geomechanics, Yerevan*, 5, 100-12.

MATHUR, S. P., 1976—Relation of Bouguer anomalies to crustal structure in southwestern and central Australia. *BMR Journal of Australian Geology & Geophysics*, 1, 277-86.

SHIRLEY, J. E., 1979—Crustal structure in north Queensland from gravity anomalies. *BMR Journal of Australian Geology & Geophysics*, 4, 309-21.

WELLMAN, P., 1978—Gravity evidence for abrupt changes in mean crustal density at the junction of Australian crustal blocks. *BMR Journal of Australian Geology & Geophysics*, 3, 153-62.

WELLMAN, P., 1979—On the isostatic compensation of Australian topography. *BMR Journal of Australian Geology & Geophysics*, 4, 373-82.

BMR Journal of Australian Geology & Geophysics, 7, 55-62.

SPECTRAL REPRESENTATION OF ISOSTATIC MODELS

Garry D. Karner*

The development of cross-spectral techniques for investigating the relation between gravity and topography has led to the representation of isostatic processes in terms of mathematical filters, or admittance functions. These filters can easily be constructed by application of Green's equivalent layer theorem. The rheology of the lithosphere principally controls the process by which isostatic compensation is achieved. As examples, admittance functions representing the isostatic process defined by elastic and visco-elastic rheologies are developed. By using admittance functions, the calculation of the free-air gravity anomaly for complicated topography, isostatic schemes, or rheology becomes computationally more efficient and simple compared to the more conventional line-integral methods.

Introduction

The observation of near-zero free-air gravity anomalies over large-scale topographic features, such as mountain ranges, led to the development of the concept of isostasy. The existence of gravity anomalies requires lateral variations of density, which, in turn, require the existence of deviatoric stresses to support the mass perturbation. A state of isostatic equilibrium results in the relaxation of these deviatoric stresses to hydrostatic stresses at some depth (the depth of compensation) in or beneath the lithosphere.

Basic to the theory of plate tectonics is the concept of a strong, rigid lithosphere overlying a weak asthenosphere (Barrell, 1914). The main argument for the existence of a strong lithosphere has come from observations that long-wavelength topographic features have been supported for many millions of years (Jeffreys, 1959). The evidence for a weak asthenosphere comes from observations that large loads on the Earth's surface, such as deltas (Walcott, 1970; Cochran, 1973), are gravitationally compensated, presumably by mass transfer within the mantle out from under the load. A characteristic parameter of the lithosphere is its flexural rigidity, which controls the mode of lithospheric flexure. As the rigidity varies from low to high values, the associated isostatic compensation of loads on the lithosphere varies from local to regional. If the rigidity approaches infinity, the lithosphere is able to support the load without flexing, regardless of topographic wavelength, and hence the load is isostatically uncompensated.

The plate or flexure model, therefore, lends itself as a first-order mechanical model for the study of isostasy. In particular, regional and Airy isostatic, and uncompensated schemes may be represented by the flexural response of the lithosphere for rigidities that range from high to low values.

To achieve Airy, or local, compensation of topographic loads would appear to involve unreasonable assumptions about the mechanical behaviour of the crust and upper mantle. However, upper crustal listric faulting and apparent lower crustal ductile stretching characterise the style of rifting in the Bay of Biscay (Montadert & others, 1979). Such crustal behaviour would lead to Airy-type compensation, in which the upper crustal blocks are locally supported. Loads on normal lithospheric thicknesses, well removed from the influence of the stretching and necking processes associated with rifting, would tend to show flexure or regional compensation. However, the gravity effects of local and regional compensation converge for long topographic wavelengths.

Recently, the application of cross-spectral techniques developed by Dorman & Lewis (1970), and Lewis & Dorman (1970) has led to an alternative way to investigate isostatic processes. The cross-spectral, or admittance function, technique assumes that observed gravity anomalies are caused by topography and its compensation, and attempts to determine a function that, when convolved with the topographic profile, produces the gravity response of both the topography and the isostatic compensation (McKenzie & Bowin, 1976; Banks & others, 1977; McNutt & Parker, 1977; Watts, 1978; Banks & Swain, 1978; Detrick & Watts, 1979; Cochran, 1979). Admittance functions represent the Fourier transform of gravity normalised by the Fourier transform of the respective topography. Observed admittances are interpreted by comparison with theoretical admittance functions representing various isostatic models.

The fast Fourier transform supplies a means of calculating free-air and isostatic gravity anomalies more rapidly than the line-integral techniques of Hubbard (1948), Talwani & Ewing (1960), and Talwani (1973), especially where a large number of station points are used in the modelling. The computation time of the Fourier transform is proportional to N ln N, rather than N^2, where N is the number of station points.

The purpose of this paper is to demonstrate the ease with which admittance functions representing isostatic models can be constructed, and that with these functions the calculation of the free-air and isostatic gravity effects become computationally efficient.

Theory

A very important concept from potential field theory is that of the equivalent stratum, which is based on the gravity effect of a surface density distribution on a horizontal plane being equivalent to that of an unknown mass distribution below that plane. The concept allows the replacement of the mass distribution below the plane by a surface density distribution in such a way that the gravity effect above the plane is the same (e.g. Grant & West, 1965, p. 214).

Consider a horizontal plane at vertical position $z = 0$ (z position down), with a surface mass distribution of $\sigma(\underline{x})$. The gravity effect at a general point on the plane due to this density distribution is

$$\Delta g(\underline{x}) = 2\pi\gamma\sigma(\underline{x}) \quad \ldots\ldots (1),$$

(Grant & West, 1965, p. 216),

* Present address: Lamont-Doherty Geological Observatory and Department of Geological Sciences of Columbia University, Palisades, New York 10964, USA.

where γ is Newton's gravitational constant. The gravity effect of the volume density distribution below the plane will be the same as that of the surface density distribution at any point above the plane.

The equivalent stratum can be further extended by allowing the surface density distribution to be equated to topography, $h(\underline{x})$, with fixed density ρ, fluctuating about a plane (at $z = d$) such that

$$\rho(\underline{x}) = \rho h(\underline{x}).$$

The topographic surface, $h(\underline{x})$, is the vertical deviation of an interface from its mean depth d. For an observational plane at $z = 0$, the gravity effect of this topographic surface is

$$\Delta g_0(\underline{x}) = \gamma\rho\left[\frac{\partial}{\partial z}\int_{-\infty}^{+\infty} d\underline{\xi} \int_{d}^{d+h(\xi)} \frac{d\zeta}{S}\right]_{z=0} \quad \ldots\ldots (2)$$

(Grant & West, 1965, p. 250), where $S = (|\underline{\xi}|^2+\zeta^2)^{1/2}$ and is the distance from the observation point to a point constrained by $z=d$ and $z=d+h(\underline{\xi})$. For max $|h(\underline{x})| << d$, (2) can be simplified to (in one dimension),

$$\Delta g_0(x) = 2\pi\gamma\rho\ h(x) * \frac{d}{d^2+x^2} \quad \ldots\ldots (3),$$

where * represents convolution in the spatial domain. The term $\frac{d}{d^2+x^2}$ is the weighting function associated with continuing the gravity effect upward from $z=d$ to $z=0$ (Dean, 1958). Similarly, this same weighting function will continue the gravity effect downward if $z=-d$, and so without loss of generality the following development will be for $d \geqslant 0$ and so $h(x)$ is a bathymetric surface. For $d<0$, $h(x)$ represents continental topography and the same results and conclusions are valid.

Isostatic models can most easily be represented by functions in the frequency domain, since spatial domain convolution becomes a simple frequency domain multiplication. (3) can be represented in the latter domain by taking the Fourier transform F of both sides,

$$F[\Delta g_0(x)] = 2\pi\gamma\rho\ F[h(x)]e^{-kd}$$
$$or\ G(k) = 2\pi\gamma\rho\ e^{-kd}\ H(k) \quad \ldots\ldots (4),$$

where k, the wave number, is related to wavelength λ by $k = 2\pi/\lambda$, and the upper case symbols refer to the Fourier transform of the corresponding spatial functions designated by lower case symbols. By the repeated use of (4) it is now possible to construct admittance functions that represent isostatic processes, as will be demonstrated in the next section.

If $|h(x)| \sim d$, the full solution of (2) is required, and is given by Parker (1972):

$$G(k) = 2\pi\gamma\rho\ e^{-kd}\sum_{n=1}^{\infty}\frac{k^{n-1}}{n!}\ F[h^n(x)] \quad \ldots\ldots (5)$$

As n, the power of the topographic function, becomes large, the n! factor rapidly dominates the series. The series is uniformly and absolutely convergent (Parker, 1972), the rate of convergence being inversely proportional to $(\max|h(x)|/d)$. The usefulness of (5) in creating admittance functions is in the accuracy of representing G(k) by the first term of the series. The conditions for which this is an acceptable approximation will be discussed later.

Isostatic models

The concept of isostasy asserts that the surface topography is somehow compensated at depth, at either one or more interfaces. Interface topography is either inversely related to the surface topography (Airy and flexural type compensation) or constant, with surface topography being inversely related to density (Pratt-Hayford and thermal type compensation). For simplicity, it is usually assumed that compensation is totally achieved at a single interface and that the depth to this interface, the depth of compensation, is the crustal thickness. Figure 1 shows the types of commonly used isostatic models.

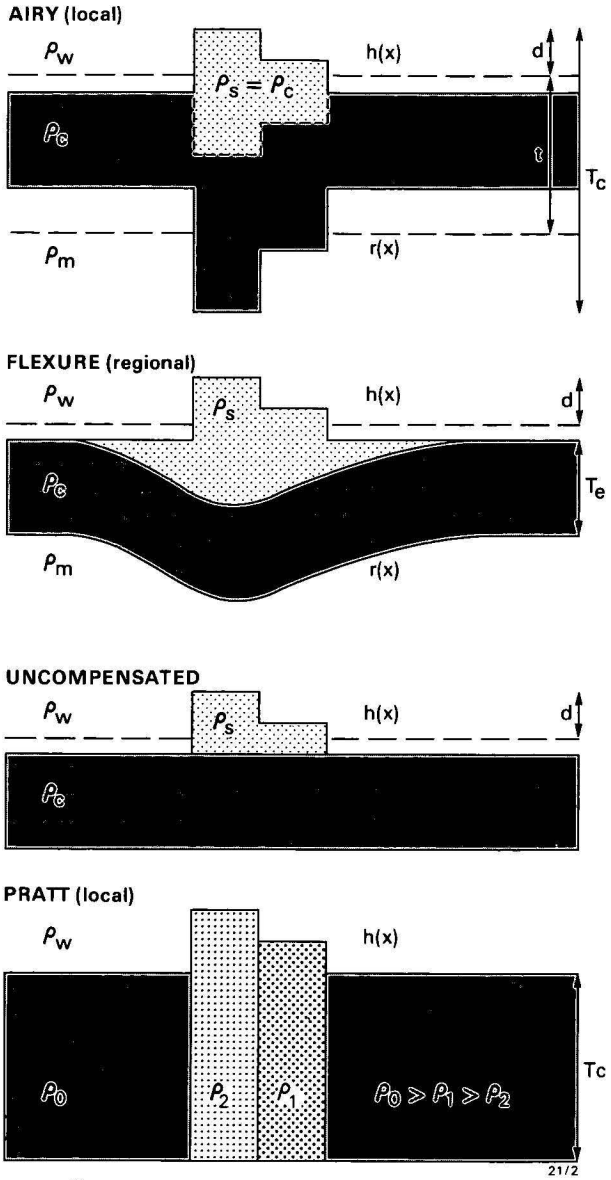

Figure 1. Schematic summary of isostatic models discussed in the paper.
The Airy, plate and uncompensated models can most conveniently be represented as the flexure of a thin elastic plate with increasing rigidity, respectively. The topography h(x) is the applied load. The mechanical response to this load implied by the models is shown for comparison. Parameters d, t, T_c and T_e are explained in the text and relate to various equations.

Because of isostatic compensation, the net gravity effect of the surface topography will result from the destructive interference of the gravity effects of the surface and the compensating interface. By equation (4), the gravity effect of the surface topography (in the Fourier domain) is

$$G_1(k) = 2\pi\gamma\Delta\rho_1\ e^{-kd}\ H(k) \quad \ldots\ldots (6),$$

where $\Delta\rho_1$ is the density contrast across the surface

Table 1. Isostatic densities.

ρ_{load}	= load density
$\rho_{displaced}$	= density of material displaced by the load
ρ_{infill}	= density of material infilling the flexural basin
ρ_a	= air density
ρ_w	= water density
ρ_s	= sediment density
ρ_c	= crustal density (Airy model)
ρ_o	= crustal density at sea level (Pratt model)
ρ_m	= mantle density
$\Delta\rho_1$	$= \rho_{load} - \rho_{displaced}$
	$= (\rho_s - \rho_a)$ for continental loading
	$= (\rho_s - \rho_w)$ for oceanic loading
$\Delta\rho_2$	$= \rho_m - \rho_c$
$\Delta\rho_3$	$= \rho_m - \rho_{infill}$ (the buoyancy force)
	$= \rho_m - \rho_s$ (implying that $\rho_s = \rho_{load} = \rho_{infill}$)

topography, d is the mean depth (if d<0, then d is the mean elevation), and H(k) the Fourier transform of the surface topography h(x). The gravity effect of the root topography is,

$$G_2(k) = -2\pi\gamma\Delta\rho_2\ e^{-k(d+t)}\ R(k) \quad \ldots\ldots (7),$$

where $\Delta\rho_2$ is the density contrast across the root topography, t is the distance between the mean surface and root topography, and R (k) the Fourier transform of the root topography, r(x). The general equation for the gravity effect of a two-interface isostatic scheme is therefore,

$$G_T(k) = 2\pi\gamma\Delta\rho_1\ H(k)\ e^{-kd}\left[1 - \frac{\Delta\rho_2}{\Delta\rho_1}\frac{R(k)}{H(k)}e^{-kt}\right] (8).$$

The rheology of the lithosphere dictates the process by which compensation is achieved, which, with the density contrasts across the interfaces involved in the compensation, determines the relation between r(x) and h(x). Density requirements and assumptions for modelling the various compensation schemes to be presented are defined in Table 1.

Elastic rheology

A useful approximation to the response of the Earth's lithosphere to applied loads is the bending of a thin elastic plate overlying a weak foundation (Hanks, 1971; Caldwell & others, 1976; Watts, 1978; Chapple & Forsyth, 1979; Goetze & Evans, 1979; Watts & others, 1980). The deformation, r(x), of an elastic beam by the loading function, h(x), is controlled by the fourth-order differential equation (Hetènyi, 1946)

$$D\frac{\partial^4}{\partial x^4}r(x) + \Delta\rho_3\ gr(x) = \Delta\rho_1\ gh(x) \quad \ldots\ldots (9),$$

where D is the flexural rigidity defined as $\frac{ET^3}{12(1-\sigma^2)}$, E is Young's modulus, T is the plate thickness, σ is Poisson's ratio, and $\Delta\rho_3$ is the density contrast between the material underlying the beam and the material infilling the deflection. Equation 9 is applicable to the bending of the Earth's lithosphere if we make the following fundamental assumptions: the lithosphere can be approximated as a thin plate, so that vertical stresses may be neglected, planar cross-sections normal to the neutral surface remain planar, and the bending moment is totally determined by the second derivative of r(x). Further, by assuming small deflections, the strains will be infinitesimal and no stretching will occur along the neutral surface. We also assume that the pre-loading, initial condition of stress in the beam is hydrostatic.

The choice of E and σ require consideration of crustal rock properties as determined from either seismology or rock mechanics. The spectrum associated with the attenuation of seismic energy appropriate to the crust and upper mantle can be related to relaxed and unrelaxed Young's moduli (Aki & Richards, 1980). The unrelaxed modulus determined from seismic frequencies ranges from 10^{12} dyn cm^{-2} to 1.9×10^{12} dyn cm^{-2} (Anderson & Minster, 1980). However, the relaxed modulus associated with geologic processes is approximately half the unrelaxed modulus (Anderson & Minster, 1980). Poisson's ratio σ is usually set to 0.25.

As T is the controlling parameter of the rigidity, it is usual to express the flexural rigidity as an equivalent plate thickness T_e. It is very likely that only the upper lithosphere can behave elastically. The thin plate is approximating only this part of the lithosphere, and, thus, estimates of plate thickness will necessarily be less than thicknesses determined seismically (Watts & others, 1980). The rigidity is, therefore, more appropriately termed the effective or equivalent flexural rigidity. The solution of (9) (Banks & others, 1977) is (for small deflections)

$$R(k) = \frac{\Delta\rho_1}{\Delta\rho_3}\left[1 + \frac{k^4D}{\Delta\rho_3 g}\right]^{-1} H(k) \quad \ldots\ldots (10).$$

As D→0, R(k)→ $\frac{\Delta\rho_1}{\Delta\rho_3}$ H(k), which corresponds to sediment loading on a very weak plate and is termed 'Airy loading'. However, as the sediment density approaches the crustal density, R(k)→ $\frac{\Delta\rho_1}{\Delta\rho_2}$ H(k), which is the familiar Airy model, more appropriately termed 'crustal Airy'. Airy loading refers to a dynamic scheme of compensation, whereas crustal Airy refers to a static scheme of compensation. As D→∞, R(k) →0, which represents uncompensated topography.

Locally compensated topography—Airy model (D=0). For a topographic load to be locally compensated, the compensating topography mirrors h(x), and is amplified according to the density contrasts across the surface and compensating interface. From (10), setting D=0 gives R(k) = $\frac{\Delta\rho_1}{\Delta\rho_3}$ H(k). Substituting this into (8) gives

$$G_T(k) = 2\pi\gamma\ e^{-kd}\ \Delta\rho_1 H(k)\left[1 - \frac{\Delta\rho_2}{\Delta\rho_3}e^{-kt}\right] (11).$$

The Airy loading admittance becomes

$$Z_l(k) = \frac{G_T(k)}{H(k)} = 2\pi\gamma\ e^{-kd}\ \Delta\rho_1\left[1 - \frac{\Delta\rho_2}{\Delta\rho_3}\ e^{-kt}\right] \quad \ldots\ldots (12a),$$

and the crustal Airy admittance function becomes ($\rho_s \rightarrow \rho_c$)

$$Z_c(k) = 2\pi\gamma\ e^{-kd}\ \Delta\rho_1\left[1 - e^{-kt}\right] \quad \ldots\ldots (12b).$$

Either Z(k), when multiplied solely by the Fourier transform of the surface topography, gives the Fourier transform of the free-air gravity effect for the topography with its respective root in one pass. For crustal Airy, the parameter t, defined earlier, can be expressed in terms of the depth of compensation T_c by $t = T_c - d(\Delta\rho_1/\Delta\rho_2)$.

Regionally compensated topography (0<D<∞). For the topographic load to be regionally compensated, the lithosphere has a finite rigidity, which compensates the

load over a broad area. Substituting (10) into (8) gives

$$G_T(k) = 2\pi\gamma\, e^{-kd}\,\Delta\rho_1\left[1 - \frac{\Delta\rho_2}{\Delta\rho_3}\left[1 + \frac{k^4 D}{\Delta\rho_3\, g}\right]^{-1} e^{-kt}\right] H(k).$$

The resultant plate admittance function becomes

$$Z_p(k) = 2\pi\gamma\, e^{-kd}\,\Delta\rho_1\left[1 - \frac{\Delta\rho_2}{\Delta\rho_3}\left[1 + \frac{k^4 D}{\Delta\rho_3\, g}\right]^{-1} e^{-kt}\right] \quad \ldots\ldots (13).$$

Uncompensated topography ($D\rightarrow\infty$). For $D\rightarrow\infty$, there is only one layer, the surface topography, to be considered. Normalising equation (4) by the topographic transform gives

$$Z_u(k) = 2\pi\gamma\,\Delta\rho_1\, e^{-kd} \quad \ldots\ldots (14).$$

Visco-elastic rheology: Maxwell substance

An alternative model to represent the lithospheric response to applied loads is to include a time-dependent creep process, which relaxes the stresses associated with the bending of the plate. Walcott (1976) considered that the lithosphere responded to applied loads as a visco-elastic (Maxwell) substance with a relaxation coefficient of 10^5 years, and this model has been used by Beaumont (1978) and Lambeck & Nakiboglu (1981) to predict sedimentary basin stratigraphy and the gravity/geoid effect over oceanic seamounts, respectively. A Maxwell substance is one in which an initial elastic strain is followed by viscous flow (diffusion creep) when subjected to a constant load—that is, its behaviour is initially elastic, but with time its rigidity decreases to zero. The differential equation for the deflection of a visco-elastic (Maxwell) beam is given by Nadai (1963):

$$D_1 \frac{\partial^4}{\partial x^4}\dot{r}(x) + \Delta\rho_3\, g\left(\frac{r}{\tau} + \dot{r}\right) = \frac{\Delta\rho_1\, gh(x)}{\tau} \quad \ldots (15)$$

where $\dot{r}$ indicates the first derivative with respect to time, t', and τ, the relaxation coefficient, is defined as $3\eta/E$, where η is the effective viscosity of the beam. Rewriting the solution by Walcott (1976),

$$R(k) = \frac{\Delta\rho_1}{\Delta\rho_3}\left[1 + \frac{k^4 D_1}{\Delta\rho_3\, g}\right]^{-1}\left[1 + \frac{k^4 D_1}{\Delta\rho_3\, g}\left[1 - \exp\frac{-t'}{\tau\left[1 + \frac{k^4 D_1}{\Delta\rho_3\, g}\right]}\right]\right] H(k) \quad \ldots\ldots (16)$$

For finite times ($0<t'<\infty$), the history of the relaxation process is controlled by $\tau[1+k^4D_1/\Delta\rho_3 g]$. Since k, the wave number, is related to the load wavelength (generally assumed to be the topographic wavelength), the rate of relaxation is dependent on the relaxation coefficient, τ, and the topographic wavelength (Beaumont, 1978). In particular, for a given depth of compensation, long-wavelength topography approaches its isostatic equilibrium position more rapidly than shorter wavelength loads (Fig. 2). Short-wavelength topography will, therefore, appear to be loading a more rigid plate relative to longer-wavelength topography. The equivalent mechanical analogue implied by a Maxwell rheology is shown in Figure 2 as a series connection of spring and dashpot elements. The rigidity D_1 refers to the spring constant and is equated to the lithospheric rigidity at the time of loading. For relatively cold lithosphere, D_1 is usually set to 10^{32} dyn.cm, which is equivalent to a seismic thickness of 100 km. The dashpot has a viscosity η, independent of time.

The free-air gravity effect over a topographic load on a visco-elastic (Maxwell) plate will, therefore, be a function of the initial plate thickness, the wavelength of the load, and the effective viscosity of the plate. The admittance function for this rheology is,

$$Z_M(k) = 2\pi\gamma\, e^{-kd}\,\Delta\rho_1\left[1 - \frac{\Delta\rho_2}{\Delta\rho_3}\left[1 + \frac{k^4 D_1}{\Delta\rho_3\, g}\right]^{-1}\left[1 + \frac{k^4 D_1}{\Delta\rho_3\, g}\left[1 - \exp\frac{-t'}{\tau\left[1 + \frac{k^4 D_1}{\Delta\rho_3\, g}\right]}\right]\right] e^{-kt}\right] \quad \ldots (17)$$

Visco-elastic rheology: general linear substance

Observations of plate flexure associated with oceanic loads, such as seamounts, large deltas, and mid-oceanic ridges, indicate that the flexural rigidity of the oceanic lithosphere is a function of its age at the time of loading (Watts, 1978) and is consistent with empirical yield-stress envelopes based on the deformation of olivine (Bodine & others, 1981). These results suggest that the elastic thickness, T_e, is significantly smaller than the seismic thickness, T_s, of oceanic lithosphere and that once T_e is acquired, it remains constant, at least over the age range of the oceans. Since T_s is determined from short duration loading associated with the propagation of seismic body waves, the systematic variation between T_s and T_e suggests that there must be a rapid relaxation from the seismic thickness to the elastic thickness. The age of most of the loads used to constrain the variation of T_e with age is greater than 1 m.y., and so the relaxation must be complete within 10 m.y.

Since the lithospheric rigidity appears to increase with age, the decaying rigidity associated with a Maxwell substance would appear to be an inappropriate rheology for the lithosphere.

A general linear visco-elastic substance, which is based on the response of a parallel combination of spring and dashpot elements, is an example of a rheology that at least is consistent with observations of oceanic flexure, in that, immediately after loading, there is a rapid relaxation of the plate rigidity from its initial rigidity, defined by the seismic thickness, to an asymptotic rigidity, defined by the age of the plate (Fig. 2). If τ is calibrated against the relaxation predicted by loading a plate whose properties are determined by the yield envelope for olivine, then τ will characterise the deformation properties of olivine.

Following the procedure for the Maxwell rheology, the differential equation associated with the loading of a visco-elastic (general linear) beam is

$$D_f \frac{\partial^4}{\partial x^4}(r + \tau\dot{r}) + \Delta\rho_3\, g\,(r + \tau\frac{D_f}{D_i}\dot{r}) = \Delta\rho_1\, gh(x) \quad \ldots\ldots (18),$$

where r, ṙ, τ, $\Delta\rho_1$, $\Delta\rho_3$, and g have been been previously defined. D_i and D_f refer to the equivalent rigidities associated with the seismic and asymptotic elastic plate thicknesses, respectively. The solution of (18) in the frequency domain is

$$R(k) = \frac{\Delta\rho_1}{\Delta\rho_3}\left[E_f + (E_i - E_f)\exp\left[\frac{-t' D_i E_i}{\tau D_f E_f}\right]\right]H(k) \quad \ldots\ldots (19),$$

where

$$E_i = \left[1 + \frac{k^4 D_i}{\Delta\rho_3 g}\right]^{-1}$$

and

$$E_f = \left[1 + \frac{k^4 D_f}{\Delta\rho_3 g}\right]^{-1}$$

At the time of loading ($t'=0$), the flexural response R(k) is $\frac{\Delta\rho_1}{\Delta\rho_3} E_i$ and represents the initial elastic deflection of the lithosphere with the maximum rigidity defined by the seismic thickness. As

$$t' \to \infty,\ R(k) \to \frac{\Delta\rho_1}{\Delta\rho_3} E_f$$

and represents the flexure of the lithosphere with an asymptotic rigidity $D_f < D_i$ (Fig. 2).

For $0<t'<\infty$, the rate of relaxation is controlled by the product $[\tau D_f E_f / D_i E_i]$ and so is dependent now not only on the topographic wavelength and the relaxation coefficient, but also the difference between T_s and T_e (Fig. 2). The respective admittance function for this rheology, using (19), is

$$Z_G(k) = 2\pi\gamma\, e^{-kd}\left[1 - \frac{\Delta\rho_2}{\Delta\rho_3}\left[E_f + (E_i - E_f)\exp\left\{\frac{-t' D_i E_i}{\tau D_f E_f}\right\}\right] e^{-kt}\right] \quad \ldots\ldots (20).$$

This section on visco-elastic models is not an exhaustive list or description of possible lithospheric rheological models, but serves as an example of how admittance functions can be created that represent complicated rheologies. These can then be compared with observed admittance functions calculated from real topographic/bathymetric and gravimetric data, so that inferences concerning isostatic mechanisms and rheologic properties of the lithosphere can be made.

Spatially varying density.

In the models considered so far the density contrasts have been assumed to be laterally constant. A second class of important isostatic models assumes that density and topography are inversely related and that there is no root topography; these local compensation schemes include the Pratt-Hayford models. Thermal effects predicted by stretching models of margin formation (for example, the crustal section of Fig. 4b, Steckler & Watts, 1980) suggest a combination of Airy and Pratt compensation—the necking of the lithosphere giving an Airy-type response, and the thermal variations across the margin giving a Pratt-type response. So far, the admittance functions considered are independent of topography. Pratt-type models, however, cannot be expressed with the same simplicity. To show this, the first-order term of equation (5) has the form

$$G(k) = 2\pi\gamma\, e^{-kd}\, F[\rho(x)\ h(x)] \quad \ldots\ldots (21).$$

For Pratt-type isostasy, $\rho(x) = \frac{\rho_o T_c - \rho_w h(x)}{T_c - h(x)}$, where T_c is the depth of compensation and ρ_o is the crustal density corresponding to topography at sea level. The resultant Fourier domain gravity effect becomes

$$G(k) = 2\pi\gamma\, e^{-kd}\ (T_c F[\rho(x) - \rho_o] + \rho_w H(k)) \quad \ldots\ldots (22).$$

An approximate linear function can be obtained for the Pratt model by calculating equivalent layers for the surface topography at mean depth d and the compensating horizontal density contrast $(\rho(x) - \rho_o)$ at a mean depth $(T_c/2 + d + h(x)) \sim d + T_c/2$. The gravity effect of the surface topography, in the Fourier domain, is

$$G_1(k) = 2\pi\gamma\, e^{-kd}\, F[(\rho(x) - \rho_o) h(x)]$$
$$\approx 2\pi\gamma\, e^{-kd}\, (\rho_o - \rho_w)\, H(k)$$

Similarly, the gravity effect of the equivalent compensating topography is,

$$G_2(k) = -2\pi\gamma\, e^{-k(d + T_c/2)}\, F[(\rho_o - \rho(x))\,(T_c + h(x))].$$

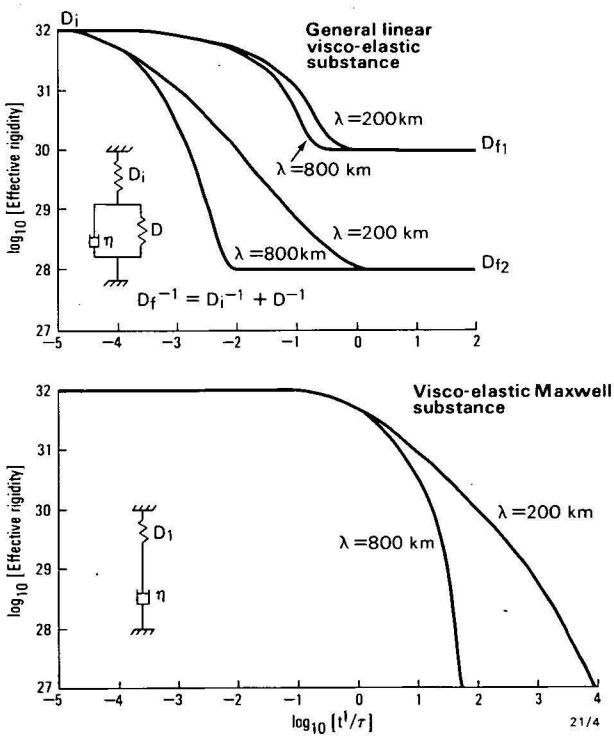

Figure 2. Theoretical flexural response of a beam to applied loads of varying wavelength for the Maxwell and general linear viscoelastic models.
The logarithm of the effective elastic rigidity (dyn.cm) is plotted against the logarithm of the ratio of the elapsed time since loading and the respective relaxation coefficient for the Maxwell and the general linear models. The equivalent mechanical system of spring and dashpot elements for each model is also shown. In either case, the shorter the topographic wavelength, the more rigid the response, which is consistent with free-air gravity observations over surface topography, viz., in general, small topographic features appear less compensated than wide topographic features. The fundamental differences between the two models are readily apparent; the decreasing rigidity with time for the Maxwell model and the asymptotic rigidity limit for the general linear model.

Since, for Pratt isostasy, $(\rho_o-\rho(x))\ (T_c+h(x)) = (\rho_o-\rho_w)h(x)$, then

$$G_2(k) = -2\pi\gamma\, e^{-k(d+T_c/2)}\ (\rho_o - \rho_w)H(k).$$

Therefore, the Fourier domain gravity effect over a given topographic surface h(x) that is compensated according to the Pratt model is

$$G(k) = G_1(k) + G_2(k) = 2\pi\gamma\, e^{-kd}\ (\rho_o - \rho_w) .H(k)\ [1 - e^{-kT_c/2}] \quad \ldots\ldots (23),$$

and so the Pratt admittance function becomes

$$Z_{PT} = 2\pi\gamma\, e^{-kd}\ (\rho_o - \rho_w)\ [1 - e^{-kT_c/2}] \ldots (24).$$

Non-linearity effects.

The basic requirement in formulating admittance functions is that the surface and root topography be linearly related. This has been achieved in the Airy and plate models by approximating the gravity effect of the two-interface system by the first term of equation (5). Thus, higher powers of the topography are not included in the gravity calculation. For example, the Fourier transform of the gravity effect for the crustal Airy model using all topographic powers becomes

$$G(k) = 2\pi\gamma\ \Delta\rho_1\ e^{-kd} \sum_{n=1}^{\infty} \frac{k^{n-1}}{n!}\ F[h^n(x)] \left[1 - \left[\frac{\Delta\rho_1}{\Delta\rho_3}\right]^{n-1} e^{-kt}\right] \quad \ldots\ldots (25).$$

The corresponding admittance function, as with the varying density models above, therefore requires knowledge of the topography, and is not as simple to use as the previous form of the admittance (e.g. equation 12).

The error associated with truncating equation (5), and, hence, in predicting gravity by this method, is controlled by the maximum slope (minimum slope width) and dominant wavelength of surface and root topographies, the depth of compensation, or plate thickness, and the data profile length. Because of the complicated interaction of these factors, a detailed error analysis is feasible only on a case-by-case basis. For each particular application of the admittance technique, a simple check of higher-order contributions should always be made (e.g. Watts, 1978; Detrick & Watts, 1979). The **maximum** possible error is obtained when the topographic slope is a maximum and the mean depth of the root topography is a minimum (i.e. $T_e=0$ and $T_c=0$, respectively). Figure 3 attempts to show empirically the error associated with predicting the free-air gravity for the simple isostatic model shown. Plotted is a contour map showing the interaction between the topographic slope width and the depth of compensation. The contours represent the percentage error in predicting gravity using equation (5) for a range of slopes and compensation depths. The T_c limit of 20 km is set by the maximum water depth and densities used in the model (d=2.5 km). In this model, the profile and plateau lengths were 800 and 200 km, respectively.

Truncating equation (5) removes the contribution by higher powers of the topography to the gravity anomaly. Higher topographic power contains information concerning the higher frequencies in gravity. Generally, the predictive accuracy will increase as the topographic waveform approaches progressively lower frequencies. Decreasing the slope essentially decreases the topographic frequency and, hence, increases the predictive accuracy.

Two slopes help control the error, one related to the surface topography and the other related to the root topography (Fig. 3). The maximum slope of the root topography will be greater than the maximum slope of the surface topography, since it is amplified by the density contrasts across the surface and root interfaces. Increasing T_c reduces the effect of the compensating root, because the upward continuation operator, e^{-kt}, acts as a low-pass filter. When the magnitude of the filtered root topography approaches the magnitude of the surface topography, the predictive error is a minimum, as can be seen in Figure 3 as a trend of local minima between slope values of 20 and 30 km. This minimum separates an upper field, where the filtered root topography is greater than the surface topography, and a lower field, where the filtered root topography is less than the surface topography. As a consequence of this, the predictive accuracy increases with decreasing T_c in the lower field.

The effects of increasing the elastic thickness in the plate model can be discussed in terms of the results

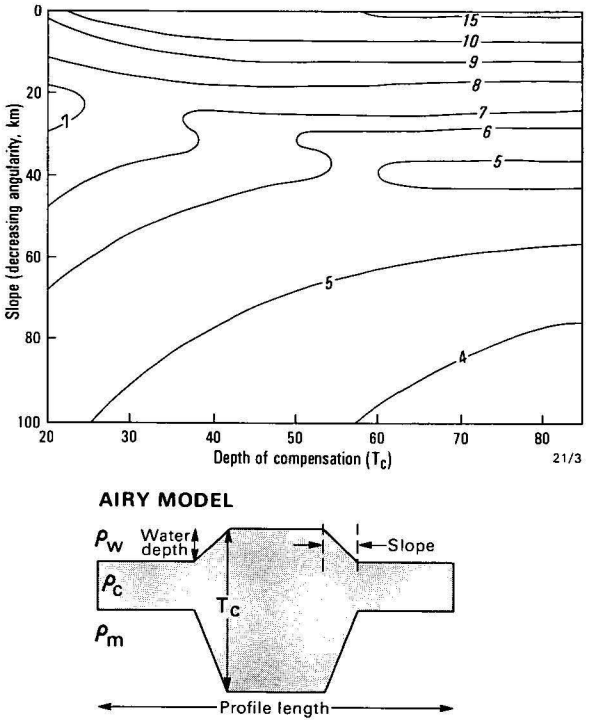

Figure 3. Predictive error associated with calculating the free-air gravity effect over a simple bathymetric shape for a range of topographic slope widths and depths of compensation, T_c.

Error here means the percentage contribution of the second-order term relative to the sum of the first and second-order terms. For the isostatic model, it was assumed that $\rho_w = 1030$, $\rho_c = 2800$, $\rho_m = 3400$ kg m^{-3}, and the profile and plateau lengths were 800 and 200 km, respectively. For most practicable applications, the maximum error is less than 10%.

in Figure 3. Loading on low plate thicknesses causes deflections with large curvatures or slopes. Increasing the plate thickness will progressively decrease the amplitude of the root topography associated with the loading. As the Airy model represents an end-member of the plate model (T_e=0), the corresponding root topography for a given load will be a maximum. Errors caused by using the plate model for a particular T_e and T_c will, therefore, be less than the error for the corresponding Airy model.

Theoretically, as the dominant wavelength approaches the data profile length, the predictive accuracy will increase. This is related to the easier approximation of the topographic waveform by longer wavelengths, which contain more energy than the shorter wavelengths. Practically however, errors associated with aliasing become increasingly significant when the dominant wavelength increases. Aliasing causes spectral contamination of the shorter wavelengths and, hence, a decrease in predictive accuracy.

For most applications (T_c>20 km and slope width > 10 km), the maximum error in predicting gravity using this admittance technique is less than 10 per cent. Because the deflection predicted by the linear theory is always over-estimated (Ribe, in prep.), the gravity effect is underestimated. Similarly, when matching observed gravity anomalies to those calculated from linear models, the plate thickness will be an upper bound.

Conclusions

Simply using the equivalent layer formula, the free-air effect of even complicated isostatic models can be rapidly computed. The analysis presented was for two-interface systems, but compensation for a third interface or more is readily apparent: the gravity effect of the n^{th} interface is calculated by defining the relation between the surface and interface topography, continued upward to the surface. The sum of the gravity effect for all interfaces normalised for the surface topography defines the equivalent admittance function.

Acknowledgements

My thanks to J. H. Bodine, J. C. Dooley, A. B. Watts, and C. L. Mrozowski for their critical appraisal of this manuscript. My thanks also to G. Grace for her painstaking efforts in typing the manuscript. This work was supported by an Australian Public Service Post-graduate Scholarship, while I was on study leave from the Bureau of Mineral Resources, Canberra.

References

AKI, K., & RICHARDS, P. G., 1980—Quantitative seismology, theory and methods. *W. H. Freeman & Co., San Francisco.*

ANDERSON, D. L., & MINSTER, J. B., 1979—The frequency dependence of Q in the Earth and implications for mantle rheology and Chandler Wobble. *Geophysical Journal of the Royal Astronomical Society*, 58, 431-40.

BANKS, R. J., PARKER, R. L., & HUESTIS, S. P., 1977—Isostatic compensation on a continental scale: Local versus regional mechanisms. *Geophysical Journal of the Royal Astronomical Society*, 51, 431-52.

BANKS, R. J., & SWAIN, C., 1978—Isostatic compensation of East Africa. *Proceedings of the Royal Society of London, Series A*, 364, 331-52.

BARRELL, J., 1914—The strength of the Earth's crust, Part VIII. Physical conditions controlling the nature of the lithosphere and asthenosphere. *Journal of Geology*, 22, 425-43.

BEAUMONT, C., 1978—The evolution of sedimentary basins on a viscoelastic lithosphere: theory and examples. *Geophysical Journal of the Royal Astronomical Society*, 55, 471-98.

BODINE, J. H., STECKLER, M. S., & WATTS, A. B., 1981—Observations of flexure and the rheology of the oceanic lithosphere. *Journal of Geophysical Research*, 86, 3695-707.

CALDWELL, J. G., HAXBY, W. F., KARIG, D. E., & TURCOTTE, D. L., 1976—On the application of a universal elastic trench profile. *Earth and Planetary Science Letters*, 31, 239-46.

CHAPPLE, W. M., & FORSYTH, D. W., 1979—Earthquakes and bending of plates at trenches. *Journal of Geophysical Research*, 84, 6729-49.

COCHRAN, J. R., 1973—Gravity and magnetic investigations in the Guiana Basin, Western Equatorial Atlantic. *Geological Society of America Bulletin*, 84, 3249-68.

COCHRAN, J. R., 1979—An analysis of isostasy in the world's oceans: 2. Mid-ocean ridge crests. *Journal of Geophysical Research*, 84, 4713-29.

DEAN, W. C., 1958—Frequency analysis for gravity and magnetic interpretation. *Geophysics*, 23, (1), 97-127.

DETRICK, R. S., & WATTS, A. B., 1979—An analysis of isostasy in the world's oceans; 3. Aseismic ridges. *Journal of Geophysical Research*, 84, 3637-53.

DORMAN, L. M., & LEWIS, B. T. R., 1970—Experimental isostasy, 1. Theory of the determination of the Earth's isostatic response to a concentrated load. *Journal of Geophysical Research*, 75, 3357-65.

GOETZE, C., & EVANS, B., 1979—Stress and temperature in the bending lithosphere as constrained by experimental rock mechanics. *Geophysical Journal of the Royal Astronomical Society*, 59, 463-78.

GRANT, F. S., & WEST, G. F., 1965—Interpretation theory in applied geophysics. *McGraw-Hill, New York.*

HANKS, T. C., 1971—The Kuril trench—Hokkaido rise system: Large shallow earthquakes and simple models of deformation. *Geophysical Journal of the Royal Astronomical Society*, 23, 173-89.

HETENYI, M., 1946—Beams on elastic foundation. *University of Michigan Press, Ann Arbor.*

HUBBARD, M. K., 1948—A line-integral method for computing the gravimetric effects of two-dimensional masses. *Geophysics*, 13, 215-25.

JEFFREYS, H., 1959—The Earth. *Cambridge University Press, 4th edition.*

LAMBECK, K., & NAKIBOGLU, S. M., 1981—Seamount loading and stress in the ocean lithosphere, 2, Visco-elastic and elastic-visco-elastic models. *Journal of Geophysical Research*, 86, 6961-84.

LEWIS, B. T. R., & DORMAN, L. M., 1970—Experimental isostasy, 2. An isostatic model for the USA derived from gravity and topographic data. *Journal of Geophysical Research*, 75, 3367-86.

MCKENZIE, D. P., & BOWIN, C., 1976—The relationship between bathymetry and gravity in the Atlantic Ocean. *Journal of Geophysical Research*, 81, 1903-15.

MCNUTT, M. K., & PARKER, R. L., 1978—Isostasy in Australia and the evolution of the compensating mechanism. *Science*, 199, 773-5.

MONTADERT, L., DE CHARPAL, O., ROBERTS, D., GUENNOC, P., & SIBUET, J.-C., 1979—North-east Atlantic passive margins: Rifting and subsidence processes. *American Geophysical Union, Maurice Ewing Series*, 3, 154-86.

NADAI, A., 1963—Theory of flow and fracture of solids, 2. *McGraw-Hill, New York.*

PARKER, P. L., 1972—The rapid calculation of potential anomalies. *Geophysical Journal of the Royal Astronomical Society* 31, 447-55.

RIBE, N. M., in prep.—On the interpretation of frequency response functions for oceanic bathymetry and gravity.

STECKLER, M. S., & WATTS, A. B., 1980—The Gulf of Lion: Subsidence of a young continental margin. *Nature*, 287, 425-9.

TALWANI, M., 1973.—Computer usage in the computation of gravity anomalies. *In* BOTT, B. A. (editor), Methods in computational physics, 13. *Academic Press, New York*, 343-89.

WALCOTT, R. I., 1970—Flexural rigidity, thickness, and viscosity of the lithosphere. *Journal of Geophysical Research*, 75, 3941-54.

WALCOTT, R. I., 1976—Lithospheric flexure, analysis of gravity anomalies, and the propagation of seamount chains. *In* SUTTON, G. H., MANGHNANI, M. H. & MOBERLY, R. (editors), *American Geophysical Union, Geophysical Monograph* 19, 431-8.

WATTS, A. B., 1978—An analysis of isostasy in the world's oceans: 1. Hawaiian-Emperor seamount chain. *Journal of Geophysical Research*, 83, 5989-6004.

WATTS, A. B., BODINE, J. H., & STECKLER, M. S., 1980—Observations of flexure and the state of stress in the oceanic lithosphere. *Journal of Geophysical Research*, 85, (B11), 6369-76.

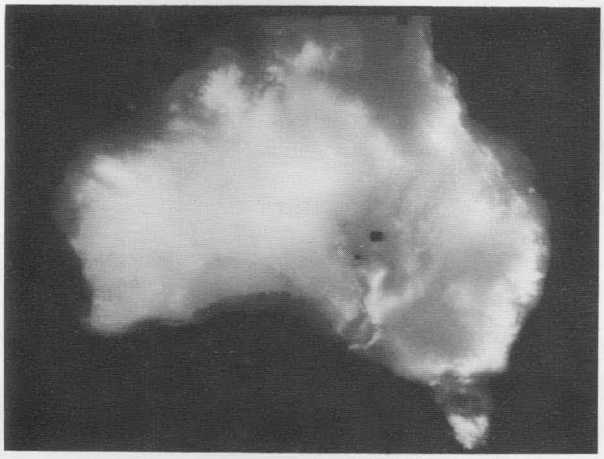

Figure 1. Initial monochrome image created from gridded spot heights and bathymetric data.
Black squares are areas where incorrect data have been removed.

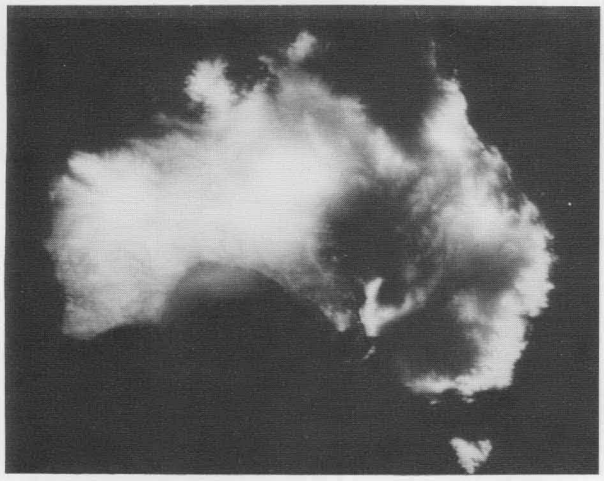

Figure 2. Image of Figure 1 data enhanced by histogram equalisation.

Figure 3. Image of topographic gradient (west to east).

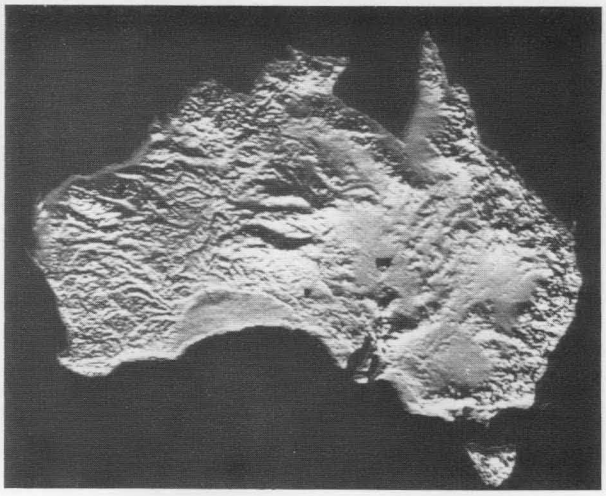

Figure 4. Image of topographic gradient (south to north).

Gonzalez & Wintz, 1977), which is incorporated in BMR's image processing system. The transformation simply assigns a colour to every pixel value in the range 0 to 255, using 256 colours. The assignment of colours can be changed for different purposes, but a maximum colour contrast between adjacent pixel values is normally desirable. The pseudocolour transformation can be equated to colouring the contour intervals on a topographic map. The top and bottom-left images on the front cover of this journal show the effects of two different pseudocolour transformations of the enhanced monochrome image shown as Figure 2. Hundreds of other pseudocolour transformations are possible and can be obtained easily on the TV monitor. Owing to the way in which digital data are displayed on the square pixel arrangement of the television monitor, a distorted projection is presented. All illustrations in this note approximate a rectangular display of meridians and parallels, and the coastline and geographic coordinates were generalised and added independently of the digital data files.

The bottom-left coloured image also shows the effect of selected colour assignment: only topography higher than 120 m above sea level is displayed in colour, all levels below 120 m being assigned to black. The level to which black is assigned on such a display can be increased in real time to give the effect of progressive 'continental flooding'.

Bit-plane images

Once a digital data set has been quantised and loaded into a digital image analysis system, a variety of manipulations can be applied to enhance the image. One technique is to look separately at each of the bit-planes that are normally stacked together to make up the total stored image. This technique can be likened to the effect of performing spatial frequency filtering. The least significant bit-plane (bit 0) shows the greatest variation and is very noisy; it shows the odd and even image values. The most significant plane (bit 7 in an 8-bit image) shows the least variation and can be likened to an over-smoothed image. These two extremes, bit 0 and bit 7, have limited value when displayed as a binary image, but several of the intermediate planes show features (particularly lineaments) more readily detectable than in other DTM manipulations (Harrington & others, 1982).

Figure 5. Synthetic reflectance images for simulated sun elevation of 15° and various sun azimuth directions.

BMR Journal of Australian Geology & Geophysics, 7, 63-7.

COMPUTER MANIPULATION OF A DIGITAL TERRAIN MODEL (DTM) OF AUSTRALIA

R. F. Moore & C. J. Simpson

Images of the topography of Australia (DTM) have been created from a digital data file of about 320 000 topographic spot heights measured during the gravity survey of Australia, resampled on a regular grid, and manipulated with a Comtal image analysis system to enhance topographic features. Three manipulations: pseudo-colour transformations, bit-plane images, and synthetic reflectance images are illustrated and discussed to give an idea of the range of computer techniques that can be used to enhance continental topography for geologic or related study. Improvements are inevitable in this new technique, which is applicable to any regional data that can be digitised, such as magnetic, gravity, or radiometric data.

Introduction

The topographic data that have long been used in geomorphological and geological research have been displayed in several ways, including contour maps, three-dimensional scale models, stacked (coulisse) profiles, stereoscopic models projected from aerial photographs, line-scanner images from space vehicles, and, more recently, computer-generated stacked profiles and isometric drawings.

Last year a black and white image and a coloured map of digital terrain data of the conterminous USA were published by Kane (1981) and Godson (1981), respectively. On the cover of this issue of the BMR Journal there are the first published examples of coloured images of the topography of Australia created from a digital data file and photographed from the screen of the Comtal image analysis system at the Bureau of Mineral Resources (BMR). The display approach used was similar to Kane's, but was developed independently, and, in addition, colour and various image analysis techniques were employed to specifically enhance topographic features so that their geologic or geomorphic significance could be more easily studied.

The Digital Terrain Model (DTM)

The basis of this work is the rather novel display of elevation data on a regular grid as a digital image. (A digital image is simply a digital representation of what is normally called a picture, and its smallest independent unit is the picture element or pixel). The image display system used in the study at BMR allows an image with 512 lines and 512 pixels per line to be displayed on a 48 cm colour television monitor.

The elevation data came from a continent-wide grid of spot heights used to correct gravity readings during the production of the 1979 Gravity Map of Australia (Anfiloff & others, 1976). The grid for the DTM, on a spacing of 6 minutes of latitude and longitude, was sampled from a 3 minute grid of about 320 000 points. This grid is held in the Australian National Gravity Repository data bank at BMR. The spot heights are not necessarily a representative sample of the extreme heights in any district, because the techniques of gravity surveying require observations to be made at sites that are locally level.

The gridding process involves the formation of a mathematical surface of minimum curvature passing through the spot heights and interpolated on to the regular grid by an iterative process, as described by Briggs (1974). When the grid was produced, the data bank had not been checked systematically for errors. Individual incorrect point values occur throughout the data, and in some districts whole blocks of data are in error. Consequently, the grid is not reliable enough to be made generally available at present, but we do not consider the errors significant for the purpose of this note. The gravity data bank is currently being checked systematically with the aim of producing a corrected grid of heights at 3-minute spacing.

Image quantisation

Because pixels have a limited range of values, before a DTM can be displayed as an image, it must be scaled down by a process termed image quantisation. For this investigation, it was necessary to quantise or scale the DTM so that the elevation data could be represented by pixel values in the range 0-255 (for an 8-bit image).

There are several ways of performing this process (Rosenfeld & Kak, 1976; Pratt, 1978), but, in this case, a simple linear quantisation was used. Bathymetric data were included, and depths of 1270 m or more below sea level were set to pixel value of zero. Heights of of 1280 m or more above sea level were set to 255. Intermediate points were scaled linearly between 0 and 255, so that sea level, for example, was quantised to pixel value 127.

After quantisation the DTM can be displayed as a monochrome (black and white) image in which a pixel value of 0 (−1270 m) is black and 255 (+ 1280 m) is white, with 255 grey level steps in between (Fig. 1). The image contrast in Figure 1 is poor because of the method of quantisation, but digital image enhancement techniques can be applied to compensate for the method of quantisation and to improve the image contrast. In this investigation, the digital image processing technique known as histogram equalisation (Hall & others, 1971; Hummel, 1975; Gonzalez & Fittes, 1977) was found to give the best result (Fig. 2).

Pseudocolour transformation

The human eye can distinguish differences in any of the three visual coordinates of hue, saturation, and intensity (luminance). In black and white images the eye responds only to differences in intensity, over the grey-scale range of black to white. If, however, the monochrome image is converted to colour, all three of the visual coordinates can be used to detect subtle variations in image values. This can be done with a pseudocolour transformation (Miller & Badler, 1977;

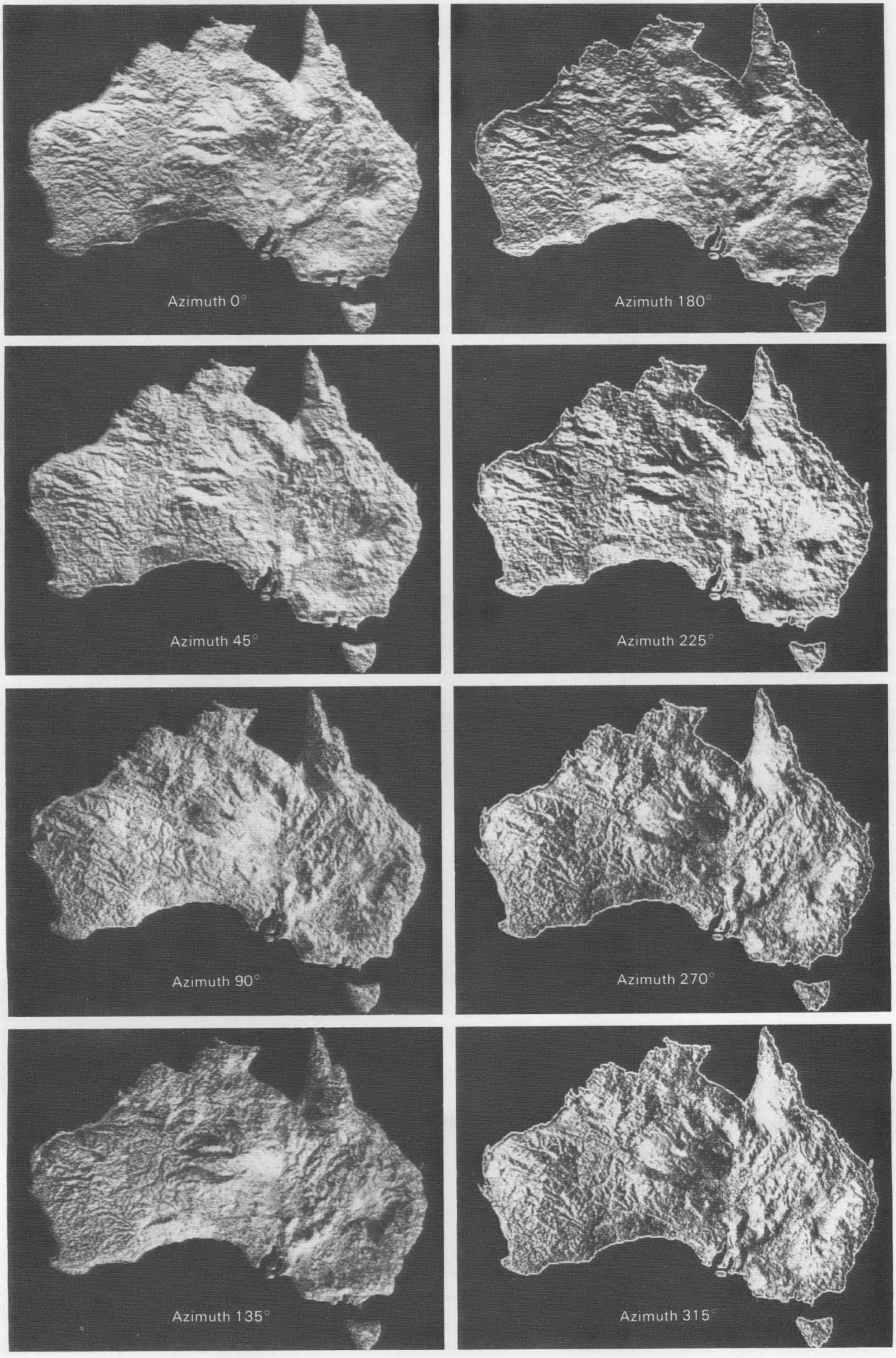
Azimuth 0°
Azimuth 180°
Azimuth 45°
Azimuth 225°
Azimuth 90°
Azimuth 270°
Azimuth 135°
Azimuth 315°

Synthetic reflectance images

The detection of lineaments with topographic expression is often facilitated by the presence of shadows, and this principle is used in terrain interpretation of aerial photographs, satellite images, and side-looking radar imagery. A constraint on its usefulness, however, is that lineaments with topographic expression aligned parallel to the illumination direction have no shadows. The strongest shadows are formed by features oriented perpendicular to the illumination. Using reflectance map techniques, synthetic images for any given conditions of sun illumination can be generated from topographic gradient data derived from a DTM (Horn & Bachman, 1978; Horn, 1981).

The reflectance of a surface element for given illumination conditions is a function of its gradient, and a reflectance map shows the relation between the apparent brightness of a surface element and its gradient in the west-to-east and south-to-north direction. Hence, for any given conditions of sun illumination (defined by azimuth θ and elevation ϕ), a synthetic image of apparent brightness at each point on the DTM under discussion can be derived and displayed as a monochrome image.

In defining the reflectance map, the topographic gradient for each surface element in the DTM must be calculated as an intermediate step. The gradient of a planar surface has two components along two mutually perpendicular directions. If the surface height, z, is expressed as a function of two coordinates, x and y, then the two components, p and q, of the gradient are defined as the partial derivatives of z with respect to x and y respectively. In this case, if the x-axis points east, the y-axis points north, and the z-axis is up, then p is the slope of the surface in the west-to-east direction and q is the slope in the south-to-north direction:

$$p = \frac{\partial z}{\partial x} \qquad q = \frac{\partial z}{\partial y}$$

One estimate of the gradient for a DTM is derived using first differences:

$$p \simeq (z_{i+1,j} - z_{ij})/\Delta$$
$$q \simeq (z_{i,j+1} - z_{ij})/\Delta$$

where $(z_{i+1,j})$ is the point immediately to the east of (z_{ij}) and $(z_{i,j+1})$ is the point immediately to the south of (z_{ij}); Δ is the grid spacing. This simple approximation was found to be sufficient for this application and has the advantage of being easy to calculate. These two intermediate gradient data sets can be displayed as monochrome images, as shown in Figures 3 and 4. In these illustrations dark areas show low (negative) gradients and light areas show high (positive) gradients, the overall impression being of illumination from the west and south, respectively.

Treatment of the DTM for a west to east gradient (Fig. 3), for example, shows a series of northwest-trending lineaments across central and western Australia, which are not so obvious in the south to north gradient image.

After derivation of the two-component gradient for each surface element in the DTM, apparent brightness, as observed looking down the z-axis (i.e. perpendicular to the plane of the DTM), can be calculated for each surface element using:

$$\Phi p,q = \frac{(1+p_s p+q_s q)}{\sqrt{1+p_s^2+q_s^2}\,\sqrt{1+p^2+q^2}}$$

where $p_s = \sin\theta \cot\phi$, and $q_s = \cos\theta \cot\phi$

Using this equation, after Horn & Bachman (1978), a series of synthetic monochrome images was displayed in which sun elevation (θ) was maintained at 15° and the sun azimuth (ϕ) was changed in increments of 45°. It should be noted that the surface albedo was assumed to be 1 (i.e. perfect reflector) and that, since the reflectance map gives reflectance as a function of the local surface gradient only, it does not take into account effects of the position of the surface element, such as mutual illumination of surface elements and cast shadows.

The images are shown in Figure 5, and for comparison are positioned so that opposing illumination directions are adjacent. The mind is not conditioned to seeing apparent relief illustrations with illumination from the south, and the illusion of inverted relief can sometimes occur. The illustrations were photographed from the TV screen and in this paper are reproduced at a very small size. Despite this, the potential of such images for studying continental structures, both linear and circular is apparent. For example, on several images a broad lineament can be seen extending from Spencer Gulf to the bottom of the Gulf of Carpentaria. Several comparable features noted in the DTM are discussed by Harrington & others (1982).

The types of display and manipulation discussed above are applicable not only to topography, but to any digital data sampled on a regular grid, for example gravity, magnetic, and radiometric data. Data can also be superimposed as multiple sets, and there is considerable scope for the development of these new techniques for structural analyses of large regions.

Acknowledgements

The authors wish to acknowledge the work of the Regional Gravity Section of the BMR. Without their long term efforts in assembling the Australian National Gravity Repository data bank, our work would not have been possible. Sources of substantial contributions of gravity data are New South Wales, South Australian and Tasmanian Mines Departments, University of Tasmania, and West Australian Petroleum Pty Ltd.

References

ANFILOFF, W., BARLOW, B. C., MURRAY, A. S., DENHAM D., & SANDFORD, R., 1976—Compilation and production of the 1976 Gravity Map of Australia. *BMR Journal of Australian Geology & Geophysics*, 1, 273-6.

BRIGGS, I. C., 1974—Machine contouring using minimum curvature. *Geophysics*, 39, 39-48.

GODSON, R. H., 1981—Digital terrain map of the United States. *United States Geological Survey, Miscellaneous Series*, Map I-1318.

GONZALEZ, R. C., & FITTES, B.A., 1977—Gray-level transformaticns for interactive image enhancement. *Mechanism and Machine Theory*, 12, 111-22.

GONZALEZ, R. C., & WINTZ, P. A., 1977—Digital Image Processing. *Addison-Wesley*, Ch. 4.

HALL, E. L., KRUGER, R. P., DWYER, S. J., HALL, D. L., MCLAREN, R. W., & LODWICK, G. S., 1971—A survey of preprocessing and feature extraction techniques for radiographic images. *IEEE Transactions on Computers*, C-20 (9), 1032-44.

HARRINGTON, H. J., SIMPSON, C. J., & MOORE, R. F., 1982—Analysis of continental structures using a digital terrain model (DTM) of Australia. *BMR Journal of Australian Geology & Geophysics*, 7, 68-72.

HORN, B. K. P., 1981—Hill shading and the reflectance map. *Proceedings of the IEEE*, 69(1), 14-47, January 1981.

HORN, B. K. P., & BACHMAN, B. L., 1978—Using synthetic images to register real images with surface models. *Communications of the ACM*, 21(11), 914-24, November 1978.

HUMMEL, R. A., 1975—Histogram modification techniques. *Computer graphics and image processing*, 4, 209-24.

KANE, M., 1981—No title (Photograph of monochrome terrain model of the United States, with caption). *EOS (American Geophysical Union, Transactions)*, 61(1), 6 January 1981.

MILLER, L. C., & BADLER, N. I., 1977—Towards a formal model for pseudocolour selection. Proceedings of the IEEE Computer Society conference on pattern recognition and image processing New York, June 1977. *IEEE Press*, 261-5.

PRATT, W. K., 1978—Digital Image Processing. *John Wiley, New York*, Chapter 6.

ROSENFELD, A., & KAK, A. C., 1976—Digital Image Processing. *Academic Press*, 98-105.

BMR Journal of Australian Geology & Geophysics, 7, 68-72.

ANALYSIS OF CONTINENTAL STRUCTURES USING A DIGITAL TERRAIN MODEL (DTM) OF AUSTRALIA

H. J. Harrington, C. J. Simpson, & R. F. Moore

Colour images of the topography of Australia, generated and manipulated by computer techniques, have been used for analysis of regional geological structures. Discussion is concentrated on lineaments, because some workers have claimed that Australia's largest metalliferous deposits are related to systems of lineaments, and much work is being done on them by the mineral and petroleum exploration industries. There is only partial correspondence of topographic lineaments with those based on gravity or aeromagnetic data, at least at the present early stage of development of DTM studies. On the other hand, some major new lineaments have been found in the DTM, for example, one that continues for hundreds of kilometres from the southeast end of the Emu Fault on which the giant HYC ore body occurs. This feature is parallel to the Roxby Downs gravity lineament. DTM images provide a new tool for recognising regional geological structures and are potentially useful for mineral exploration.

Introduction

Australia has a long history in the use of topography for identifying regional structures, which perhaps started seriously with the celebrated study of eastern Australia by Griffith Taylor (1911). Hills (1956, 1961) was the first to discuss "morphotectonic" features and patterns in Australia as a whole, and he emphasised the value of scale models and aerial photographs for detecting major structural lineaments. There was a major upsurge of interest in that kind of work with the advent of spacecraft pictures of the Earth and, particularly, with the introduction of the Landsat series of satellites in 1972. The satellites have stimulated an expanding, multibillion dollar business on a world-wide basis, and within that framework Australia has built its own Landsat receiving and processing facility. Studies of Landsat images have shown many regional linear structural features, the recognition of which is proving valuable in several Australian geological investigations ranging from mineral exploration to the prediction of zones of weak strata in coal mines (O'Driscoll & Keenihan, 1980; Shepherd & others, 1981).

The purpose of this paper is to draw attention to quite a different method of studying linear or areal features in the topography. The new technique is based on computer manipulation of a digital terrain model (DTM) as described in the previous paper of this issue (Moore & Simpson, 1982).

Though the technique is in an early stage of development we believe it is potentially very valuable for morphotectonic studies, and possibly in exploration. We have chosen in this note to emphasise lineaments, straight or curved, some of them new and some of them detected or postulated earlier by others using techniques such as geological mapping, gravity surveys, and the study of Landsat images. Individual incorrect spot-height values occur throughout the data, and in some districts whole blocks of data are in error, but we do not consider the errors significant for the interpretations in this note.

Many apparently geologically significant features in the topography of the DTM are most obvious when contour interval colour contrasts are rapidly varied in real time on the TV monitor. It is impossible to illustrate those real time effects by using only the few images that can be reproduced with this note. Therefore, where a specific feature is discussed in the text, the reader is advised to compare the expression of that feature in all figures. It should be emphasised also that, owing to the way in which digital data are displayed on the square pixel arrangement of the television monitor, a distorted projection is presented. It does not correspond exactly with any standard map projection. The accompanying illustrations approximate a rectangular display of meridians and parallels, and for this paper the coastline and geographic coordinates were generalised and added independently of the digital data files. The coloured illustrations at the top, bottom-left and bottom-right on the cover are reproduced in the text in monochrome as Figures 1, 2, and 3 respectively.

Although only selected features are discussed below, the reader will observe many others, particularly lineaments, which may often be detected more easily by viewing the cover pictures at low oblique angle.

The Darling River Lineament

Hills (1956, 1961) studied a relief model of the topography of Australia and pioneered the recognition of lineaments and patterns of lineaments. He stated (1956, p. 13) that in the continent of Australia as a whole 'the overall picture is very clearly revealing a great many relatively straight lineaments, either linked or intersecting', and he considered that the pattern shows many major trends that are parallel with the global network of shear planes drawn by Vening Meinesz (1947). Particular emphasis was given by Hills (1956) to the Darling Lineament, along the Darling River and its tributary, the Birrie River. This feature is very clear along part of its length (e.g. A-B on Fig. 1) and some workers have claimed that it extends from the Birrie River towards Brisbane or the region north of Brisbane (Rod, 1966). O'Driscoll & Keenihan (1980) made the Darling River Lineament even longer than others had done, extending it from Spencer Gulf north of Adelaide through the Adelaide Fold Belt and the Broken Hill mining district to the Queensland coast at Fraser Island, north of Brisbane. Part of the Darling River Lineament can be seen in the pseudocolour images on the cover (possible extensions of this can be seen in the synthetic reflectance images of Moore & Simpson, 1982, fig. 5) but we could find no definite DTM expression of the Darling River Lineament northeast of the Toowoomba Charleville Lineament (Fig. 4), a feature which is discussed below. Exon (1976) made a detailed study of the Surat Basin, and did not mention the lineament, presumably because it does not appear in the surface

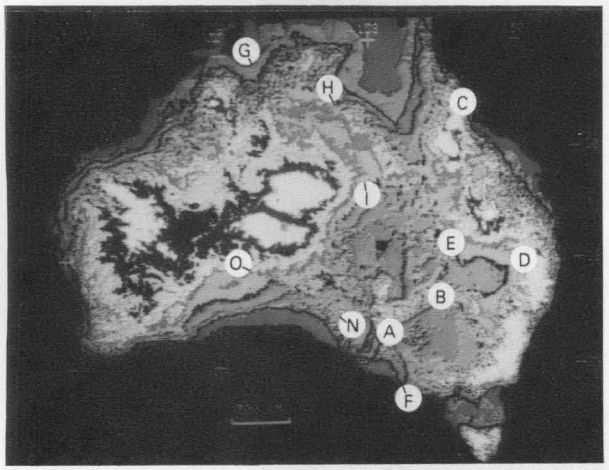

Figure 1. Monochrome reduction of the pseudocolour DTM image in the upper part of the front cover of the journal.

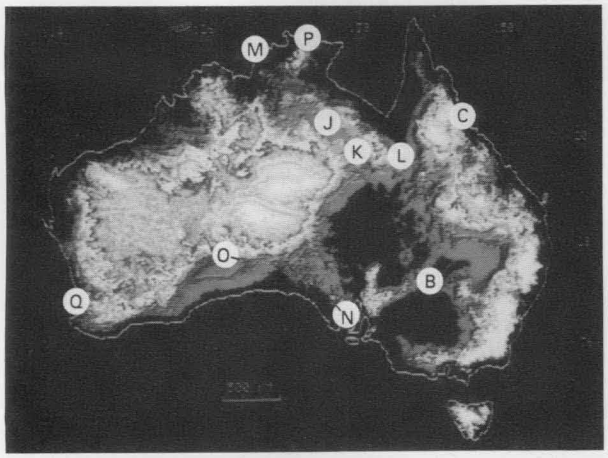

Figure 2. Monochrome reduction of the pseudcolour DTM image in the lower left section of the front cover of the journal.
On the cover only the topography above 120 m is shown in colour.

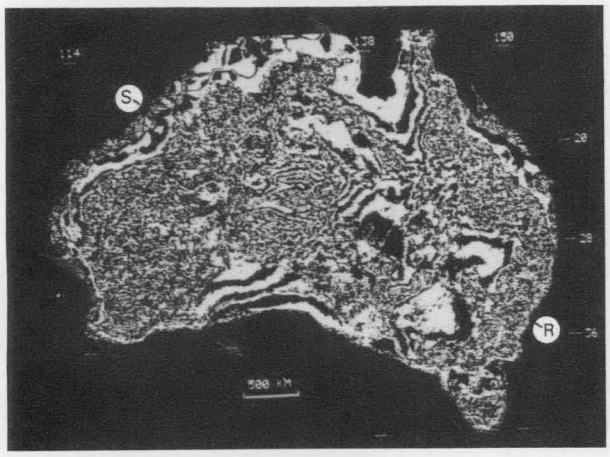

Figure 3. Monochrome representation of the bit-plane image in the lower right section of the front cover of the journal.

geology or in his structure contours on various units in the Bowen and Surat Basins. Similarly, Harrington (1974) could not find evidence of the lineament crossing either the northeast Surat Basin, or the Yarrol

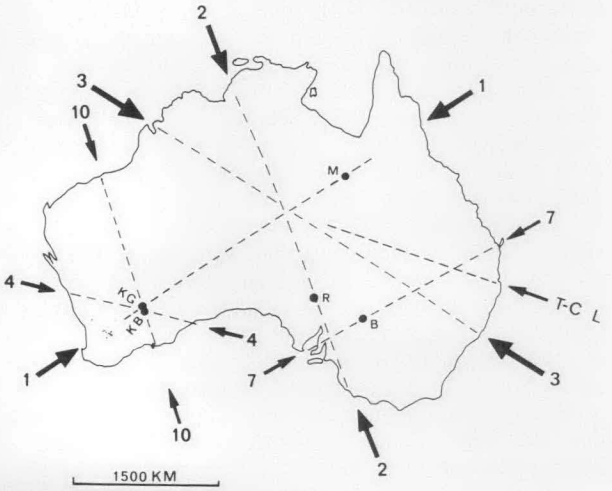

Figure 4. Lineaments recognised by O'Driscoll & Keenihan (1980) using Bouguer gravity maps.
The Toowoomba-Charleville Lineament (T-CL) has been added. Major ore bodies are indicated: KG, Kalgoorlie; KB, Kambalda; R, Roxby Downs; B, Broken Hill; M, Mount Isa. Originally published in *The APEA Journal* 20 (1), p. 17, and reproduced with permission.

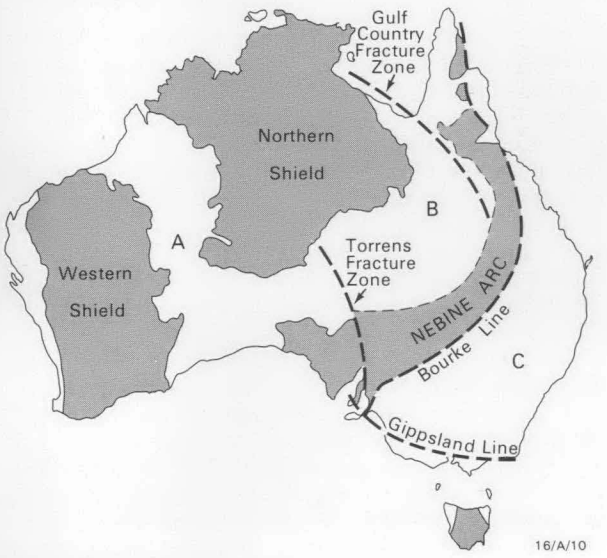

Figure 5. Late Proterozoic to Early Cambrian break-up of the Precambrian craton (shaded) according to the hypothesis of Harrington (1974).
Extensions of the craton are known under parts of regions A and B, and suspected under C. A, Canning, Officer and Eucla basins; B, Eromanga Basin and infrabasins; C, Tasman Orogen and successor basins.

Orogen in the vicinity of Fraser Island, Maryborough, and Gympie. He claimed that in the vicinity of Bourke the lineament curves to the north, passing through faults and folds to the junction of the Nebine Ridge and Anakie High with the Bowen Basin. Harrington called this curved lineament the Bourke Line (Fig. 5), because part of it diverged from the traditional Darling River Lineament and passed along the western side of the Bowen Basin.

Nebine Arc

The Nebine Ridge is a west-southwest-trending subsurface continuation of the exposed Anakie High (Senior, 1971). There is a cover of Jurassic and

Cretaceous sediments on it that strikes northwest, concealing the underlying basement ridge, but water bores and petroleum exploration wells have enabled the concealed part of the ridge to be delineated quite well (Senior, 1971; Exon, 1976, Section AB; Hind & Helby, 1969; Scheibner, 1974). In the portion termed the Eulo Ridge, streams have cut through the Mesozoic sediments to expose small areas of granite basement as shown on the 1960 Tectonic Map of Australia (BMR, 1960). In New South Wales, however, the trend of the ridge has been in dispute. Most workers (Battersby, 1981, fig. 1) have considered that it trends south from Queensland, joining the Cobar Spur section of the Lachlan Orogen southwards from Bourke through Cobar. Harrington (1974) studied the depths to basement found in many water bores, and claimed that the ridge trends southwest from Queensland to Broken Hill, forming part of a basement feature that extends from South Australia to North Queensland. (He called this feature the Nebine Island Arc, in part because of its arc-like shape and its rough similarity to present day Japan in length and shape). The southwest trend from the Queensland border shows very clearly on the Tectonic Map of New South Wales (Scheibner, 1974), but so also does the possible link with the Cobar Spur.

It was, therefore, very interesting to us to notice that the Nebine Arc showed clearly on many of the pseudo-colour images of the topography, (particularly Fig. 2) except in that portion in central Queensland where it is crossed obliquely by the cover of resistant ridge-forming Triassic and Jurassic sediments at the north-eastern edge of the Great Artesian Basin. The Bourke Line at the eastern edge of the arc is less distinct, but can be seen on some images. There is another very distinct and previously undescribed lineament (Figs. 1 & 2, B-C) that is mainly inside the Nebine Arc, trending southwards from west of Townsville through Lake Galilee, thence just west of Charleville and down the long straight Warrego River through Cunnamulla, to west of Bourke. This "Lake Galilee" lineament does not correspond with any known structural feature. It is unexplained. We can note only that Taylor (1911, p. 11) considered Lake Galilee anomalous in having no outlet, a fact that he attributed to disruption of drainage patterns by recent warping producing a 'New Divide' west of an 'Old Divide'. His 'Old Divide' was on a high part of the Yarrol Orogen, his 'New Divide' on the Nebine Arc.

The Toowoomba-Charleville Lineament

The Toowoomba-Charleville Lineament (Fig. 4, T-CL) was postulated by O'Driscoll & Keenihan (1980) using gravity data. They considered it a straight zone that extends west-northwest from the east coast south of Brisbane, through Toowoomba to Charleville, and then to the border of the Northern Territory. In its eastern part it is sub-parallel for about 300 km to the Main Divide, where the divide trends west-northwest to converge with the Nebine Arc. No immediately obvious expression of the T-CL could be found within the topography of the DTM. Minor topographic alignments at different levels do coincide with the lineament, but at the scale of the screen display they are too small to be given independent significance. On the other hand, the DTM shows clearly that contours on the lowland plain to the south of the Main Divide are essentially linear and subparallel to the T-CL (Fig. 1, D-E). In a zone 100 km wide and about 600 km long to the south of the T-CL, there is a surface sub-parallel to the T-CL and dipping south. This suggests that the T-CL is at the upper edge of the south dipping plain. The T-CL would not have been detected from DTM, but nevertheless, at the scale of the DTM regional topographic features may be easily identified and provide useful supplementary information about a major feature defined by other workers from other sources of information.

Other structural lineaments, and ore deposits

O'Driscoll & Keenihan (1980, p. 17) claimed that five of the largest Australian ore deposits are on continental gravity lineaments, namely the Broken Hill, Kambalda, Kalgoorlie, Mount Isa, and Roxby Downs deposits (Fig. 4). Their work has, therefore, attracted close attention from economic geologists, especially since the discovery of the huge concealed Roxby Downs deposit. Their lineaments were based largely on BMR Bouguer gravity anomaly maps.

The southwestern end of the Kalgoorlie-Mount Isa lineament of O'Driscoll & Keenihan (Fig. 4, lineament 1) is not obvious in Figure 1, but it can be traced for over 1000 km by manipulation in real time of contour colour contrasts on the image display system. Similarly, the northwest-trending Roxby Downs gravity lineament (Fig. 4, lineament 2; Fig. 1, F-G) has discontinuous topographic expression for about one-third of its length in South Australia, and, in the Northern Territory, nearly continuous expression between Mount Peake and Wave Hill. Moreover, on the western side of the Northern Territory segment, there are significant sub-parallel contours in a zone 150 km wide and 500 km long. This zone suggests a relatively uniform topographic gradient dipping towards the lineament and terminating at it.

Inside the Arnhem Land Block, the Emu Fault system forms the eastern side of the Batten Trough (Plumb & others, 1981) and has attracted much attention because the very large HYC lead-zinc deposit is located on it. Manipulation of colour contrasts on the DTM showed that the line of the fault continues south-south-eastward as a lineament along the eastern side of the Barkly Tableland (which is also the eastern side of the northwesterly parallelogram of the Georgina Basin, discussed later) and along the western side of the Georgina River (Fig. 1, H-I; cf. also Fig. 3). The northern part of this lineament was previously observed on a Gemini V oblique space photograph of the region (taken 27 August 1965). The lineament is parallel to the northwestern portion of the Roxby Downs gravity lineament of O'Driscoll & Keenihan (1980) and approximately 500 km from it.

The Halls Creek Mobile Zone is a major structural feature in the northeastern part of Western Australia. Extending southwards from it is a subtle linear zone that crosses the Canning Basin and the Yilgarn Province and trends towards Perth (part of it shows between P and Q on Fig. 2). It is weakly expressed, and is not continuous on any single DTM image, but several observers have agreed that it can be followed during real-time manipulation of contour colour contrasts on the screen. It is mentioned here as an example of the

many lineaments apparent in the DTM images for which, over much of their length, there is at present no geological explanation.

There are several potential applications of the DTM display in addition to the study of straight or curved linear topographic features. The system can be used to study specific height levels on a continental scale as discussed by Moore & Simpson (1982). For example, the topography above 120 m is displayed in colour on Figure 2, the levels below 120 m being assigned to black. Changes in the minimum contour on such a figure can be made in real-time to give the effect of progressive 'continental flooding'. The resultant changes in the shapes of basins and highs as the 'sea rises and falls', and changes in the shapes and positions of province boundaries, some of which are major lineaments, provide a new method of studying topographic relationships. The effect is similar to watching a moving film instead of a single still photograph. For example, on specific contour levels the Barkly Tableland region of the Georgina Basin (Fig. 2, J) is divided into two rhombs or parallelograms (Fig. 2, J and K in the blue colour level). During real-time 'flooding' of the contour levels, the pattern of the two Georgina rhombs is continued northwestwards by similar patterns in the interconnected Wiso and Daly River basins. Such features can not be adequately illustrated in the single level photographs. In some real-time sequences the pattern extends further to the Bonaparte Gulf Basin. When the value of the minimum contour is progressively increased a simulated opening of the basins by a spreading movement of the Arnhem Land block away from the remainder of the northern shield is very apparent in successive images on the screen. The pattern is like the pattern of transform faults and spreading segments in, say, the Gulf of California, and it really might be a result of a Late Proterozoic or earliest Cambrian spreading event of the kind postulated by Harrington (1974). Another possibility is that the boundaries of the parallelograms are expressions of reactivated Early Proterozoic faults of the kind postulated in a paper by Rossiter & Ferguson (1980, p. 215). In other words, the DTM images suggest regional structural patterns that were previously unrecognised, though they tell us nothing of the processes by which the patterns formed.

In the same northern region, geologists have speculated about the meaning of the linear southwestern coastline of the Gulf of Carpentaria. Harrington & others (1973), and Harrington (1974), related it to a postulated Gulf Country Fracture Zone, which was regarded as a transform fault that had allowed the Carpentaria Basin and its infrabasins to open, and the Nebine Arc to move away from the northern shield (Fig. 5) in the Later Proterozoic or earliest Cambrian. Rossiter & Ferguson (1980, p. 219) extended the fracture zone northwest through Arnhem Land to the major Bulman Fault. That lineament shows in the DTM, but there is also another even more prominent sub-parallel lineament 200 km southwest of the coastline (Fig. 2, L-M). This extends 1500 km from Winton to south of Darwin (and beyond, according to bathymetry). The Northern Territory part of this topographic feature was discussed by Hays (1967, p. 186) and called the Pine Creek Upwarp. Extrapolation of the feature to the southeast brings it in line with a gravity lineament that is not visible on the DTM, but which was claimed by Evans & Roberts (1980) to extend from Longreach to Roma and, possibly, to Lismore.

Other lineaments, discussed by Harrington & others (1973, 1974) and Harrington (1974), have topographic expression on the 'flooded' DTM image of Figure 2. They are the Torrens Fracture Zone (or Hinge) in South Australia, and the Gippsland Line (cf. Fig. 5) The latter coincides with the southern flank of the Gippsland highlands in eastern Victoria, and in western Victoria it appears as a distinct straight line on the DTM, although it is not distinct in ground-based field work. Harrington (1974, fig. 3) drew the Gippsland Line as far west as Spencer Gulf. The DTM shows a major topographic discontinuity (Figs. 1 & 2, N-O) in line with the Gippsland Line and continuing for 1000 km from Spencer Gulf along the southern side of the Gawler Ranges to the Ooldea Sand Range, a curious feature near the inner edge of the Eucla Basin (Krieg, 1971, p. 7; Pitt & others, 1980, p. 218).

The technique of displaying, in image form, individual bit-planes of the total stored data as discussed by Moore & Simpson (1982) also appears to have advantages for lineament detection. When the third least significant bit-plane is displayed as a binary image (Fig. 3) it shows lineaments that are not obvious when the total data set is displayed as in Figures 1 and 2. For example, a northwest trending lineament (Fig. 3, R-S) extends across the continent and is expecially apparent in low-angle viewing. The geological significance of this feature is unknown. It is believed to be a valid feature, for no mechanism is known that could randomly create an artifact of that dimension in the data set. Many other lineaments can be seen also on Figure 3.

Synthetic reflectance images, as discussed by Moore & Simpson (1982) may provide more specific lineament information than either the pseudocolour images of the bit-plane images discussed here. All types of images appear to provide complementary data and probably should be interpreted in conjunction. The scale of reproduction of the reflectance images, though adequate to demonstrate the technique, is too small for meaningful interpretation. However specific lineaments and structures discussed in this note can often be identified in part in some synthetic reflectance images.

Discussion

It is clear that some topographic lineaments lie along major faults or plate boundaries. Others are of unknown origin, some might not relate directly to surface geological features, and some are probably of doubtful authenticity. If most of the major topographic and gravity lineaments are surface expressions of really deep faults, they should end in triple junctions (active or inactive), but such junctions are seldom or never detected. There is much that is cryptic, and much that has yet to be developed in the fields of observation, structural interpretation, and economic application. Nevertheless, the new DTM techniques should be useful in morphotectonic studies, and have potential value in exploration.

References

BATTERSBY, D. G., 1981—New discoveries in the Surat/Bowen Basin. *The APEA Journal*, 21 (2), 39-44.

BMR., 1960—Tectonic Map of Australia, 1:253 400 scale, First edition. *Bureau of Mineral Resources, Australia.*

EVANS, P. R., & ROBERTS, J., 1980—Evolution of central eastern Australia during the late Palaeozoic and early Mesozoic. *Journal of the Geological Society of Australia*, 26, 325-40.

EXON, N. F., 1976—Geology of the Surat Basin in Queensland. *Bureau of Mineral Resources, Australia, Bulletin*, 166.

HARRINGTON, H. J., 1974—The Tasman Geosyncline in Australia. *In* The Tasman Geosyncline—a symposium in honor of Professor Dorothy Hill. *Geological Society of Australia, Queensland Division*, 385-407.

HARRINGTON, H. J., BURNS, K. L., & THOMPSON, B. R., 1973—Gambier-Beaconsfield and Gambier-Sorell fracture zones and the movement of plates in the Australia-Antarctica-New Zealand region. *Nature Physical Science*, 245 (146), 109-12.

HARRINGTON, H. J., BURNS, K. L., THOMPSON, B. R., & OZOLINS, A. P., 1974—Regional geology of Victoria in relation to satellite imagery, a preparatory study. *CSIRO Minerals Research Laboratories, and Mines Department, Geological Survey of Victoria, Investigation Report* 106.

HAYS, J., 1967—Land surfaces and laterites in the north of the Northern Territory. *In* JENNINGS, J. N., & MABBUTT, J. A., (editors), Landform studies from Australia and New Guinea. *Australian National University Press, Canberra*, 182-210.

HILLS, E. S., 1956—A contribution to the morphotectonics of Australia. *Journal of the Geological Society of Australia*, 3, 1-15.

HILLS, E. S., 1961—Morphotectonics and the geomorphological sciences with special reference to Australia. *Quarterly Journal of the Geological Society, London*, 117, 77-89.

HIND, M. C., & HELBY, R. J., 1969—The Great Artesian Basin in New South Wales. *Journal of the Geological Society of Australia*, 16, 481-97.

KRIEG, G., 1971—Comments on Noorina, Wyola, Maurice 1:250 000 geological sheets. *Department of Mines South Australia Report Book* 71/4.

MOORE, R. F., & SIMPSON, C. J., 1982—Computer manipulation of a digital terrain model (DTM) of Australia. *BMR Journal of Australian Geology & Geophysics*, 7, 63-7.

O'DRISCOLL, E. S. T., & KEENIHAN, S. L., 1980—The Toowoomba-Charleville lineament in southern Queensland. *The APEA Journal*, 20 (1), 16-24.

PITT, G. M., BENBOW, M. C., & YOUNGS, B. C., 1980—A review of recent geological work in the Officer Basin, South Australia. *The APEA Journal*, 20 (1), 209-20.

PLUMB, K. A., DERRICK, G. M., NEEDHAM, R. S., & SHAW, R. D., 1981—The Proterozoic of northern Australia. *In* HUNTER, D. R., (editor), Precambrian of the southern hemisphere. *Developments in Precambrian Geology*, 2, *Elsevier, Amsterdam*, 205-307.

ROD, E., 1966—Clues to ancient Australian geosutures. *Eclogae geologicae Helvetiae*, 59, 849-83.

ROSSITER, A. G., & FERGUSON, J., 1980—A Proterozoic tectonic model for northern Australia and its economic implications. *Proceedings of the International Uranium Symposium on the Pine Creek Geosyncline, Sydney, 4-8 June 1979, International Atomic Energy Agency, Vienna*, 209-32.

SCHEIBNER, E., 1974—Tectonic map of New South Wales, scale 1:1 000 000. *Geological Survey of New South Wales, Sydney*.

SENIOR, B. R., 1971—Structural interpretation of the southern Nebine Ridge area, Queensland. *Australasian Oil and Gas Review*, February 1971, 2-8.

SHEPHERD, J., HUNTINGTON, J. F., & CREASY, J. W., 1981—Surface and underground geological prediction of bad roof conditions in collieries of the Western Coalfield, New South Wales. *Institution of Mining & Metallurgy (London), Transactions, Section B*, 90, B1-B14.

TAYLOR, G., 1911—Physiography of eastern Australia. *Commonwealth Bureau of Meteorology, Australia, Bulletin* 8.

VENING MEINESZ, F. A., 1947—Shear patterns in the Earth's crust. *Transactions of the American Geophysical Union*, 28, 1-16.

BMR Journal of Australian Geology & Geophysics, 7, 73-7.

ON *AUSTRALINA* CLARKE—AND ITS JUNIOR SYNONYMS *LISSATRYPA, LISSATRYPOIDEA,* AND *TYROTHYRIS* (SILURIAN-DEVONIAN BRACHIOPODA).

D. L. Strusz

The Silurian-Devonian lissatrypid genera *Lissatrypa, Tyrothyris* and *Lissatrypoidea* are shown to be congeneric, and junior synonyms of *Australina* Clarke, 1913; the tiny naviculate *Nanospira* is treated as a subgenus. *Meifodia* differs in the shape of the ventral median platform and the orientation of the spiralia. *Gracianella lissumbra* differs only in lacking inner hinge plates, and (*contra* Johnson & Boucot, 1972) is considered most unlikely to be either ancestral to the Carinatininae, or closely related to *Dnestrina,* which is an anoplotheciid.

The small smooth atrypoids allied to *Lissatrypa* Twenhofel, 1914, type of the family Lissatrypidae, have long been difficult to deal with. In this paper, the morphology of a number of related genera is re-examined in the light of recent work (especially that of Copper, 1973a) and a new species from the Wenlock of Canberra, Australia (Strusz, in press) (Fig. 1). The systematic result is to place *Lissatrypa, Lissatrypoidea* and *Tyrothyris* in synonymy with *Australina* Clarke, 1913, and to treat *Nanospira* as a subgenus of *Australina.*

Clarke (1913) erected *Australina* for an Argentinian Wenlock species, *A. jachalensis,* but it remained poorly known until redescribed by Castellaro (1959), and has not been widely used since then. It is a rather small smooth lenticular to planoconvex atrypoid, with a faint dorsal sulcus and small suberect ventral beak. The ventral valve lacks dental plates, but has a median platform of chevron or barbed arrow-head outline, steeper and concave anteriorly. The structure of the cardinalia is not ideally illustrated, but judged from the serial sections, the hinge plates are narrowly disjunct, give rise to crura from their ventral faces, and are sessile on a thick posterior shelf that merges with a strong median ridge. There are widely divergent sockets, and the spiralia are directed dorsomedially.

Twenhofel (1914) gave a reasonable description of his new genus *Lissatrypa* and its types species *L. atheroidea* —although some nomenclatural problems ensued (see Kirk & Amsden, 1952)—but a fuller understanding of its internal structure awaited serial sectioning of topotypes by Copper (1973a). It, too, is a smooth lenticular atrypoid, with a small incurved beak. There are no dental plates, the teeth being attached to the valve sides, while the cardinalia comprise disjunct hinge plates resting on a median ridge and giving rise to small crura; the spiralia are directed dorsomedially. A ventral platform is barely developed in this thin-shelled species; none of the illustrations clearly shows its outline. In the serial sections, Copper discovered a small pedicle collar and tiny deltidial plates.

Öpik described *Tyrothyris* in 1953, basing it on the Victorian Llandovery species *T. tyro,* known only from moulds in siltstone. He thought the species to be punctate, and therefore a rostrospiracean, but the presumed punctae have since been shown to be a problematical boring organism (Talent, 1964; Boucot & others, 1964).

Talent considered first that, if punctae are absent, "*Tyrothyris* ... could perhaps be construed as a synonym of *Lissatrypa* ...". Having shown that punctae are indeed absent, he then commented "... the genus *Tyrothyris* fails as a synonym of *Meifodia* Williams (1951), likewise described as a meristellid and recently shown to be an atrypoid ...". Boucot & others (1964) placed *Tyrothyris* in synonymy with *Meifodia*—also first described from moulds—but did not draw comparisons with either *Lissatrypa* or *Nanospira* Amsden, 1949. Savage (1974) concurred with Talent in making a close comparison between *T. tyro* and the Early Devonian Australian species *Lissatrypa lenticulata* Philip, 1962, and suggested that *Tyrothris* is probably a junior synonym of *Lissatrypa* rather than *Meifodia.* The spiralia are directed dorsally in the latter, dorsomedially in the other two (Talent, 1964; Boucot & others, 1964; Copper, 1973a). Perhaps more importantly, the ventral median platform in *Meifodia* is distinctive, being in the form of a double-ended wedge, steeper and somewhat concave posteriorly. In *Tyrothyris* and those species (the majority) of *Lissatrypa* thick-shelled enough for it to develop, the ventral platform is as in *Australina*—chevron-shaped. There remain two features reported in *Lissatrypa* but not *Tyrothyris*: the presence in *L. atheroidea* of a pedicle collar and narrow deltidial plates, demonstrated by Copper (1973a). However, Copper (1967, p. 1168) had already noted that pedicle collars are "... not always present in all atrypid shells of a single species", and (p. 1174) "... cannot be employed as diagnostic biocharacters because of their irregular and only sporadic calcification." Moeover, most species of the lissatrypids being discussed here have erect to incurved ventral beaks, which makes detection of small deltidial plates, easily lost upon disarticulation, difficult. This indeed was the case with *L. atheroidea,* where the plates were only detected in serial sections. The new Canberra species that has prompted this note has a relatively prominent suberect beak, and both complete shells and ventral internal moulds show that the delthyrium is closed by conjunct deltidial plates, which are often lost during disarticulation.

Thus, these two characters, pedicle collar and deltidial plates, cannot be used in lissatrypid systematics. As their external and internal structures are, in all significant respects, the same, I conclude that *Tyrothyris* and *Lissatrypa* are junior synonyms of *Australina* Clarke, 1913.

Nanospira was erected by Amsden (1949) for the diminutive North American Silurian species *N. parvula,* which he contrasted with the similarly shaped *Glassia* Davidson, 1881, but not with *Lissatrypa.* He considered *Nanospira* to be distinct because of a prominent ven-

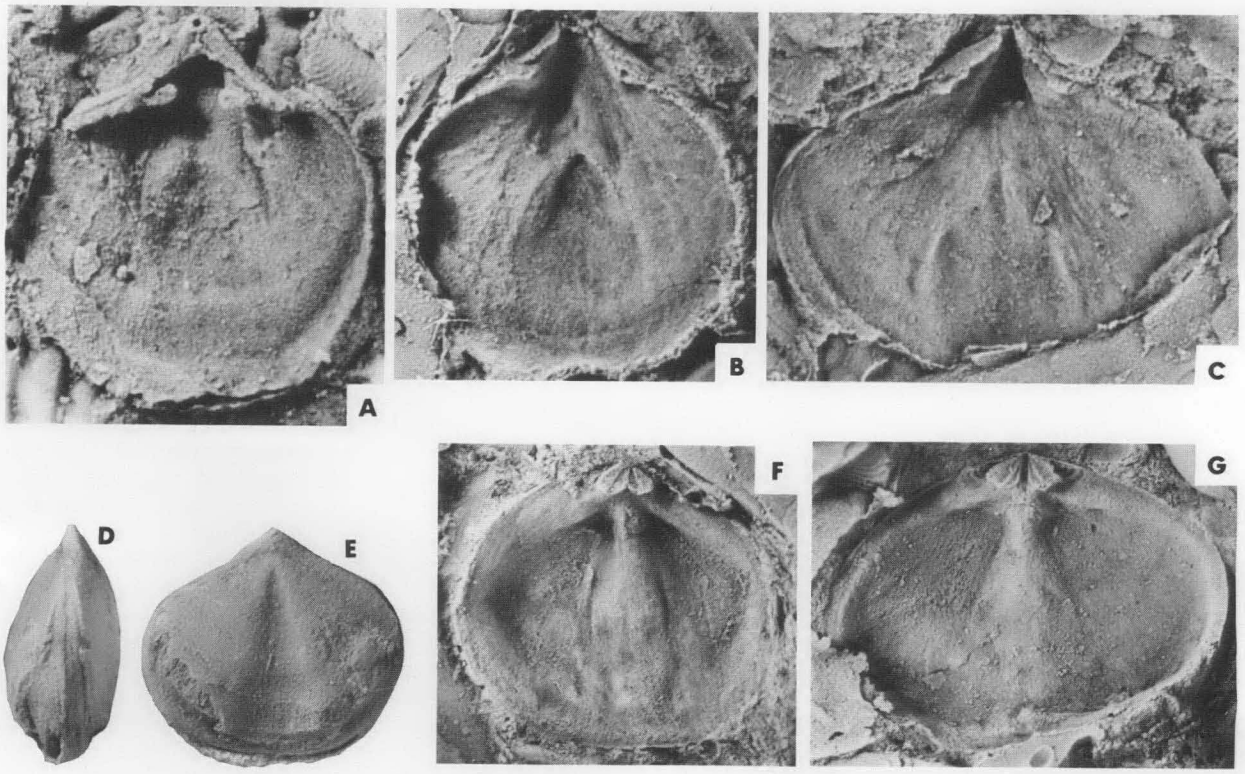

Figure 1. *Australina (Australina)* **n. sp.; Walker Volcanics, right bank of Molonglo R. below Coppins Crossing, west of Canberra; Wenlock.**

A-C ventral valves (latex replicas), x10; D, E, complete shell, x6; F, G, dorsal valves (latex replicas), x10. A, CPC 20442, showing foramen, conjunct deltidial plates, fairly deep cella and wide median platform; B, CPC 20473, with deep ogival cella and narrow platform, deltidial plates lost; C, CPC 20474, with shallow cella, low wide platform, deltidial plates lost. D, E, CPC 20518 in lateral and dorsal aspects, showing lenticular shape, suberect beak, closed delthyrium, and shallow sulcus. F, CPC 20475, with conjunct hinge plates; G, CPC 20455, with disjunct hinge plates clearly showing crural bases.

tral median platform (lacking in *Glassia*), spiralia with fewer turns, and a jugum arising much farther forward. Moreover, the spiralia are directed dorsomedially in *Nanospira*, and medially in *Glassia*. The cardinal structures are, however, similar (see Siehl, 1962, and Rubel, 1970).

Boucot & Amsden (1958) placed some American species in a new genus, *Lissatrypoidea*, with type species *Nucleospira concentrica* Hall, 1859. The new genus was held to differ from *Lissatrypa* in having medially conjunct hinge plates and a knob-like cardinal process. No comparison was made with *Nanospira*, presumably because of the disparity in size and shape. However, Amsden (1968) concluded that *Lissatrypoidea* was synonymous with *Nanospira*, on the basis that the conspicuous cardinal process indentified by Boucot & Amsden (1958) was in fact "... only a further build-up of shell material between the hinge plates, a feature presumably ... gerontic ...", and also that the hinge plates in both are conjunct. Re-examination of *N. parvula* shows disjunct (though sessile) hinge plates, "... somewhat filled in between with what I would regard as adventitious shell material" (R. E. Grant, personal communication 27.2.1980). The new Canberra lissatrypid species mentioned above shows considerable variation in the sessile hinge plates, from conjunct to distinctly disjunct, but without infilling of the cleft between. From this I conclude that no generic distinction can be made on conjunct versus disjunct hinge plates in this group of lissatrypids, and I concur with Amsden on the lack of a true cardinal process. Internally, the only difference between *Nanospira* and the other forms so far considered is the small number of turns to the spiralia, but this is clearly a function of shell size. Externally, it is distinguished by its small size, and, more significantly, by its distinctive shape. *N. parvula* is strongly naviculate, with a deep, anteriorly expanded dorsal sulcus, and averages only 3.5 mm wide. *Australina jachalensis* is ventribiconvex, but lacks the distinctive sulcus, while *Lissatrypa atheroidea* is lenticular, with an average width of about 14 mm, and its typical in both respects for most of the species concerned—e.g. *Lissatrypoidea concentrica* is lenticular and up to 12 mm wide. *Nucleospira clairensis* Thomas, 1926, placed in *Nanospira* by Amsden, 1968, is intermediate in size, with an average width of about 7 mm, and also in shape, since some specimens are ventribiconvex—but again, the dorsal sulcus is shallow, even anteriorly. From this, I conclude that a close relationship exists, but that a distinction, probably best drawn at the subgeneric level, can be made between *Nanospira parvula* on the one hand, and all the other species now placed in *Australina* (including those previously referred to *Nanospira*) on the other.

Systematics

Superfamily **Atrypacea** Gill, 1871

Family **Lissatrypidae** Twenhofel, 1914

Genus **Australina** Clarke, 1913

Type species. *Australina jachalensis* Clarke, 1913, pp. 346-348, revised Castellaro, 1959, pp. 60-62, pl. 3, figs. 1-9, 21, pl. 5, figs. 11-18; Wenlock, Precordillera de San Juan, Argentina.

Revised diagnosis. Small lissatrypids with subhypothyrid foramen, and delthyrium open or with deltidial plates; sulcus may develop on dorsal or both valves; shell surface finely spinose. Teeth crytomatodont, unsupported by dental plates; ventral muscle field bilobed, impressed posteriorly, divided anteriorly by variably elevated median platform in shape of chevron; front of platform steep, generally excavated as cella. Sockets widely divergent, contained between valve margin and massive inner hinge plates, may be transversely corrugated; hinge plates sessile on thick posterior shelf that merges forward with strong median ridge, may be disjunct or conjunct; cleft between plates may be partly or completely filled with secondary tissue, which in gerontic shells may overflow to simulate elevated cardinal process; small crura arise from ventral faces of hinge plates. Spiralia directed dorsomedially.

Remarks. I follow Copper (1973a) and Cocks (1978) in not recognising separate subfamilies within the Lissatrypidae. The closest genera to *Australina* are *Meifodia*, *Glassia*, and *Holynatrypa* Havlíček, 1973. *Meifodia* differs in being dorsibiconvex, with short dental plates in some species, in having a ventral platform of double wedge shape, steeper posteriorly, and in having dorsally directed spiralia. In *Glassia*, which is lenticular to naviculate, there is no ventral platform, and the spiralia are directed medially. *Holynatrypa* has a widely crescentic front to its ventral platform, with the cella excavated therein divided by a strong ridge that extends forward to the shell margin.

Also very like *Australina* is *Gracianella* Johnson & Boucot, 1967, especially the type species *G. lissumbra* and non-costate specimens of *G. umbra* (Barrande). Their surface ornament is the same, and the erect foramenate beak and closed delthyrium are as in the new Canberra species of *Australina*. The internal structure also is very similar, differing only in the lack of inner hinge plates in *Gracianella*. The resemblance is far greater than that between *Gracianella* and Devonian Carinatininae such as *Biconostrophia*. The Carinatininae have long hinge-lines, a different ventral musculature, very obvious impressions of the spiralia on the ventral valve floor, and a distinctive transverse ridge joining the posterior edges of the socket ridges (as in *Dnestrina* and *Coelospira*). Copper (1973c, p. 486) left *Gracianella* in the Carinatininae, pending information on the spiralia, but suggested that at least some of its species could be dayiaceans. I consider *Gracianella* to be a most unlikely ancestor for the Carinatininae, *contra* Johnson & Boucot, 1972, and would definitely remove it from the subfamily, although further investigation will be needed to find it a home. Johnson & Boucot (1972, p. 35) also considered *Gracianella* and *Dnestrina* to be related, but I concur with Copper (1973b, pp. 121-122) in placing *Dnestrina* with *Coelospira* in the Anoplotheciidae.

Subgenus **Australina** Clarke, 1913

= *Lissatrypa* Twenhofel, 1914
= *Tyrothyris* Öpik, 1953
= *Lissatrypoidea* Boucot & Amsden, 1958

Type species. As for the genus

Diagnosis. Lenticular *Australina* with dorsal sulcus, where developed, shallow throughout.

Species included

atheroidea Twenhofel, 1914, p. 33, pl. 1, figs 11-15; type species, *Lissatrypa*; Llandovery, Anticosti I., Canada; possibly also Lochkovian, Kazakhstan, USSR (Ushatinskaya & Nilova, pp. 113-114 in Menner, 1975).

clairensis Thomas, 1926, pp. 397-398, pl. 54, fig. 11; as *Nucleospira*; assigned to *Nanospira* by Amsden, 1968, p. 79; Wenlock, Arkansas, USA.

concentrica Hall, 1859, p. 223, pl. 28B, fig. 16 (*partim*), as *Nucleospira*; emend. Boucot & Amsden, 1958, p. 159; type species, *Lissatrypoidea*; synonym *Lissatrypa decaturensis* Amsden, 1949; Ludlow, Tennessee-Oklahoma-Missouri, USA.

henryhousensis Amsden, 1951, p. 89, pl. 19, figs. 32-38, as *Lissatrypa*; Ludlow, Oklahoma, USA.

jachalensis Clarke, 1913, pp. 346-348, figs. 1-3; type species; Wenlock, Precordillera de San Juan, Argentina.

?*kazachstanica* Borisiak, 1955, pp. 53-54, pl. VI, figs. 19-24; Lochkovian (Aynasuy horizon), Kazakhstan, USSR.

lenticulata Philip, 1962, pp. 220-221, pl. 34, figs. 4, 17-21, as *Lissatrypa*; Lochkovian, Victoria and New South Wales, Australia.

leprosa Kozłowski, 1929, pp. 167-169, pl. 5, figs. 15-21, as *Lissatrypa*; Lochkovian, Podolia, USSR.

?*sulcata* Lindström, 1861, p. 364, pl. 12, fig. 4, as *Spirigerina*; to *Lissatrypa*? by Bassett & Cocks, 1974, p. 31, pl. 9, fig. 1; Wenlock to Ludlow, Gotland, Sweden.

?*minuta* Rybnikova, 1967, *fide* Kul'kov, 1978, pp. 85-88,, pl. X, figs. 1, 2, as *Glassia*; has ventral median platform of *Australina* form; spiralia unknown; Llandovery, Latvia and Tuva, USSR.

tyro Öpik, 1953, pp. 15-17, pl. 4, figs. 23-29, pl. 5, figs. 30-31; type species, *Tyrothyris*; synonym *T. melicerta* Öpik, 1953; Llandovery, Victoria, Australia.

sp. nov., figured herein, fully described in Strusz (in press); Wenlock, Canberra, Australia.

Species rejected

Lissatrypa columbella (Barrande), Kul'kov, 1967, pp. 91-93, pl. 14, figs. 1-6, 10, pl. 15, fig. 11; Ludlow (Chagyr suite), Altai Mts, USSR; = *Atrypoidea*.

Lissatrypa linguata (Buch), Kul'kov, 1967, pp. 93-94, pl. 14, figs. 8, 9; Ludlow (Chagyr suite), Altai Mts, USSR = *Atrypoidea*.

Lissatrypa minuta Kul'kov, 1967, 1967, pp. 96-97, pl. 16, fig. 12; Ludlow (Chagyr suite), Altai Mts, USSR; = *Atrypoidea*.

Lissatrypa operosa Kul'kov, 1967, pp. 94-96, pl. 15, figs. 1-7; Ludlow? (Kuimov suite), Altai Mts, USSR; = *Atrypoidea.*

Lissatrypa recta Nikiforova & Andreeva, 1961, pp. 228-230, pl. 48, figs. 1-11; Llandovery, Siberian Platform, USSR; placed in *Meifodia* by Boucot, Johnson, & Staton, 1964, p. 812, but more likely to be *Atrypoidea.*

Glassia tenella Williams, 1951, pp. 114-115, pl. 5, figs. 16-18; Llandovery, UK; referred to *Australina* by Castellaro, 1959, but is *Glassia.*

Subgenus **Nanospira** Amsden, 1949

Type species. *Nanospira parvula* Amsden, 1949, p. 203; Amsden, 1951, p. 91, pl. 19, figs. 1-9; Ludlow, Oklahoma, USA.

Species included. Monospecific.

Acknowledgements

V. G. Walmsley and L. R. M. Cocks gave help and advice at the start of my work on the Silurian brachiopod faunas of Canberra, R. E. Grant provided information on the U.S. National Museum types of *Nanospira*, while A. J. Boucot and J. G. Johnson commented usefully on an early draft of this account. Photography was done by R. W. Brown and H. M. Doyle. To all, my thanks.

References

AMSDEN, T. W., 1949—Two new genera of brachiopods from the Henryhouse formation (Silurian) of Oklahoma. *Journal of the Washington Academy of Science,* 39, 202-3.

AMSDEN, T. W., 1951—Brachiopods of the Henryhouse Formation (Silurian) of Oklahoma. *Journal of Paleontology,* 25, 69-96, 15-20.

AMSDEN, T. W., 1968—Articulate brachiopods of the St. Clair Limestone (Silurian), Arkansas, and the Clarita Formation (Silurian), Oklahoma. *Paleontological Society, Memoir* 1.

BASSETT, M. G., & COCKS, L. R. M., 1974—A review of Silurian brachiopods from Gotland. *Fossils and Strata,* 3.

BORISIAK, M. A., 1955—Siluriyskie (Venlokskie) brakhiopody iz Karagandinskoy oblasti (Silurian (Wenlockian) brachiopods in the Karaganda region). *Materialy Vsesoyuznyy Nauchno-issledo-vatel'skiy Geologicheskiy Institut (VSEGEI), n.s., Paleontologiya i Stratigrafiya,* 3. (In Russian).

BOUCOT, A. J., & AMSDEN, T. W., 1958—Stratigraphy and paleontology of the Hunton Group in the Arbuckle Mountain region. Part IV—new genera of brachiopods. *Bulletins of the Oklahoma Geological Survey,* 78, 159-170, 12, 14 (*pars*).

BOUCOT, A. J., JOHNSON, J. G., & STATON, R. D., 1964—On some atrypoid, retzioid, and athyridoid Brachiopoda. *Journal of Paleontology,* 38, 805-22, 125-8.

CASTELLARO, H. A., 1959—Braquiopodos gotlándicos de la Precordillera de San Juan. *Revista de la Asociacion Geologica Argentina,* 13, 41-65, I-V.

CLARKE, J. M., 1913—Fosseis devonianos do Paraná. *Monographica do Serviço Geologico e Mineralogica do Brasil,* I (not seen; *fide* MOORE, 1965).

COCKS, L. R. M., 1978—A review of British Lower Palaeozoic brachiopods, including a synoptic revision of Davidson's Monograph. *Palaeontographical Society, Monograph.*

COPPER, P., 1967—Pedicle morphology in Devonian atrypid brachiopods. *Journal of Paleontology,* 41, 1166-75, 153-4.

COPPER, P., 1973a—The type species of *Lissatrypa* (Silurian Brachiopoda). *Journal of Paleontology,* 47, 70-6, 1-2.

COPPER, P., 1973b—*Bifida* and *Kayseria* (Brachiopoda) and their affinity. *Palaeontology,* 16, 117-38, 4-7.

COPPER, P., 1973c—New Siluro-Devonian atrypoid brachiopods. *Journal of Paleontology,* 47, 484-500, 1-3.

DAVIDSON, T., 1881—Descriptions of new Upper Silurian brachiopods from Shropshire. *Geological Magazine,* (2) 8, 145-56, 5.

HALL, J., 1859—containing descriptions and figures of the organic remains of the lower Helderberg group and the Oriskany sandstone. *New York State Geological Survey, Natural History of New York, Paleontology,* 3(1), 1-532 (text only; pl. 1-120 published 1861; not seen; *fide* MOORE, 1965).

HAVLÍČEK, V., 1973—New brachiopod genera in the Devonian of Bohemia. *Věstník Ustredního Ustavu Geologického,* 48, 337-40, 1-2.

JOHNSON, J. G., & BOUCOT, A. J., 1967—*Gracianella,* a new late Silurian genus of atrypoid brachiopods. *Journal of Paleontology,* 41, 868-73, 109-10.

JOHNSON, J. G., & BOUCOT, A. J., 1972—Origin and composition of the Carinatininae (Devonian Brachiopoda). *Journal of Paleontology,* 46, 31-8, 1-3.

KIRK, E., & AMSDEN, T. W., 1952—Upper Silurian brachiopods from southeastern Alaska. *United States Geological Survey Professional Paper* 233-C, 53-66, 11-13.

KOZLOWSKI, R., 1929—Les Brachiopodes gothlandiens de la Podolie polonaise. *Palaeontologia Polonica,* I.

KUL'KOV, N. P., 1967—Brakhiopody i stratigrafiya Silura gornogo Altaya (Brachiopods and stratigraphy of the mountainous Altai). *Nauka, Moscow* (in Russian).

KUL'KOV, N. P., 1978—Nekotorye gladkie Spiriferida iz Silura Tuvy (Some smooth Spiriferda from the Silurian of Tuva). *Trudy Instituta Geologii i Geofiziki Sibirskoe Otdelenie Akademiya Nauk SSSR,* 405, 85-94, X. (In Russian).

LINDSTRÖM, G., 1861—Bidrag till kännedomen om Gotlands brachiopoder. *Öfversigt af Kongliga Svenska Vetenskapsakademiens Förhandlingar, Stockholm,* 17 (for 1860), 337-82, 12-13 (not seen; *fide* BASSETT & COCKS, 1974).

MENNER, V. V. (editor), 1975—Kharakteristika fauny pogranichnykh sloev Silura i Devona tsentral'nogo Kazakhstana. (Materialy po geologii Tsentral'nogo Kazakhstana, XII). (Characteristic faunas of the Siluro-Devonian boundary beds of central Kazakhstan. Materials on the geology of central Kazakhstan, 12). *Nedra, Moscow.*

MOORE, R. C. (editor), 1965—Treatise on Invertebrate Paleontology. Part H, Brachiopoda. *Geological Society of America & University of Kansas Press, Lawrence.*

NIKIFOROVA, O. I., & ANDREEVA, O. N., 1961—Stratigrafiya Ordovika i Silura sibirskoy platformy i ee paleontologicheskoe obosnovanie (brakhiopody) (Stratigraphy of the Ordovician and Silurian of the Siberian Platform and its palaeontological basis (brachiopods)). *Trudy Vsesoyuznogo Nauchno-issledovatel'skogo Geologicheskogo Instituta (VSEGEI), 56, Biostratigrafiya paleozoya sibirskoy platformy* 1. (In Russian).

ÖPIK, A. A., 1953—Lower Silurian fossils from the "Illaenus Band", Heathcote, Victoria. *Geological Survey of Victoria, Memoir* 19.

PHILIP, G. M., 1962—The palaeontology and stratigraphy of the Siluro-Devonian sediments of the Tyers area, Gippsland, Victoria. *Proceedings of the Royal Society of Victoria,* 75, 123-246, 11-36.

RUBEL, M., 1970—Brakhiopody Pentamerida i Spiriferida Silura Estonii (Silurian brachiopods Pentamerida and Spiriferida of Estonia). *Eesti NSV Teaduste Akadeemia Geoloogia Instituut, 'Valgus', Tallinn* (in Russian).

SAVAGE, N. M., 1974—The brachiopods of the Lower Devonian Maradana Shale, New South Wales. *Palaeontographica, Abteilung A,* 146, 1-51, 1-11.

SIEHL, A., 1962—Der Greifensteiner Kalk (Eiflium, rheinisches Schiefergebirge) und seine Brachiopodenfauna. I. Geologie; Atrypacea und Rostrospiracea. *Palaeontographica, Abteilung A,* 119, 173-221, 23-40.

STRUSZ, D. L. (in press)—Wenlock brachiopods from Canberra, Australia. *Alcheringa,* 6.

TALENT, J. A., 1964—The Silurian and early Devonian faunas of the Heathcote District, Victoria. *Geological Survey of Victoria, Memoir* 26.

THOMAS, N. L., 1926—Brachiopods from the St. Clair Limestone, Arkansas. *Journal of the Science Laboratories, Denison University,* 21, 385-401, 1.

TWENHOFEL, W. H., 1914—The Anticosti Island faunas. *Museum Bulletin of the Geological Survey of Canada,* 3, Geological Series, 19, 1-39, 1.

WILLIAMS, A., 1951—Llandovery brachiopods from Wales with special reference to the Llandovery district. *Quarterly Journal of the Geological Society, London,* 107, 85-134, 3-8.

BMR Journal of Australian Geology & Geophysics, 7, 78-9.

THE STRATIGRAPHIC IMPLICATIONS OF *MONOGRAPTUS EXIGUUS* FROM CAMP HILL, CANBERRA, ACT

D. L. Strusz & C. J. Jenkins [1]

The Camp Hill Sandstone of Öpik (1958) is unconformable not only on the Black Mountain Sandstone but also the State Circle Shale (whose age is established as Late Llandovery by the occurrence of *Monograptus exiguus*). It is almost certain that the Black Mountain Sandstone overlies the State Circle Shale, and is thus of Late Llandovery age, not Early Ordovician.

In the seventy years since Pittman (1911) reported on the geology of the Canberra area, the age assigned to the prominently outcropping Black Mountain Sandstone has changed from Silurian to earliest Ordovician and back. Yet still there is no direct evidence, all interpretations being deduced from its relation with the surrounding rocks (Öpik, 1958; Strusz & Henderson, 1971; Crook & others, 1973)—and those relations have themselves been subject to disagreement (Link, 1970, 1971; Öpik, 1971).

The stratigraphic units most involved, of those erected by Öpik, are the Camp Hill Sandstone and the State Circle Shale. The former contains a Silurian shelly fauna, including the brachiopod *Rhipidium*, which Öpik took to be of Llandovery age, but which is now known to be a Wenlock-Ludlow form (Strusz & Henderson, 1971). The State Circle Shale contains a graptolite fauna, of which the commonest species is *Monograptus exiguus*, restricted to two zones in the middle of the Late Llandovery. Öpik thought that the State Circle Shale was conformable on the Camp Hill Sandstone (the contact was not exposed) and passed upwards into his calcareous Turner Mudstone. However, excavations for Capital Circle and the widened State Circle in 1969-71 revealed a different and more complex situation (Henderson, 1973). At the summit of Capital Hill (now removed during excavation for the new Parliament House), the Camp Hill Sandstone lay unconformably on quartz sandstone identified by Öpik as the Black Mountain Sandstone. In a pedestrian underpass below Capital Circle about 400 metres west of the summit, and 300 metres south of the type locality of the State Circle Shale, the same quartz sandstone conformably overlay shale similar to the State Circle Shale. In cuttings on Capital Circle 350 metres north-northeast of the summit, a tectonically disturbed area showed the quartz sandstone definitely interbedded with State Circle Shale (containing *M. exiguus*). None of the excavations contained rock resembling the Turner Mudstone.

A major fault separates most of Capital Hill from Camp Hill to the northeast, type locality of the Camp Hill Sandstone, and the deepened road cutting on State Circle exposed the unconformity at the base of the Camp Hill Sandstone. The underlying slumped pinkish buff siltstone is quite unlike the Black Mountain Sandstone, and, though unfossiliferous, was identified as the State Circle Shale. A trunk sewer tunnel behind the present Parliament House, less than 300 metres northeast, but with no outcrop intervening, had yielded shale with a good *M. exiguus* fauna in 1958, but a fault separated it from rocks of Öpik's Canberra Group, so it could not be put in proper stratigraphic context. While examining test pits for the new Parliament House with Henderson in 1979, one of us (D.L.S.) collected a single specimen of *M. exiguus* from a pinkish buff siltstone exposed in a pit on Camp Hill behind the northern end of the Parliament House car park. The exposure clearly showed the same unconformity as in State Circle, and the graptolite came from below it, so the stratigraphic context is unequivocal. The identity of the specimen (Fig. 1) has been confirmed by the other author (C.J.J.).

It is thus now certain that the Camp Hill Sandstone is unconformable on both State Circle Shale and Black Mountain Sandstone. The interbedding of the State

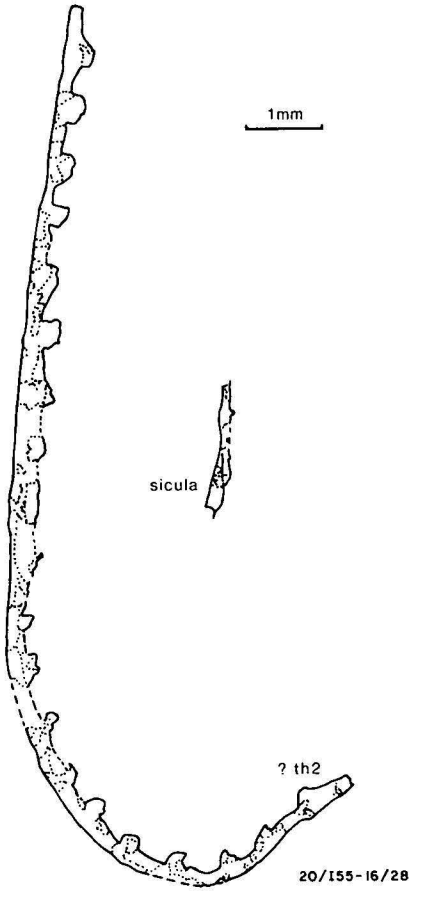

Figure 1. *Monograptus exiguus* **(Nicholson, 1868), CPC 21458.**
The dimensions and shape of the specimens most closely match those of the *M. e. exiguus* described in Hutt (1975), and from the *Monograptus turriculatus* and *Monograptus crispus* Zones of the Upper Llandovery in Britain.

[1] James Cook University of North Queensland, Townsville, Queensland 4811.

Circle Shale with quartz sandstone assigned to the Black Mountain Sandstone on Capital Circle, while not conclusive, strongly supports the more recent thesis, based on reappraisal of the outcrops at the southern end of Black Mountain (Strusz & Henderson, 1971; Crook & others, 1973), that the Black Mountain Sandstone is conformable above the State Circle Shale. While definite proof of this thesis remains elusive, Öpik's alternative concept that the Black Mountain Sandstone is below everything, including the Pittman Formation (of known Ordovician age), is becoming increasingly difficult to support.

Acknowledgements

We would like to thank R. Abell, H. F. Doutch, M. Owen, and D. Wyborn for their helpful criticisms of an early draft of this note.

References

CROOK, K. A. W., BEIN, J., HUGHES, R. J., & SCOTT, P. A., 1973—Ordovician and Silurian history of the southeastern part of the Lachlan Geosyncline. *Journal of the Geological Society of Australia,* 20, 113-43.

HENDERSON, G. A. M., 1973—Geology of the Capital Hill area, Canberra, A.C.T. *Bureau of Mineral Resources, Australia, Record* 1973/35 (unpublished).

HUTT, J. E., 1975—The Llandovery graptolites of the English Lake District. Part 2. *Palaeontographical Society, Monograph,* 2, 57-137.

LINK, A. G., 1970—Age and correlations of the Siluro-Devonian strata in the Yass Basin, New South Wales. *Journal of the Geological Society of Australia,* 16, 711-22.

LINK, A. G., 1971—Reply (to correspondence by Öpik on the Silurian of Canberra). *Journal of the Geological Society of Australia,* 17, 232.

ÖPIK, A. A., 1958—The geology of the Canberra City district. *Bureau of Mineral Resources, Australia, Bulletin* 32.

ÖPIK, A. A., 1971—The Silurian of Canberra. *Journal of the Geological Society of Australia,* 17, 231-2.

PITTMAN, E. F., 1911—Reports on the geology of the Federal Capital site. *Government Printer, Melbourne.*

STRUSZ, D. L., & HENDERSON, G. A. M., 1971—Canberra City, A.C.T., 1:50 000 Geological Map and Explanatory Notes. *Bureau of Mineral Resources, Australia, Canberra.*

CONTENTS

K. S. Jackson
Geochemical evaluation of the petroleum potential of the Toko Syncline, Georgina Basin, Queensland 1

J. P. Cull
An appraisal of Australian heat-flow data 11

C. M. Brown, K. S. Jackson, K. L. Lockwood, & V. L. Passmore
Source rock potential and hydrocarbon prospectivity of the Darling Basin, New South Wales 23

R. V. Burne
Relative fall of Holocene sea level and coastal progradation, northeastern Spencer Gulf, South Australia 35

V. Anfiloff
Elevation and gravity profiles across Australia: some implications for tectonism 47

G. D. Karner
Spectral representation of isostatic models 55

NOTES

R. F. Moore & C. J. Simpson
Computer manipulation of a digital terrain model (DTM) of Australia 63

H. J. Harrington, C. J. Simpson, & R. F. Moore
Analysis of continental structures using a digital terrain model (DTM) of Australia 68

D. L. Strusz
On *Australina* Clarke and its junior synonyms, *Lissatrypa*, *Lissatrypoidea*, and *Tyrothyris* (Silurian-Devonian Brachiopoda) 73

D. L. Strusz & C. J. Jenkins
The stratigraphic implications of *Monograptus exiguus* from Camp Hill, Canberra, ACT 78

R81/103(1) Cat. No. 81 1834 0